

## N O T I C E

THIS DOCUMENT HAS BEEN REPRODUCED FROM  
MICROFICHE. ALTHOUGH IT IS RECOGNIZED THAT  
CERTAIN PORTIONS ARE ILLEGIBLE, IT IS BEING RELEASED  
IN THE INTEREST OF MAKING AVAILABLE AS MUCH  
INFORMATION AS POSSIBLE

The Electrical Conductivity of the Earth's  
Upper Mantle as Estimated from  
Satellite Measured Magnetic  
Field Variations

by

Edna M. Didwall

A dissertation submitted to The Johns Hopkins  
University in conformity with the requirements  
for the degree of Doctor of Philosophy

Baltimore, Maryland

1981

(NASA-CR-163938) THE ELECTRICAL  
CONDUCTIVITY OF THE EARTH'S UPPER MANTLE AS  
ESTIMATED FROM SATELLITE MEASURED MAGNETIC  
FIELD VARIATIONS Ph.D. Thesis (Johns  
Hopkins Univ.) 174 p HC A08/MF A01 CSCL 08G G3/46

N81-17648

Unclas  
41419



## ABSTRACT

The electrical conductivity of the upper mantle is estimated from low latitude magnetic field variations (magnetic storms) caused by large fluctuations in the equatorial ring current. The data base is derived from satellite magnetic field measurements which offer better global coverage than land based observatories.

The procedures of analysis consist of i) separation of the disturbance field into internal and external parts relative to the surface of the earth, ii) estimation of a response function " $Q(\omega)$ " which relates the internally generated magnetic field variations to the external variations due to the ring current, and iii) interpretation of the estimated response function using theoretical response functions for known conductivity profiles. Special consideration is given to possible ocean effects.

Magnetic field variations are derived from magnetic field magnitude data measured by satellites Ogo 2,4, and 6 which collected data from October, 1965 to July, 1971. Flying nearly polar orbits, these satellites sampled the field every  $\frac{1}{2}$  minute over an altitude range of 400 km to 1500 km (Cain and Langel, 1971; Langel, 1974).

Best estimates of the response function  $Q(\omega)$  were obtained using stacked, smoothed power spectra from eight storms. The frequency range for these smoothed estimates is from 0.2 cycles/day to

2.0 cycles/day. Also, to examine a possible source of noise in the data, a model of the crustal anomaly field (model by Mayhew, 1980) was removed from the magnetic field data and a "corrected" Q was calculated. Although the corrected Q differed slightly from the original Q for individual storms, the stacked corrected Q did not differ from the uncorrected stacked results. It is concluded that within the reliability limits of the data, the anomaly field has no significant contribution.

Using a finite difference algorithm, a theoretical  $Q(\omega)$  is calculated for a given conductivity profile. Matching a theoretical Q to the measured Q implies a model where most of the upper mantle has a conductivity of order  $10^{-2}$  mho/m. This value agrees with Banks' (1972) model but differs from Parker's (1970) value of order  $10^{-1}$  mho/m. Considering the high temperatures implied by Parker's model, geochemical and petrological evidence favors the  $10^{-2}$  mho/m mantle.

Since the frequency range (.2 to 2. cpd) extends beyond that used by Banks and Parker, considerations were made for possible ocean effects. Representing the top 3 km of the earth with a shell of conductivity equal to a weighted sum of oceanic and continental conductivities, the ocean effect did not appear in our frequency range until the continental conductivity was raised to  $10^{-2}$  mho/m -- this sets an upper limit of  $10^{-2}$  mho/m on the top 3 km of crust. Also suggested by the data is a lower crust-upper mantle conductivity of  $10^{-3}$  mho/m, extending downward to 30 km (upper limit).

A temperature profile is proposed using conductivity-temperature data for single crystal olivine ( $\sim\text{Fo}_{90}$ ) (Duba, 1976). The resulting temperature profile is reasonable for depths below 150-200 km, but is too high for shallower depths. Apparently, conductivity is not controlled solely by olivine at shallow depths.

As a new application of satellite data, the results are most promising. Reliability of the estimates of  $Q(\omega)$  will be greatly improved if more data sets are stacked.

## PREFACE

My introduction to this rather exotic genre of satellite application came about during my summer employment at NASA- Goddard Space Flight Center in 1974. With the encouragement of Robert Langel, I played various fun and games with the Ogo 2, 4, and 6 satellite data sets. Later, while attending graduate school at Johns Hopkins University, I continued my research into the global induction problem using satellite data. As with any new approach -- and satellite data has problems unique onto itself -- there were many difficulties. There are numerous people that I would like to thank for their help and encouragement. The following are people that I particularly would like to thank.

Professor Bruce Marsh, my advisor, has put up with alot (and vice versa) . I am very grateful for his help and support over the years.

Professor Peter Olson, also my advisor, has endeavored to keep me to the "straight and narrow",scientifically speaking. I appreciate his help.

Frances Fisher not only helped my sanity with a few piano lessons, but also encouraged me to write chapters I through V in English rather than "pigeon computerese".

Jens Pedersen (formerly of Brown University) and Professor Jack Hermance (Brown University) enlightened me on a number of

statistical and data reduction techniques. They gave a great deal of assistance and are probably still wondering how they got roped into it.

Maxene Mote typed most of this thesis and offered valuable advice on how to put it together. Maxene also gave a great deal of moral support.

Finally, I thank my "cheering section" -- Elvera Mitchell, Mingo and Chief, and my mother.

This research was generously supported by NASA, grants NSG5269 and NCC5-18.

## TABLE OF CONTENTS

Chapter I: Introduction .....	1-8
Chapter II: Sources of Magnetic Variations .....	9-16
Chapter III: Data .....	17-23
Chapter IV: Data Reduction and Analysis .....	24-49
Chapter V: Interpretation of the Estimated Response	
Function Q .....	50-101
Chapter VI: Temperature in the Mantle .....	102-130
Chapter VII: Conclusion .....	131-132
Appendix A: Polar Orbit .....	133-134
Appendix B: Main program for finding $e(t)$ and $i(t)$ .....	135-141
Appendix C: Data reduction programs for estimating $\hat{Q}(\omega)$ ..	142-148
Appendix D: Programs for calculating $Q(\omega)$ .....	149-158
Appendix E: Glossary of Symbols .....	159-162

TABLE OF ILLUSTRATIONS

Fig. 1.1: Banks' 1972 conductivity profile.....5-6

Fig. 1.2: Parker's 1970 conductivity profile.....5-6

Fig. 2.1: The earth's magnetosphere and ionosphere.....11-12

Fig. 3.1: Field separation into external (E(t)) and internal (I(t))  
for March 5, 1970 magnetic storm.....22-23

Fig. 4.1: Response function estimates for the March 5, 1970  
magnetic storm.....29-32

Fig. 4.2: Response function for stacked data listed in  
Table 3.1.....33-36

Fig. 4.3: Response function for stacked data of Table 3.1  
with  $\gamma_{12}^2 \geq .6$  .....37-40

Fig. 4.4: Response function for September 29, 1969 magnetic  
storm with anomaly correction.....42-45

Fig. 4.5: Response function for September 29, 1969 magnetic  
storm without anomaly correction.....46-49

Fig. 5.1: Parker's 1970 model compared to homogeneous sphere  
of 0.1 mho/m .....59-62

Fig. 5.2: Banks' 1972 model compared to homogeneous sphere  
of .01 mho/m .....64-67

Fig. 5.3: Response functions of homogeneous sphere of  
varying conductivity .....68-71

Fig. 5.4: Comparison of best estimate of response function to  
those of homogeneous spheres.....73-76

Fig. 5.5: Banks' 1972 conductivity profile as used in this study .....	77-84
Fig. 5.6: Comparison of estimated magnitudes to calculated magnitudes for Banks' profile with and without 30 km surface layer of .001 mho/m .....	87-88
Fig. 5.7: Effects of variation of second layer from .01 to .02 mho/m (boundary at 500 km).....	89-92
Fig. 5.8: Effects of variation of second layer thickness.....	93-96
Fig. 5.9: Effects of variation of second layer from .01 to .02 mho/m (boundary at 350 km).....	97-98
Fig. 5.10: Conductivity profile for estimated response function.....	100-101
Fig. 6.1: Band scheme for an intrinsic semiconductor.....	103-104
Fig. 6.2: Resistivity vs. 1/T for germanium doped with gallium .....	105-106
Fig. 6.3: P-T diagram for the reaction $En + Mag = Fo + CO_2$ .....	109-110
Fig. 6.4: Stability field of $Fo_{90}$ with respect to $f_{O_2}$ and $f_{O_2}$ region for conductivity measurements.....	112-113
Fig. 6.5: Variation of conductivity with temperature for single crystal olivine.....	115-116
Fig. 6.6: Electrical conductivity as a function of temperature with controlled $f_{O_2}$ for basalt.....	117-118
Fig. 6.7: Oxygen fugacity calculations for basalt .....	120-121

Fig. 6.8: Temperature profiles estimated from response function  
Q .....122-123

Fig. 6.9: Geotherm estimates based on detailed compositional  
analysis of lherzolite nodules from kimberlites...125-126

Fig. 6.10: Comparison of "Q" geotherm to pyroxene geotherm  
of Boyd and Nixon .....127-128

Fig. 6.11: Expected electrical conductivities for the top  
250 km assuming pyroxene geotherm.....129-130

TABLES

Table 3.1: Data: Magnetic storm dates and local times.....19

## CHAPTER I: INTRODUCTION

This thesis concerns the earth's electrical conductivity as determined from low latitude magnetic field variations (magnetic storms) caused by large fluctuations in the equatorial ring current. Using satellite observations of these magnetic field variations, information about the electrical conductivity structure and the associated temperature profile can be obtained.

The procedures of analysis consist of i) separation of the disturbance field into internal and external parts relative to the surface of the earth, ii) estimation of a response function "Q( $\omega$ )" which relates the internally generated magnetic field variations to the external variations due to the ring current, and iii) interpretation of the estimated response function using theoretical response functions for known conductivity profiles. Special consideration is given to possible ocean effects.

### I.1 Previous investigations.

In 1889, Schuster used observations of the diurnal (Sq) magnetic variations to infer the general conductivity structure of the earth. Using Gauss's spherical harmonic representation of magnetic scales potential

$$U = a \sum_{\ell, m} [i_{\ell}^m \left(\frac{a}{r}\right)^{\ell+1} + e_{\ell}^m \left(\frac{r}{a}\right)^{\ell}] P_{\ell}^m(\theta, \phi) \quad (1.1)$$

where  $a$  is the radius of the earth,  $r$  is the radial distance of the observer,  $i_{\ell}^m$  is the internal source coefficient and  $e_{\ell}^m$  is the external source coefficient for spherical harmonic  $P_{\ell}^m(\theta, \phi)$  of degree  $\ell$  and

order m, Schuster estimated  $i_{\ell}^m$  and  $e_{\ell}^m$  and concluded that the earth could be represented by an equivalent conducting sphere with a smaller radius than the Earth's. Chapman (1919) improved upon Schuster's analysis and concluded that the equivalent sphere has a conductivity of  $3. \times 10^{-2}$  mho/m and a radius of 250 km less than that of the earth.

Chapman and Price (1930) also studied diurnal variations and obtained estimates of electrical conductivity compatible with Chapman's (1919) earlier estimates. However, in their study of a non-periodic phenomenon, namely magnetic storms, they found a significantly higher conductivity estimate of about  $4. \times 10^{-1}$  mho/m. This higher conductivity estimate was taken as an indication of a non-uniform conductivity structure.

Lahiri and Price (1939) further developed the theory for non-uniform conductors and obtained results which supported Chapman and Price's view that an increase in conductivity existed at a depth of 250 km. They also concluded that an additional large increase in conductivity (one to two orders of magnitude) exists at a depth of 700 km. Their results indicated an enhanced conductivity near the surface of the earth, which they attributed to the oceans.

To improve the resolution of the electrical conductivity structure, analysis of more magnetic variations of differing frequencies was needed. Intuitively, this becomes apparent when one considers the electromagnetic skin depth,  $\delta = (2/\omega\sigma\mu)^{1/2}$ , which is inversely proportional to frequency  $\omega$ , conductivity  $\sigma$  and magnetic permeability  $\mu$ . To obtain resolution near the surface of the earth,

one needs magnetic variations with small skin depths. These have high frequency components which are attenuated before reaching far into the interior. To probe deeper into the earth, the magnetic variations must have larger skin depths and therefore lower frequency components so they can reach the interior before they are greatly attenuated. Theoretically, a necessary condition for obtaining a unique model of the earth's conductivity structure is that magnetic variations with an infinite range of frequencies must be sampled (Bailey, 1970).

However, an infinite frequency range of magnetic variations is not available for induction studies. At the low frequency end, below  $10^{-3}$  cpd (cycles per day) the geomagnetic spectrum is dominated by "secular" variations originating internally at the core-mantle boundary. At the high frequency end, above 0.25 cpd, lack of global coverage along with possible lateral variations in the upper 400 km of the earth hinders application of induction theory (Anderson, et al., 1979).

Not until the application of cross-spectral analysis techniques (Banks, 1969, 1972) could the intervening continuum as well as some major peaks associated with periodic phenomena (i.e. "Sq") be included in induction studies. Using Gauss's potential field representation (eqn. 1.1), Banks separated the observed magnetic variations into internal and external origin. He then defined a frequency response function  $Q_{\ell}^m(\omega)$  by

$$Q_{\ell}^m(\omega) = \frac{I_{\ell}^m(\omega)}{E_{\ell}^m(\omega)} \quad (1.2)$$

where  $I_{\ell}^m(\omega)$  and  $E_{\ell}^m(\omega)$  are the frequency spectra for the internal and external coefficients of degree  $\ell$  and order  $m$  in eqn. 1.1. Using standard cross-spectral techniques (Blackman and Tukey, 1958), Banks estimated the response function (mainly  $Q_1^0(\omega)$  harmonic) and conducted a Monte Carlo search for the most compatible conducting profile (fig. 1.1).

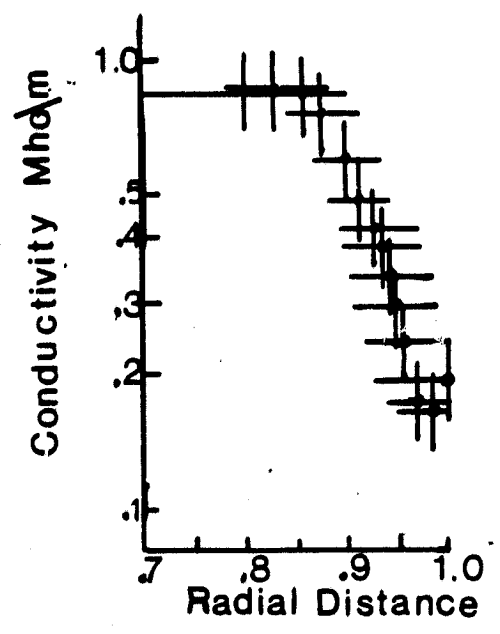
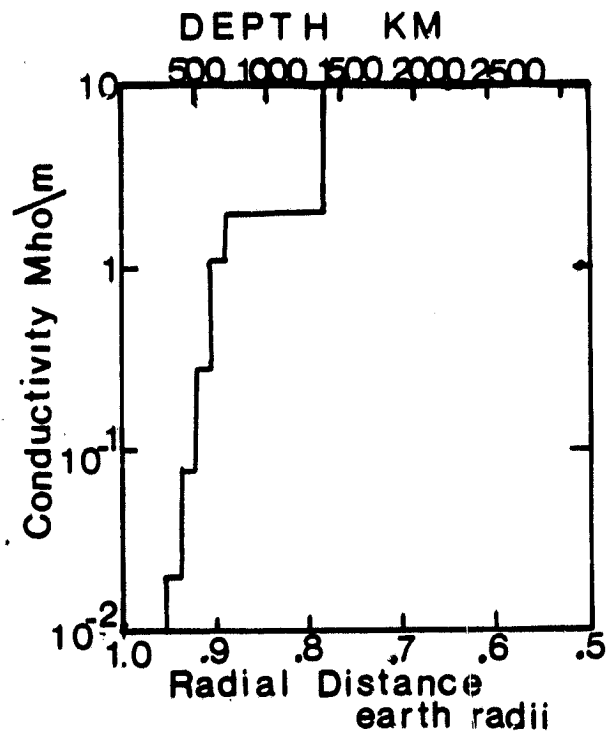
Banks' estimate of  $Q_1^0(\omega)$  and his resulting conductivity profile are based on his analysis of magnetic variations of frequencies 0.003 cpd to 0.25 cpd. For frequencies above 0.25, estimates of  $Q_1^0(\omega)$  had nonphysical, negative phases. He attributed this lack of reliability for high frequency estimates to lack of global coverage and/or lateral variations in the upper mantle and crust.

Using Banks' data, Parker (1970) suggested another conductivity profile. Parker obtained this profile (fig. 1.2) by applying inverse theory after the fashion of Backus and Gilbert. As compared to Banks' original 1969 model, Parker's model confirms the sharp rise in conductivity at 400 km but differs in its near surface value: near 0.1 mho/m as opposed to Banks' figure of  $10^{-2}$  mho/m.

In the models thus far presented, existence of the oceans is not considered. Since the high frequency estimates of  $Q_1^0(\omega)$ , near 0.25 cpd, is from the zonal (local time independent) part of magnetic storm variations, 'Dst,' which is assumed to have only  $P_1^0$  component (eqn. 1.1), the effect of oceans are considered unimportant for Dst variations (Lahiri and Price, 1939). For Sq variations (1 cpd and harmonics) which have higher harmonic components, the oceans probably

Figure 1.1: Banks' 1972 conductivity profile. (J. Geomag.  
Geoelectr., 24, 337-351, 1972)

Figure 1.2: Parker's 1970 conductivity profile. (Geophys. J.  
R. astr. Soc. (1970) 22, 121-138)



ORIGINAL FILED  
C7 P001 QUALITY

have a significant effect (Lahiri and Price, 1939; Bullard and Parker, 1970; Banks, 1972, Jady, 1974a,b). Banks (1972) later reworked his data to include  $S_q$  variations, but he does not include a layer for ocean conductivity. Ocean effects are usually included in local studies only. More discussion of ocean effects will be presented in chapter V.

As noted earlier, the low frequency end of the geomagnetic spectrum is dominated by "secular variations." Since these variations are of purely internal origin, induction methods used in the studies already described are not appropriate. However, secular variations still can yield information about the earth's deep interior.

In a method developed by McDonald (1957), the attenuation behavior of a sinusoidal magnetic variation originating at the core-mantle boundary is used as an indicator of lower mantle conductivity. Assuming spherical symmetry and a power law function for conductivity, McDonald calculates ratios of attenuation functions of differing harmonic degree as would be observed at the earth's surface for different conductivity structures. Comparing these predicted ratios to those obtained from spherical harmonic representation of observed secular variations, McDonald inferred a conductivity profile with the lower mantle conductivity of  $10^2$  mho/m.

As McDonald's work estimates the conductivity of the lower mantle, local magnetotelluric studies estimate crustal conductivities. Local measurements show the first few kilometers of the earth may be fairly conductive, typically 0.01 to 0.1 mho/m while the underlying rock may be as low as  $10^{-4}$  mho/m (Gough, 1973). Sea water varies in

conductivity according to temperature and salinity, but typically is 3.3 mho/m.

The global coverage essential to conductivity studies of the upper 400 km of the earth can be provided by satellite observations.

## CHAPTER II: SOURCES OF MAGNETIC VARIATIONS

Part of the objective of this study is to estimate a response function (eqn. 1.2) relating the time-varying magnetic field external to a conductor to that generated internally. Chapman (1919) concluded that this "conduction" was within the earth and that the upper 250 km and the surrounding space were nonconductors. Later investigations concluded that the upper 250 km did have significant conductivity and the boundary between conductor and nonconductor became the earth's surface. In this study, the boundary shall be the surface of the earth. This is a valid assumption if there are no electric currents (hence, no conductors) between the satellite and the surface of the earth. Ionospheric currents do exist between the satellite and the earth surface, but these will be demonstrated to be unimportant in this study.

Another assumption in this study is that the equatorial ring current, represented by a  $P_1^0$  harmonic magnetic variation, is the sole source of external magnetic field variations. This implies that the observed magnetic variations of internal origin are due only to induction effects from the ring current. This assumption is valid if other current systems in the ionosphere and magnetosphere and their induced fields are accounted for.

To examine the validity of these assumptions, we shall consider the various electric current systems with regard to the position of the satellite. The trajectories of satellites Ogo-2, 4, and 6 place them in a polar orbit with altitudes varying 400 km to 1500 km. This

orbit situates the satellite above the denser regions of the ionosphere and well inside the magnetosphere.

In the following section, electric current systems will be presented as "external" or "internal" to the satellite's orbit.

### II.1 External current systems.

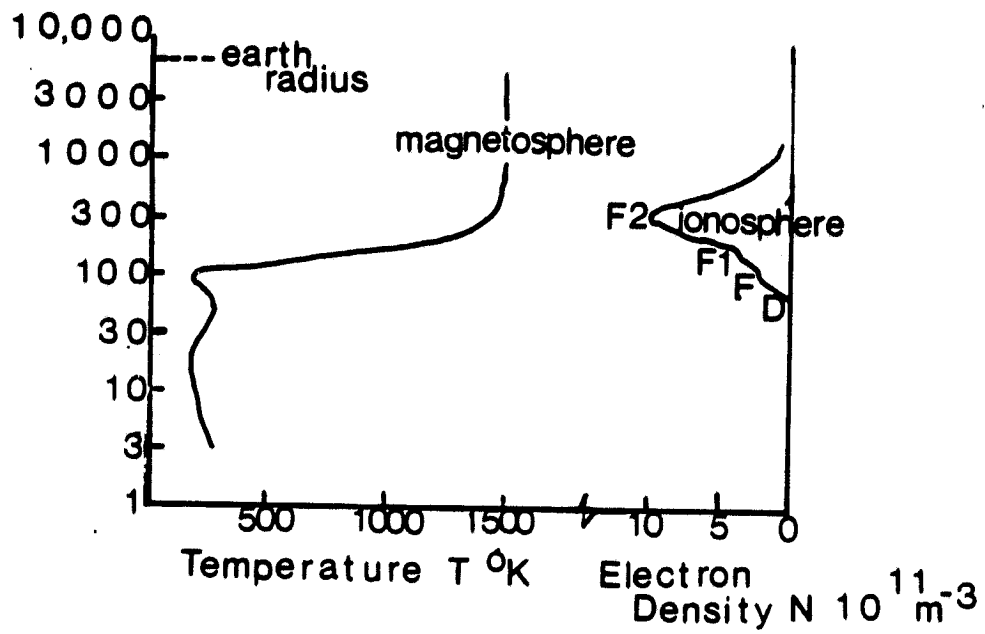
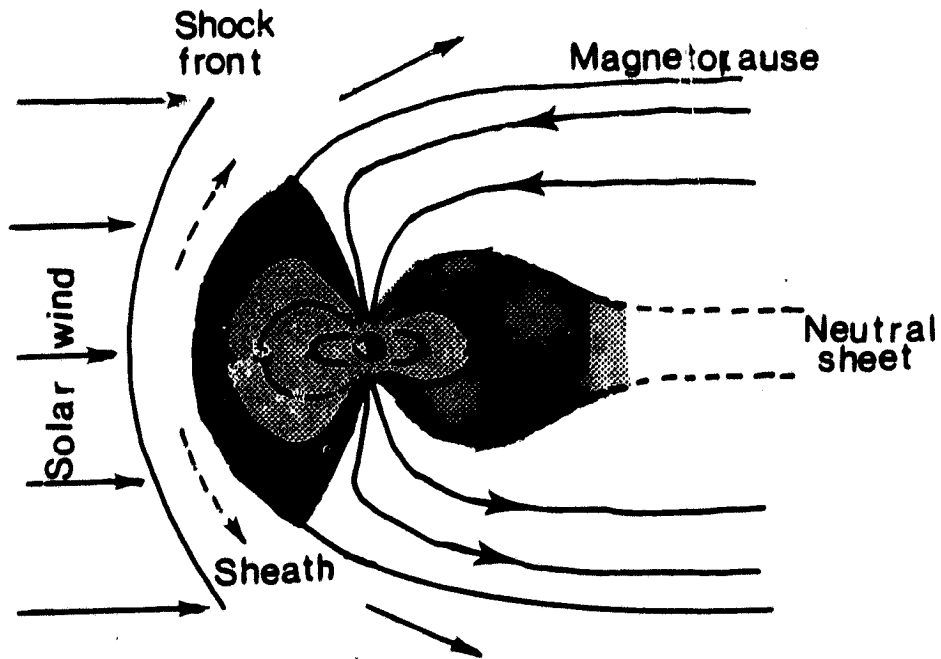
The equatorial ring current and its associated magnetic variations provides the source field for this study. Represented approximately by a toroidal current flow, its influence on magnetic field variations during magnetic storms is fairly uniform over the mid- and low latitudes of the earth. However, as the earth's magnetic field is distorted towards the sunward side, the ring current is also asymmetric in shape with respect to the sun. This causes a slight local time dependence for these variations. As for location, its inner boundary is generally located at a distance greater than 3 earth radii from the earth, though occasionally it will extend into the upper ionosphere (fig. 2.1). In any case, it is located well outside of the orbits of the satellites.

From a long tradition in characterizing land observatory data, the magnetic disturbance field "D" is expressed in terms of an axially symmetric part "Dst" and a longitudinal or local time dependent part "DS." Dst or "storm time variation" is the average value of the change in the horizontal component of the disturbance field measured along the equator. This is the principal influence of the equatorial ring current for low and mid-latitudes. DS or "disturbance local-time inequality" is the variation in D which depends on local time (Rishbeth

Figure 2.1: (a) The earth's magnetosphere as viewed from the equatorial plane.

(b) Location of the ionosphere in the atmosphere.

(Rishbeth and Garriott, Introduction to Ionospheric Physics, Academic Press, New York, 1969)



and Garriott, 1969).

$$D = \text{Dst}(t) + DS$$

where

(2.1)

$$DS = \sum_n \tilde{C}_n \sin(n\lambda + \tilde{E}_n)$$

$t$  is universal time,  $\lambda$  is longitude (relative to the sun), and  $\tilde{C}_n$  and  $\tilde{E}_n$  are the series coefficients. For studies using land observatory data, the DS component of the variation must be removed before analysis of the ring current variation can be made.

However, with satellite observations, the trajectories are such that measurements over the mid- and low latitudes are at a constant local time. Hence, the disturbance field is measured at a constant local time over successive orbits (see Ch. III) and local time variations need not be removed. Unlike land observatories, the satellite is constantly changing in latitude " $\theta$ ", so different sources of magnetic variations are measured. This is particularly true in the polar regions of the earth.

Current systems in the auroral zones are exceptionally active during magnetic disturbances. During such times, charged particles from the upper ionosphere and magnetosphere are absorbed in the polar regions of the earth. These charged particles contribute to the "polar electrojet" and other related current systems causing increased magnetic variations in the high latitudes. Current systems associated with auroral phenomena are more complicated in geometry and in temporal behavior than the equatorial ring current. They also involve regions of space both above and below the orbits of the satellites

and hence are not suitable for induction studies, at least not in the manner presented here. Therefore, the best way to deal with polar current systems is to exclude magnetic data taken in the higher latitudes.

## II.2 Internal currents.

The electric currents induced within the earth by the magnetic variations due to the ring current are the currents of interest in this study. However, other currents exist in the earth and in the intervening ionosphere between the earth and the satellite.

The daytime ionospheric current systems originate in the "E-layer" of the ionosphere at altitude ranges of 90-130 km. During the course of a day, the tidal effects of the sun (and moon) produce electric currents in the ionosphere. This "Sq" system causes the diurnal variations observed in daily magnetic records with its peak disturbance at local noon. Sq variations also induce electric currents within the earth and oceans that contribute roughly one-third to the total observed magnetic variation attributed to Sq (Rishbeth and Garriott, 1969).

The geometry of the Sq current system is very complicated and, when given a spherical harmonic representation, requires several degrees of spherical harmonics. The currents induced in the earth, particularly in the oceans, also are complicated in shape. In their study of ocean effects, Bullard and Parker (1970) have analysed the effect of Sq variations induced within the oceans. Because of the ocean shapes and the insulating effects of the continents, the main influence of Sq is in harmonics higher than  $P_1^0$ .

Sq is associated not only with the tidal effects of the sun, but also with the density of free electrons in the ionosphere; the degree of ionization and, therefore, the magnetic variations due to Sq are local-time dependent (contribute to DS in equation 2.1), and are at a minimum near local midnight.

Sometimes considered part of the Sq system is the "equatorial electrojet." This current flows eastward along the dipole equator during the day, causing large magnetic variations at equatorial land observatories. A return current flows at night, but the effect is much less intense than during the day.

These "quiet day variations," Sq, L (lunar variations), and the equatorial electrojet, occur every day and are periodic in nature. They are easily detected by land observatories. Their effects on the data can be minimized by applying a one-cycle/day filter to the data or by simply considering data at one local time, particularly at night.

During magnetic disturbances, additional currents appear or are enhanced in the ionosphere; in the polar regions, current systems associated with increased auroral activity are stimulated. Higher electron densities appear in the E-layer, principally in the high latitudes. Other currents are induced in lower latitudes, but these are strongly local-time dependent because of solar effects on ionization. It then follows that DS variations from ionospheric currents are minimized during the night for the low and mid-latitudes; in the polar regions where particle absorption from the upper ionosphere and the magnetosphere takes place, magnetic variations can be active in nighttime as well as the daytime.

The  $P_1^0$  magnetic variations due to the ring current induce currents within the ionosphere. However, the integrated conductivities for the ionosphere, measured over hundreds of kilometers, vary from 10 to 1,000 mhos (dependent on direction of integration) and therefore imply a very low conductance with regard to this study. Induction effects in the ionosphere will be essentially noise in the data.

As for induction in the ocean from ring current fluctuations, the  $P_1^0$  currents should be much less than the  $P_2^1$  and  $P_3^2$  currents associated with Sq. This reduced effect is because of the insulating influence of the continents on a current that would have to flow around the equatorial regions of the earth. The ocean effect is further discussed in Chapter V.

## CHAPTER III: DATA

III.1 Data collection.

The magnitude of the magnetic field was measured by satellites Ogo-2, 4, and 6 which collected data from October, 1965 to July, 1971. Flying nearly polar orbits, these satellites sampled the field every 1/2 minute over an altitude range of 400 km to 1500 km (Cain and Langel, 1971; Langel, 1974). These magnetic field measurements were made by a rubidium vapor magnetometer with an accuracy of 6 gammas ( $10^{-5}$  gauss =  $10^{-9}$  tesla.).

With each orbit taking approximately 90 minutes, the flight path from pole to pole essentially followed a longitudinal line. Since it took about 20 minutes to fly between  $-50^{\circ}$  to  $+50^{\circ}$  latitude, measurements at mid- and low latitudes were made at a constant local time (relative position of the sun). During the course of one orbit, the satellite crossed the equator twice and hence can be characterized by two local times corresponding to the two equatorial crossings. Over a period of a few days, these local times for equatorial crossings remain almost constant.

Data types for these satellites included geographic longitude and latitude, geomagnetic latitude, local time, universal time, and altitude for each data point. This arrangement allows for easy elimination of data collected over the polar regions. It also allows for selection of data at particular local times.

### III.2 Data selection.

In studying magnetic field variations associated with fluctuations in the equatorial ring current, one needs data drawn from periods of large magnetic disturbances. Such data are here defined as having negative deviations in magnetic field magnitude greater than 50 gammas as compared to normal daily variations.

Further selection of data was based on local time. Since the satellite orbit is characterized by two local times which remain constant over a few days, one has the option of selecting only that data which corresponds to one local time. Since the field fluctuations due to the ring current have a local time dependence, only data from one local time can be used. Furthermore, the nighttime data has been selected in order to minimize the effects of ionization currents.

The data and local times for data used in this study are presented in Table 3.1.

### III.3 Field separation into internal and external coefficients.

For each data set listed in Tables 3.1, two time series  $e(t_n)$  and  $i(t_n)$  are extracted from the satellite data. These time series correspond to the external coefficient " $e_1^0$ " and internal coefficient " $i_1^0$ " of a harmonic representation of the scalar potential for disturbance field  $\bar{D}$

$$\bar{D} = -\nabla U$$

$$U = a(e_1^0 \left(\frac{r}{a}\right) + i_1^0 \left(\frac{a}{r}\right)^2) P_1^0(\cos \theta) \quad (3.1)$$

TABLE 3.1: DATA

<u>Date</u>	<u>Modified Julian Date</u>	<u>Local Time (Hrs.)</u>
March 5, 1970	40650-40657	19.50
July 26, 1969	40428-40430	0.50
*April 21, 1970	40697-40698	1.75
June 11, 1968	40018-40022	23.00
December 31, 1967	39855-39860	15.75
October 30, 1968	40159-40165	21.00
February 8, 1968	39894-39900	23.00
September 29, 1969	40493-40498	16.25
†March 22, 1966	39206-39209	15.75

\* included only in stacked data with anomaly correction.

† included only in stacked date without anomaly correction.

where  $a$  is the radius of the earth,  $r$  is the radial distance of the observer,  $\theta$  is the colatitude and  $P_1^0(\cos \theta)$  is the spherical harmonic of degree 1 and order 0. During the course of the magnetic disturbance, the coefficients  $e_1^0$  and  $i_1^0$  change with universal time  $t$ , so the time series for  $e_1^0$  and  $i_1^0$  can be defined.

To identify these time series, the disturbance field  $\bar{D}$  must be extracted from the observed field magnitude data  $|\bar{B}^0|$ . This is done by defining an observed change in total field, " $\Delta B^0$ " by

$$\Delta B^0 = |\bar{B}^0| - |\bar{B}^m| \quad (3.2)$$

where  $|\bar{B}^m|$  corresponds to the quiet day field represented by a field model of degree 12 (Langel, 1974). A theoretical  $\Delta B^t$ , which includes disturbance field  $\bar{D}$ ,

$$\Delta B^t = |\bar{B}^m + \bar{D}| - |\bar{B}^m| \quad (3.3)$$

is then fitted to the observed  $\Delta B^0$ . Since  $\bar{D}$  varies with colatitude  $\theta$ , this fit is performed for data points between  $-50^\circ$  to  $50^\circ$  for each orbit. This results in one estimate of  $e_1^0$  and  $i_1^0$  per orbit. When data is considered for the whole magnetic storm, each  $e_1^0$  and  $i_1^0$  is estimated at a different universal time  $t$ , defined to be the time of crossing the geomagnetic equator.

The resulting time series  $e(t_n)$  and  $i(t_n)$  are equally spaced in time by approximately 90 minutes and have a total period equal to the duration of the storm.

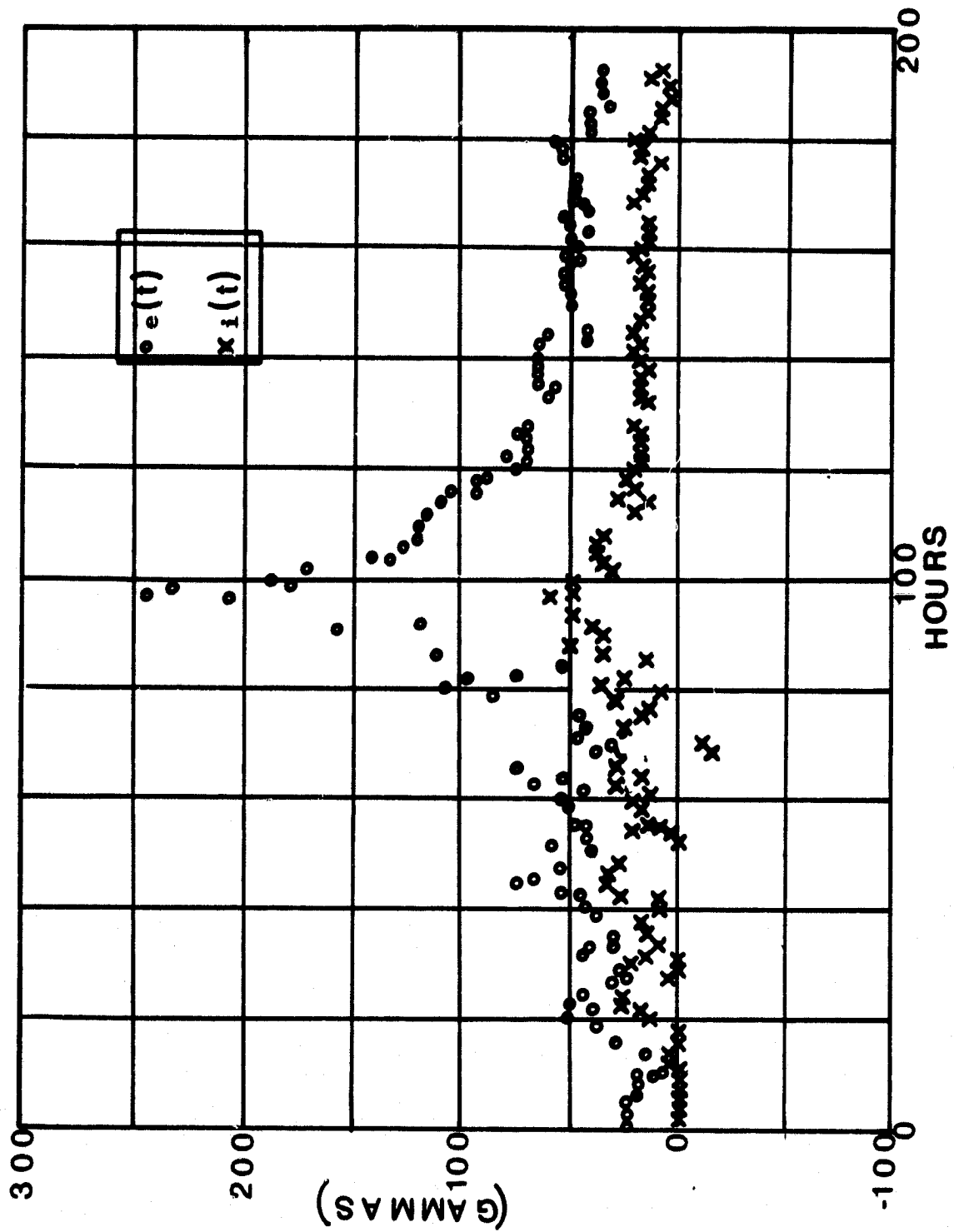
This  $e(t_n)$  and  $i(t_n)$  analysis is a slightly different approach than that applied to land observatory data. Since observations on land vary with local time, the DS part of the disturbance field is

subtracted from the observations--only Dst is used for magnetic storm analysis. In this satellite data, local time is constant, so the analysis includes more than just Dst.

An example of a field separation for the strong magnetic disturbance of March 5-9, 1970 is presented in fig. 3.1.

A possible source of error in this field separation is the crustal anomaly field. To explore this effect, a field model (courtesy of Mike Mayhew, 1980) is subtracted from the total field measurements before the field separation is performed. This anomaly field proved to have small effect on large magnetic disturbances and on stacked data (see Ch. IV), but has some effect on field separation for weaker magnetic disturbances.

Figure 3.1: Field separation into external ( $e(t)$ ) and Internal ( $i(t)$ ) parts for March 5, 1970 magnetic storm.



ORIGINAL PAGE 1  
OF POOR QUALITY

## CHAPTER IV: DATA REDUCTION AND ANALYSIS

The magnetic field data measured by the satellites are expressed in terms of two time series  $e(t_n)$  and  $i(t_n)$ ,  $n = 1, \dots, N$  for each magnetic disturbance observed. The external field variation represented by  $e(t_n)$  is the "input" and the internal field variation represented by  $i(t_n)$  is the "output" for the linear system

$$i(t) = q(t) * e(t) \quad (4.1)$$

where "\*" denotes convolution and "q(t)" is the linear impulse function. This operation can also be represented in the frequency domain by

$$I(\omega) = Q(\omega) E(\omega) \quad (4.2)$$

where  $I(\omega)$  and  $E(\omega)$  are the Fourier transforms of  $i(t)$  and  $e(t)$  and  $Q(\omega)$  is the "frequency response function." To ascertain the conductivity structure of the earth, we first must estimate  $Q(\omega)$ .

From eqn. (4.2), the frequency response function can be defined by

$$Q(\omega) = \frac{I(\omega)}{E(\omega)} \quad (4.3)$$

If the above definition were applied to the original time series  $e(t_n)$  and  $i(t_n)$ ,  $n = 1, \dots, N$ , the resulting estimate of  $Q(\omega_n)$ ,  $n = 1, \dots, N/2$  would have the highest resolution that the data could provide, but the least reliability.

To improve reliability of an estimate of  $Q(\omega)$ , one needs to smooth the data, either in the time domain or the frequency domain. However if one were to smooth the frequency spectra  $I(\omega)$  and  $E(\omega)$  and

then estimate  $Q(\omega)$  with eqn. (4.3), one would have a very biased estimate of  $Q(\omega)$  (Bendat and Piersol, 1971). Instead, a better estimate of  $Q(\omega)$  involves smoothed estimates of the cross-power spectrum  $\hat{C}_{12}(\omega)$  and power spectrum  $\hat{C}_{11}(\omega)$

$$\hat{Q}(\omega) = \frac{\hat{C}_{12}(\omega)}{\hat{C}_{11}(\omega)} \quad (4.4)$$

knowing that the cross-power spectrum can be expressed as

$$C_{12}(\omega) = E^*(\omega) I(\omega) \quad (4.5)$$

where  $*$  denotes complex conjugate, and the power spectrum  $C_{11}(\omega)$  is

$$C_{11}(\omega) = E^*(\omega) E(\omega) \quad (4.6)$$

one can easily see that eqn. (4.4) is an equivalent definition to eqn. (4.3). The difference between the two definitions is in the amount of bias when one smooths in the frequency domain. Eqn. (4.4) will yield a less biased estimate than eqn. (4.3).

To obtain a reliable estimate of  $Q(\omega)$  for each data set listed in Table 3.1, the following procedure as recommended by Bendat and Piersol (1971) was followed:

- 1) preprocess time series  $e(t_n)$  and  $i(t_n)$ ,  $n = 1, \dots, N$ .
- 2) calculate the Fourier transforms of  $e(t_n)$  and  $i(t_n)$
- 3) calculate the raw estimates of the cross-power spectrum  $\hat{C}_{12}(\omega)$  and power spectrum  $\hat{C}_{11}(\omega)$
- 4) smooth the spectra  $\hat{C}_{12}(\omega_i)$  and  $\hat{C}_{11}(\omega_i)$  for frequencies  $\omega_i$ ,  $i = 1, \dots, M$
- 5) estimate  $\hat{Q}(\omega_i)$ ,  $i = 1, \dots, M$ ,  $M < N/2$ .

The preprocessing in step (1) involves removing a linear trend, defined as the line which was tangent to the endpoints of the time series. The resulting time series starts and ends at the zero base line with the maximum well above zero.

The Fourier transforms of  $e(t_n)$  and  $i(t_n)$  are routinely calculated using the fast Fourier transform or FFT algorithm. The resulting spectra have half the number of original data points due to folding around the zero frequency axis.

In step (4) the raw estimates  $\hat{C}_{12}(\omega_n)$  and  $\hat{C}_{11}(\omega_n)$ ,  $n = 1, \dots, N/2$  are made using eqn. (4.4).

Smoothed estimates of  $\hat{C}_{12}(\omega_i)$  and  $\hat{C}_{11}(\omega_i)$  are made for selected frequencies  $\omega_i$ ,  $i = 1, \dots, M$ , where  $M \ll N/2$ . This is to improve the reliability of estimates of  $\hat{Q}(\omega_i)$ .

Finally,  $\hat{Q}(\omega_i)$  is estimated for the selected frequencies  $\omega_i$ ,  $i = 1, \dots, M$ .

The best procedure found for step 4 was one formerly applied to magnetotelluric studies, known as a "constant Q" analysis (Thayer, 1975). After selection of "centered frequencies"  $\omega_i$ ,  $i = 1, \dots, M$ ,  $M < N/2$ , the raw estimates of  $\hat{C}_{12}(\omega_n)$ ,  $\hat{C}_{11}(\omega_n)$  and  $\hat{C}_{22}(\omega_n)$  are smoothed around each frequency  $\omega_i$  using a Gaussian window  $W(\omega_i - \omega_n)$

$$W(\omega_i - \omega_n) = (2\sqrt{\pi}/\omega_i S) \exp(-(\omega_i - \omega_n)^2 / \omega_i^2 S^2) \quad (4.7)$$

where  $S$  is the "selectivity." The selectivity defines the width of the Gaussian windows, which was set at  $S = 0.2$  in this analysis. A "constant Q analysis" is one where the selectivity is held constant for all frequencies  $\omega_i$ . This kind of window smooths less at longer

periods than shorter periods, which is necessary in order to maintain relatively the same resolution at depth as near the surface of the earth. Specific listings of the programs used for this window are given in Thayer (1975).

As noted earlier, smoothing increases the reliability of the estimate. Statistically, it increases the "degrees of freedom" of the estimate at frequency  $\omega_1$ . By increasing the window width, more data points are included in the smoothing and higher degrees of freedom are provided for the estimate. Since the constant Q analysis varies the window width with frequency, the number of degrees of freedom also varies with frequency.

Within the "95% confidence interval" around an estimate of  $\hat{Q}(\omega_1)$ , there is a 95% probability that the true value of  $Q(\omega_1)$  will exist. This confidence interval depends upon the number of degrees of freedom.

For complex number  $\hat{Q}(\omega_1)$ , the confidence interval is defined in terms of a radius  $\hat{r}(\omega_1)$  and a phase range  $\Delta\hat{\phi}(\omega_1)$  where

$$|\hat{Q}(\omega_1)| - \hat{r}(\omega_1) \leq |Q(\omega_1)| \leq |\hat{Q}(\omega_1)| + \hat{r}(\omega_1) \quad (4.8)$$

$$\hat{\phi}(\omega_1) - \Delta\hat{\phi}(\omega_1) \leq \phi(\omega_1) \leq \hat{\phi}(\omega_1) + \Delta\hat{\phi}(\omega_1)$$

where '^' denotes "estimate." These are defined by Bendat and Piersol (1971).

$$\hat{r}^2(\omega_1) = \frac{2}{(n-2)} F_{2,n-2;\alpha} [1 - \hat{\gamma}_{12}^2(\omega_1)] \frac{\hat{C}_{22}(\omega_1)}{\hat{C}_{11}(\omega_1)} \quad (4.9)$$

$$\Delta\hat{\phi}(\omega_1) = \sin^{-1} \left[ \frac{\hat{r}(\omega_1)}{|\hat{Q}(\omega_1)|} \right]$$

where

$n$  = number of degrees of freedom

$F_{2,n-2;\alpha}$  = 100 $\alpha$  percentage point of an F distribution

with  $n_1 = 2$  and  $n_2 = n-2$  degrees of freedom

$\hat{\gamma}_{12}(\omega_1)$  = estimate of the coherency function between  $E(\omega_1)$

and  $I(\omega_1)$  defined by

$$\hat{\gamma}_{12}^2(\omega_1) = \frac{|\hat{C}_{12}(\omega_1)|^2}{\hat{C}_{11}(\omega_1) \hat{C}_{22}(\omega_1)} \leq 1$$

An example of  $|\hat{Q}|$  and  $\hat{Q}$  estimates for March 5-9, 1970 magnetic storm is presented in fig. 4.1a,b.

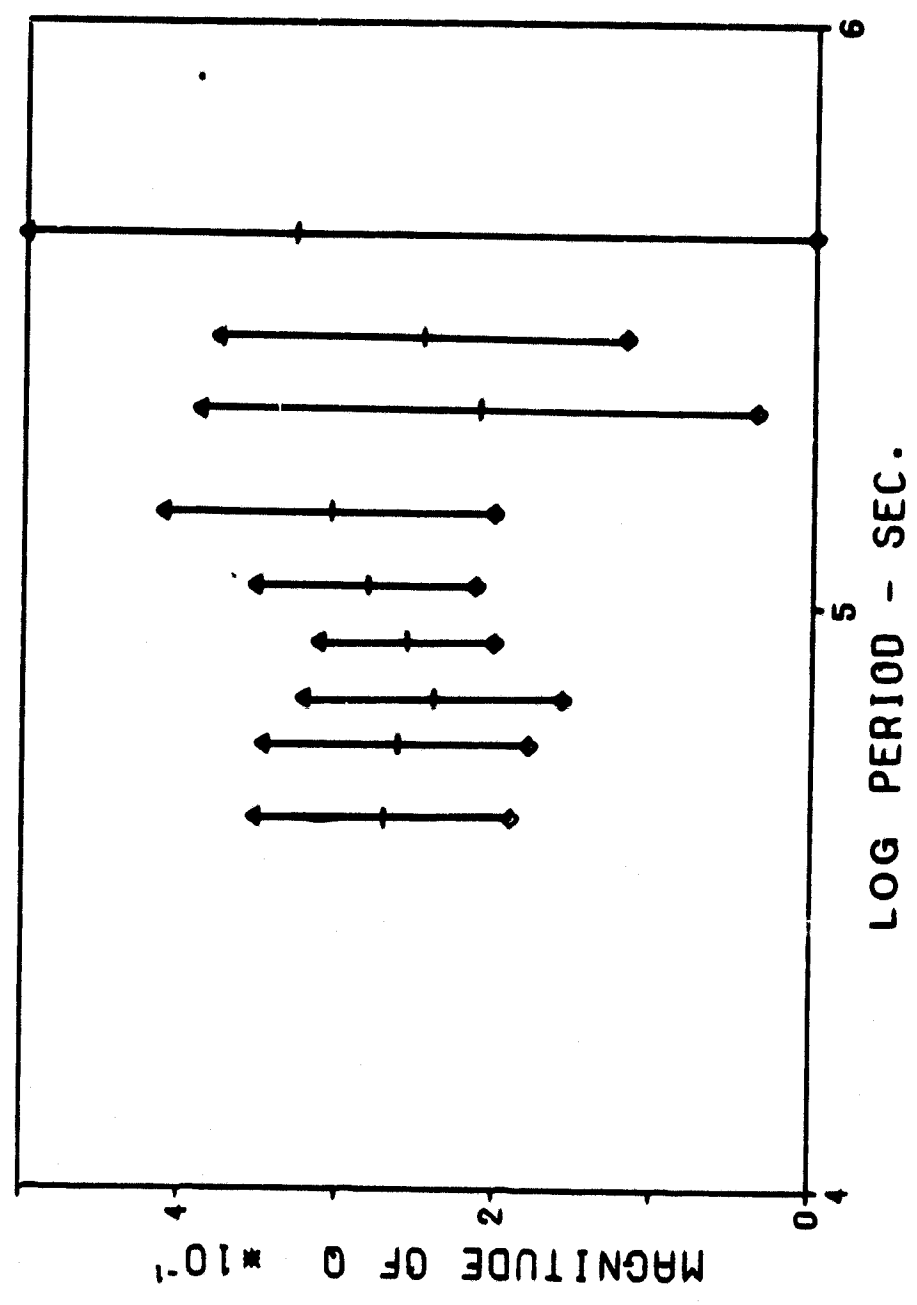
To obtain a better estimate of  $Q(\omega_1)$ , the power spectra of  $\hat{C}_{12}(\omega_1)$  and  $\hat{C}_{11}(\omega_1)$  from several magnetic disturbances were "stacked." Stacking was accomplished by forming a weighted sum of spectra at each frequency  $\omega_1$  from eight data sets listed in Table 3.1. Each spectral estimate of  $\hat{C}_{12}(\omega_1)$  and  $\hat{C}_{11}(\omega_1)$  at frequency  $\omega_1$  for data set  $j$  was weighted with the factor  $n_j(\omega_1) / \sum_j n_j(\omega_1)$  where  $n_j$  is the number of degrees of freedom for that estimate at frequency  $\omega_1$  of data set  $j$ . The results for magnitude and phase are in fig. 4.2a and fig. 4.2b.

To improve the reliability of estimates of  $\hat{Q}$ , power spectra estimates at frequencies  $\omega_1$  which had squared coherencies  $\hat{\gamma}_{12}^2(\omega_1)$  less than 0.60 were eliminated from the stacking procedure. This resulted in estimates of  $\hat{Q}$  which have better reliabilities as shown in fig. 4.3a and fig. 4.3b.

Figure 4.1: Response function estimates for the March 5, 1970  
magnetic storm.

(a) Magnitude of  $\hat{Q}$

MAGNITUDE OF Q VS PERIOD



ORIGINAL PAGE 1  
OF FOUR QUALITY

Figure 4.1: Response function estimates for the March 5, 1970  
magnetic storm.  
(b) Phase of  $\hat{Q}$

PHASE OF Q VS. PERIOD

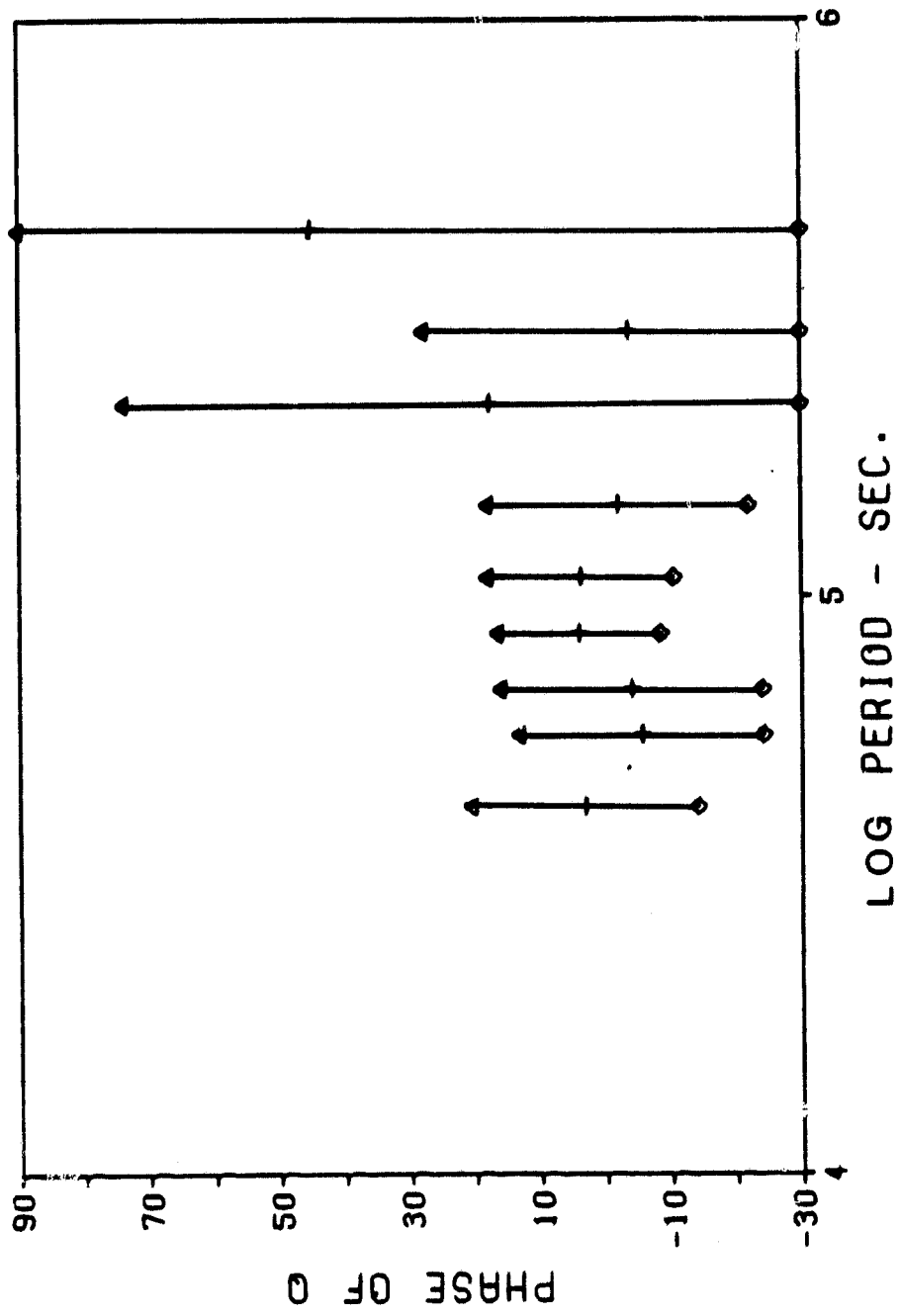


Figure 4.2: Response function for stacked data listed in Table 3.1

(a) Magnitude of  $\hat{Q}$

MAGNITUDE OF Q VS PERIOD

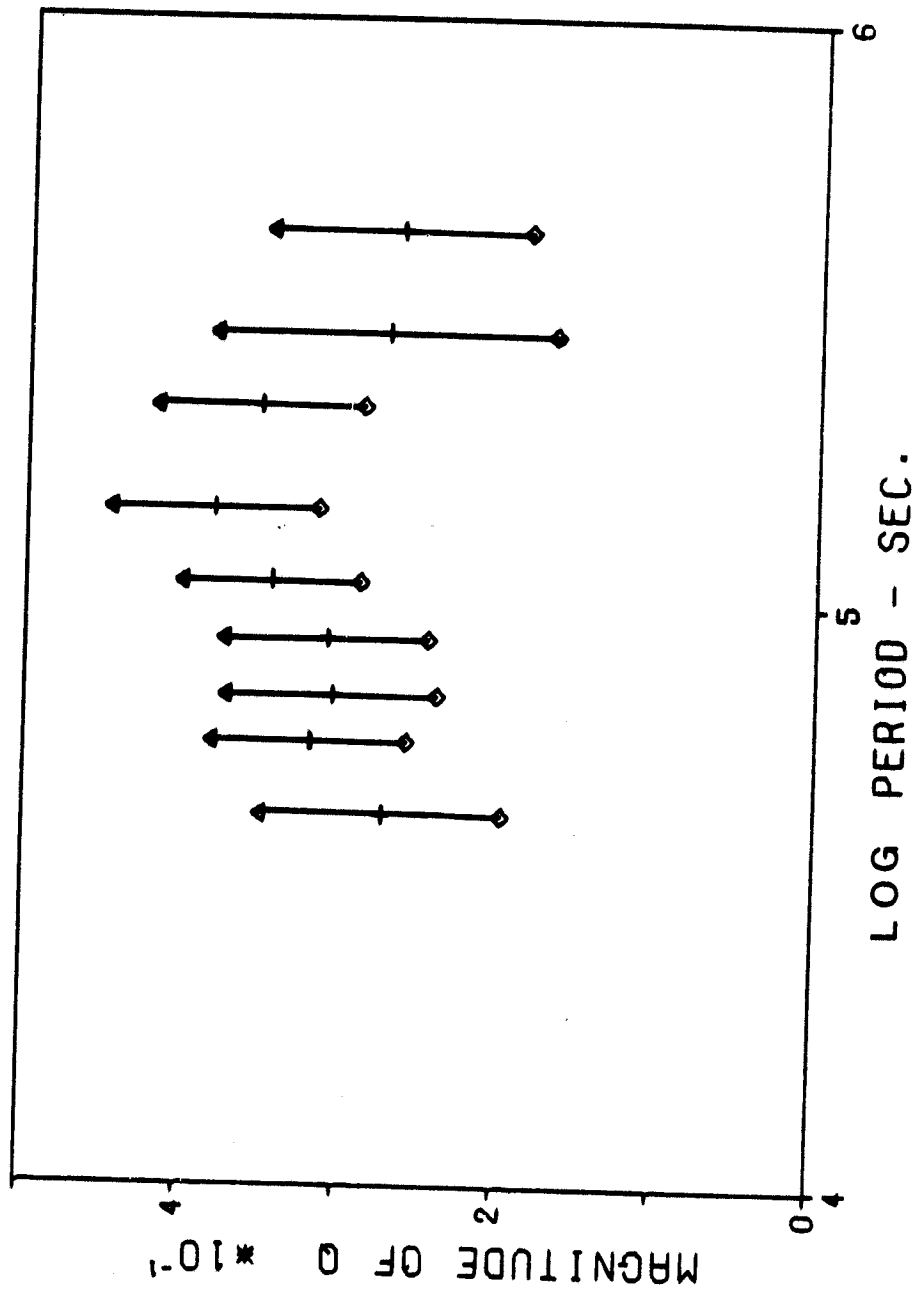
ORIGINAL PAGE IS  
CONTAINED IN

Figure 4.2: Response function for stacked data listed in Table 3.1

(b) Phase of  $\hat{Q}$

PHASE OF Q VS. PERIOD

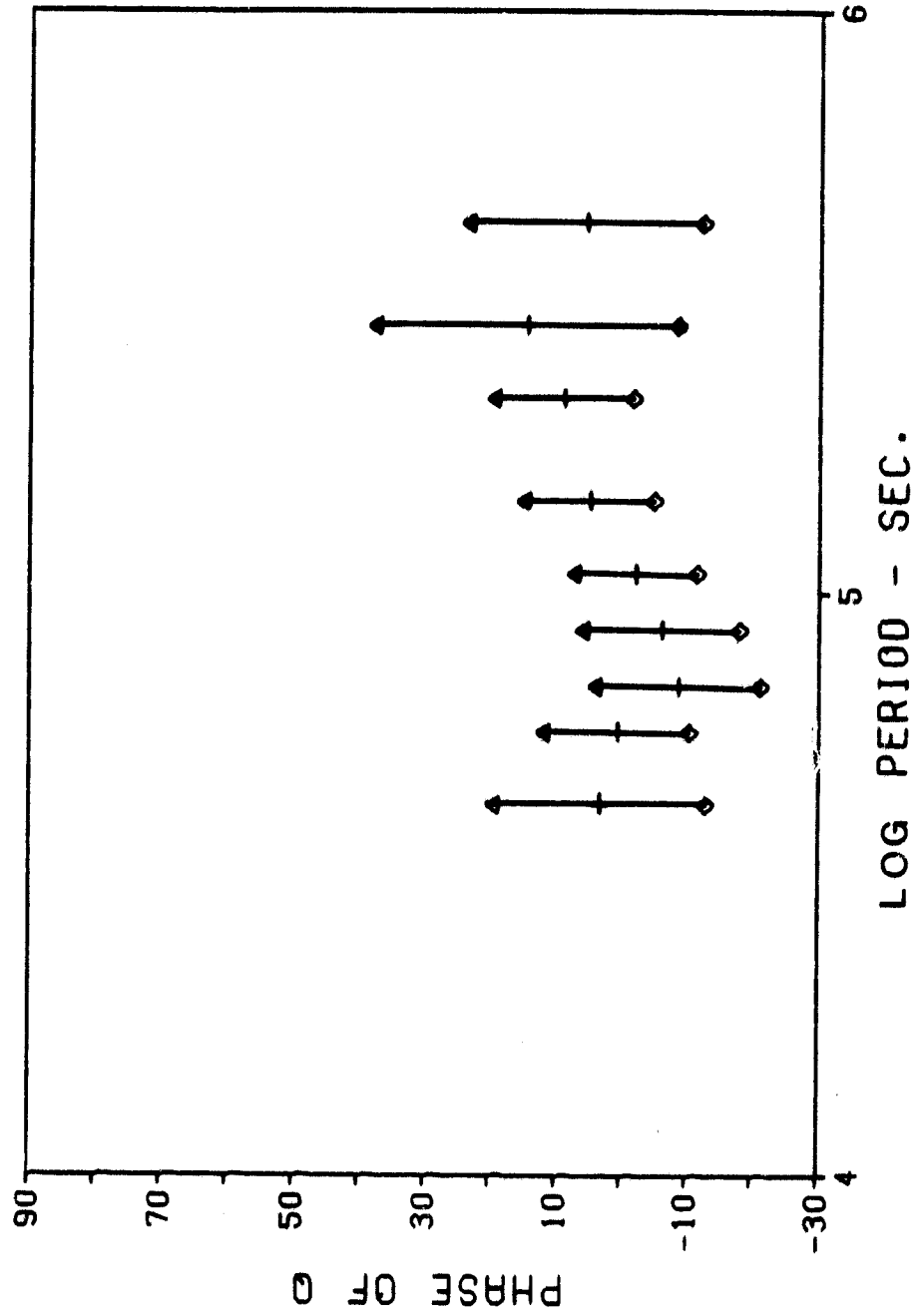


Figure 4.3: Response function for stacked data of Table 3.1 with

$$\gamma_{12}^2 \geq .6.$$

(a) Magnitude of  $\hat{Q}$

MAGNITUDE OF Q VS PERIOD

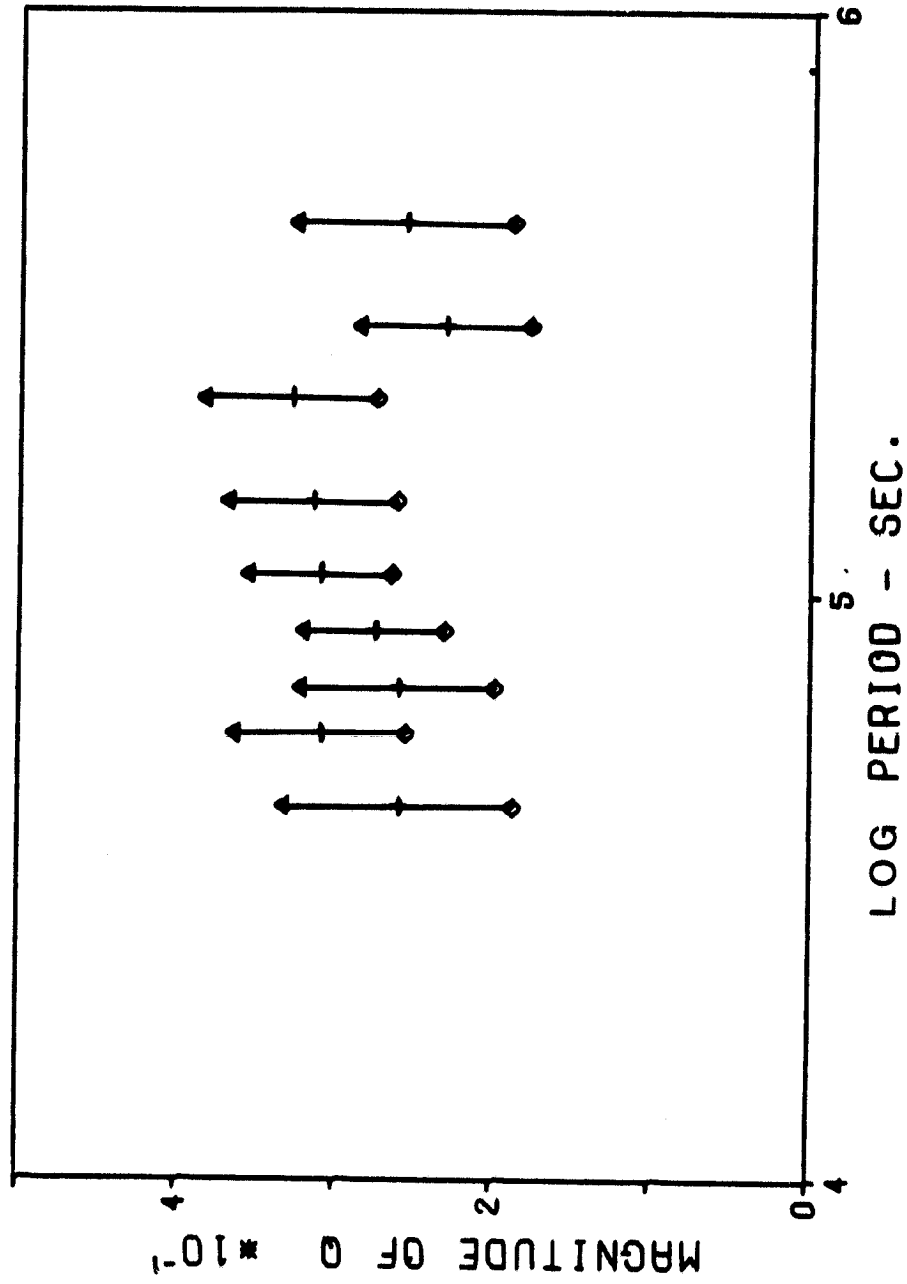
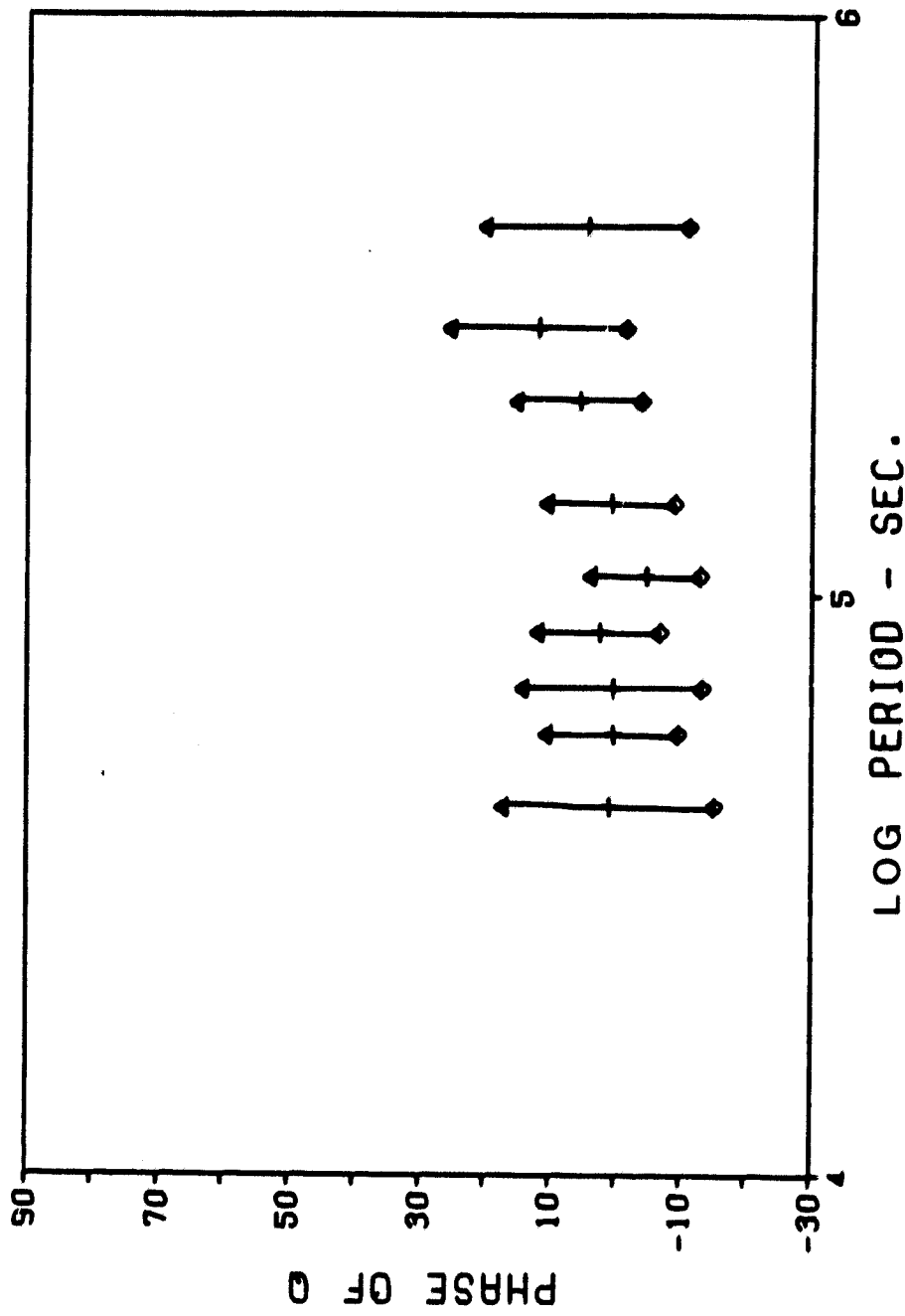


Figure 4.3: Response function for stacked data of Table 3.1 with

$$\hat{\gamma}_{12}^2 \geq .6.$$

(b) Phase of  $\hat{Q}$

# PHASE OF Q VS. PERIOD



A possible source of error in these estimates of  $\hat{Q}$  comes from contamination of the total field measurements by the crustal anomaly field. Using a field model developed by Mayhew (1980), the crustal anomaly field is subtracted from the total field before separation into  $e(t_n)$  and  $i(t_n)$  contributions (Table 3.1). In larger magnetic disturbances such as of March 5, 1970, there is little change in  $e(t_n)$  and  $i(t_n)$  or in the response function. In smaller magnetic disturbances such as Sept. 29, 1969 there is a slight difference in estimates of  $Q(\omega)$  between the anomaly corrected data and the uncorrected data (fig. 4.4 and 4.5). There appears to be no significant difference between stacked corrected and stacked uncorrected data sets.

Figure 4.4: Response function for September 29, 1969 magnetic storm  
with corrections for crustal magnetic anomalies.

(a) Magnitude of  $\hat{Q}$

MAGNITUDE OF Q VS PERIOD

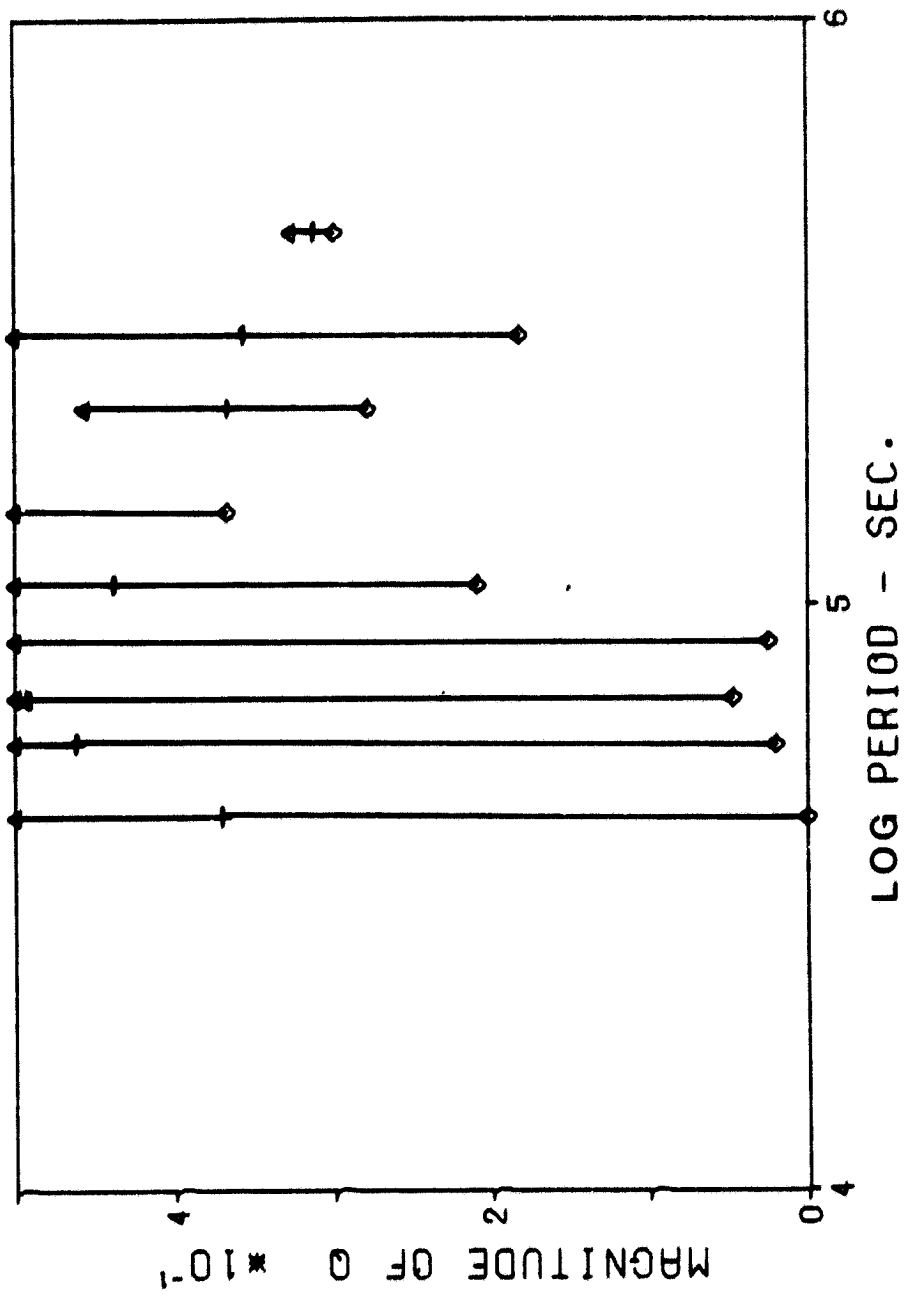
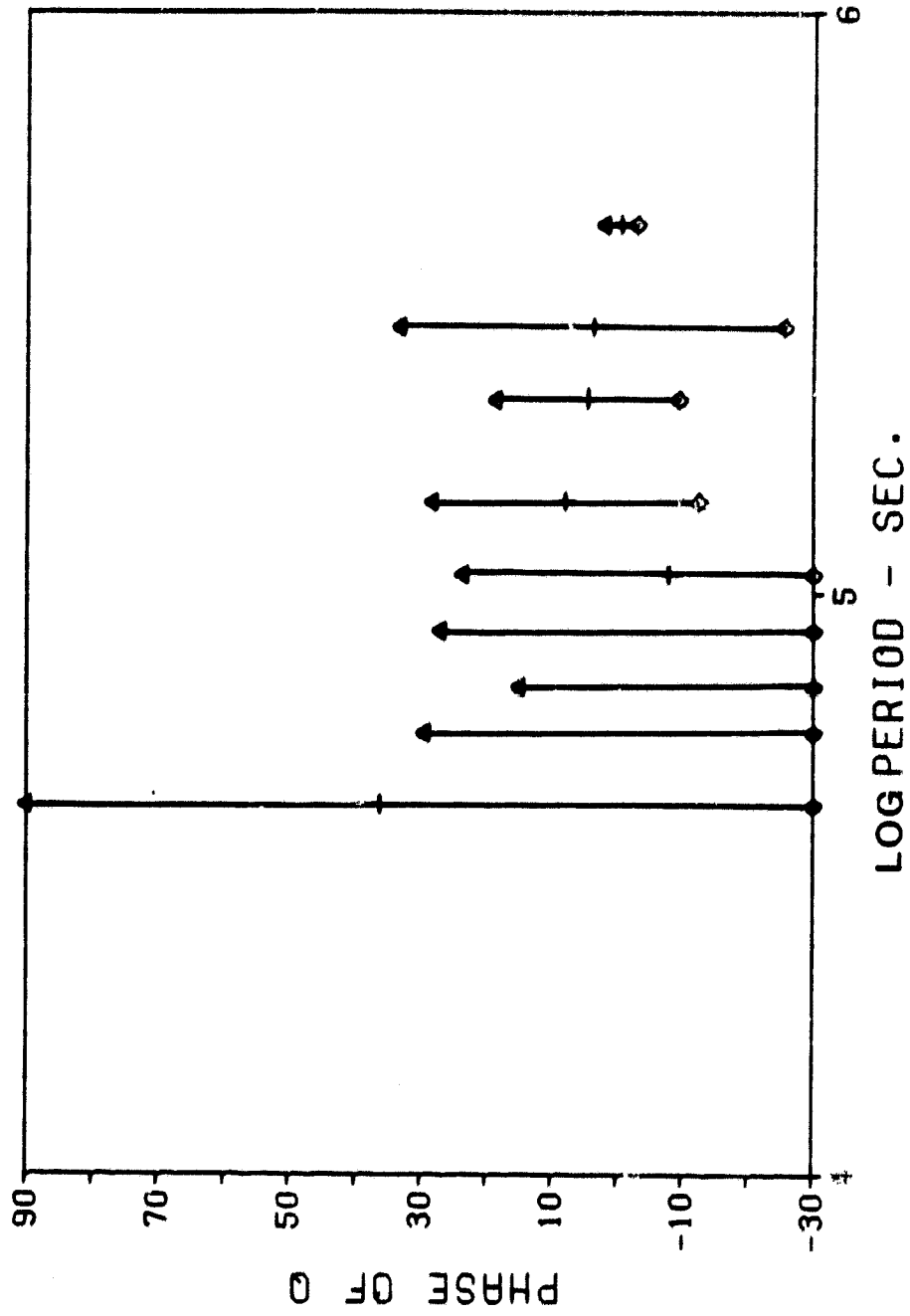


Figure 4.4: Response function for September 29, 1969 magnetic storm  
with corrections for crustal magnetic anomalies.

(b) Phase of  $\hat{Q}$

PHASE OF Q VS. PERIOD



ORIGINAL PAGE  
POOR QUALITY

Figure 4.5: Response function for September 29, 1969 magnetic storm  
without anomaly corrections.  
(a) Magnitude of  $\hat{Q}$

MAGNITUDE OF Q VS PERIOD

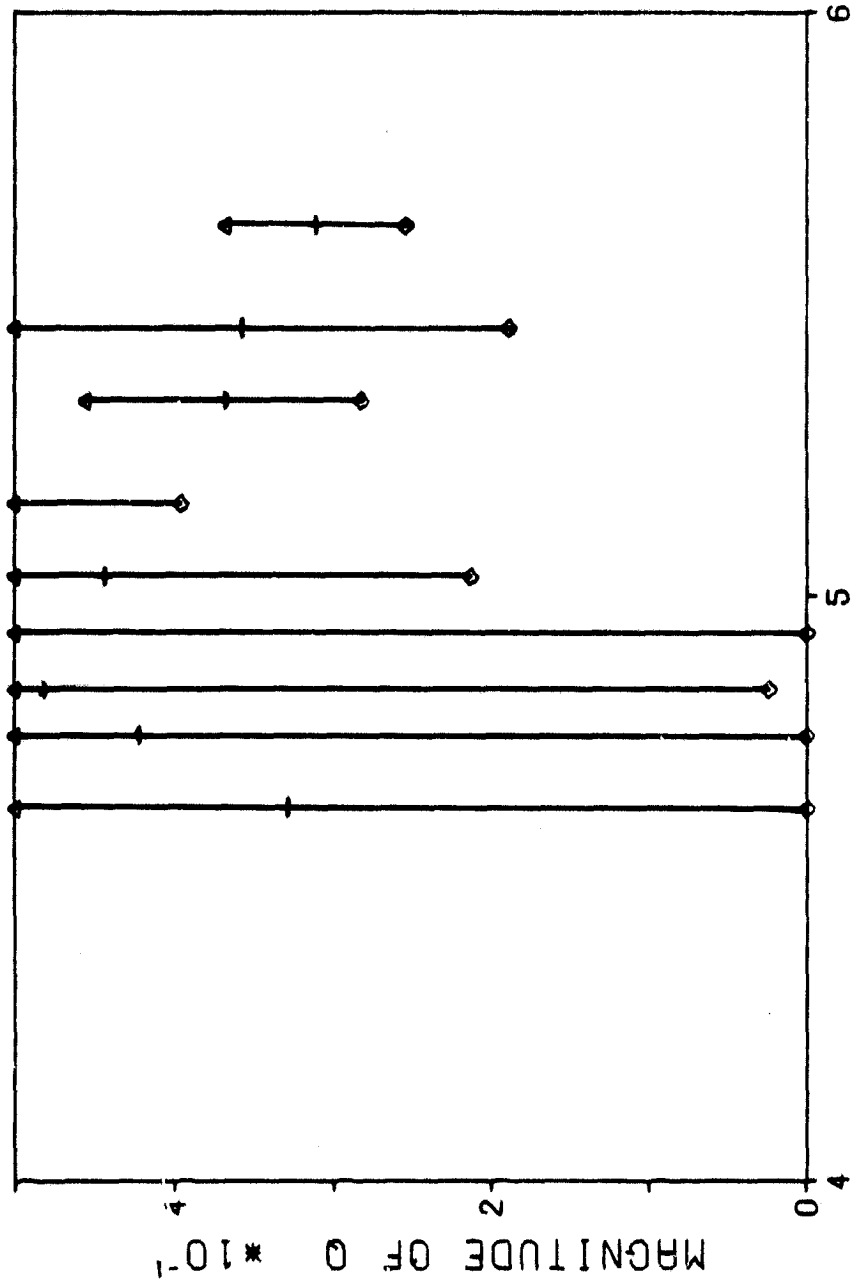
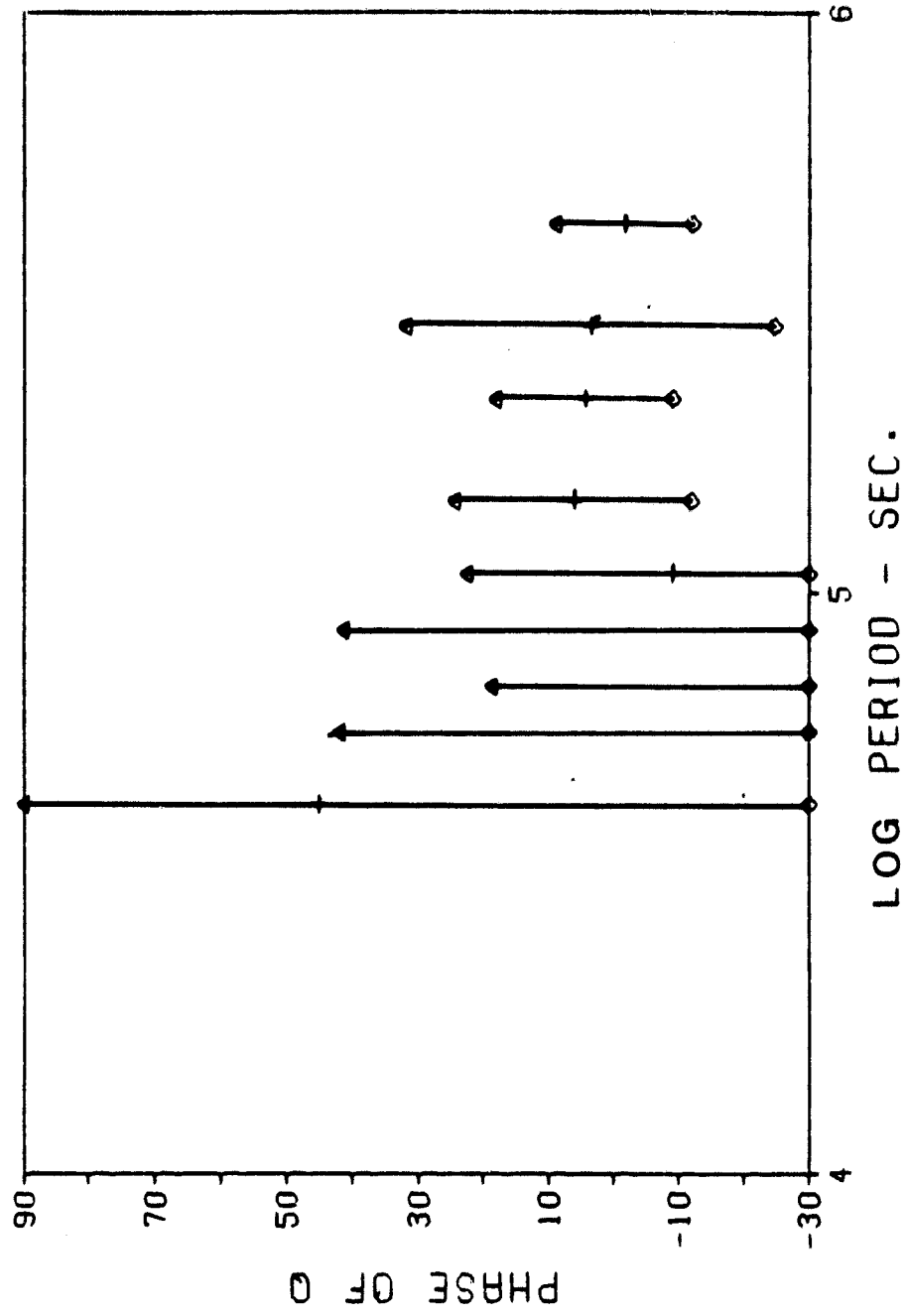


Figure 4.5: Response function for September 29, 1969 magnetic storm  
without anomaly corrections.

(b) Phase of  $\hat{Q}$

## PHASE OF Q VS. PERIOD



CHAPTER V: INTERPRETATION OF THE ESTIMATED RESPONSE FUNCTION Q.

In order to interpret the response function  $Q(\omega)$  obtained from the satellite data (fig. 4.3), one must solve the "forward problem": given a conductivity profile, what is the response function?

The response function  $Q$  is calculated for various conductivity profiles and compared to our best estimates of  $\hat{Q}$ . All response functions are calculated for periods  $10^4$  to  $10^6$  seconds which includes the range of our data. Chosen conductivity profiles include homogeneous sphere, profiles by Banks (1972), Parker (1970) and other profiles with various upper mantle and near surface conductivities.

V.1. Solution of the Forward Problem.

The method presented here is a finite difference method operating with real notation.

Consider a sphere with some known conductivity profile dependent upon radius only. Surrounding the sphere is a nonconducting space with some source of time varying magnetic field. From Maxwell's equations, in MKS units

$$\nabla \times \bar{H} = \frac{\delta \bar{D}}{\delta t} + \bar{J}_f \quad (5.1)$$

where magnetic field  $\bar{B} = \mu \bar{H}$ ,  $\bar{D}$  is the displacement field  $\bar{D} = \epsilon \bar{E}$  and  $\bar{J}_f$  is the free current density. For slowly varying magnetic field, displacement current is negligible,  $\frac{\delta \bar{D}}{\delta t} = 0$ . So, inside of the sphere

$$\nabla \times \bar{H} = \bar{J}_f \quad (5.2)$$

Taking the curl of (5.2) and using  $\bar{\mathbf{B}} = \mu\bar{\mathbf{H}}$  results in

$$\nabla^2 \bar{\mathbf{B}} = -\mu \nabla \times \bar{\mathbf{J}}_f \quad (5.3)$$

Knowing  $\sigma \bar{\mathbf{E}} = \bar{\mathbf{J}}_f$  and  $\nabla \times \bar{\mathbf{E}} = -\frac{\delta \bar{\mathbf{B}}}{\delta t}$ , this becomes

$$\nabla^2 \bar{\mathbf{B}} = \mu \sigma \frac{\delta \bar{\mathbf{B}}}{\delta t} - \mu \nabla \sigma \times \bar{\mathbf{E}} \quad (5.4)$$

For constant conductivity, the  $\nabla \sigma \times \bar{\mathbf{E}}$  term will vanish. For conductivity that varies only in the radial direction, the  $\bar{\mathbf{B}}$  field produced by  $\nabla \sigma \times \bar{\mathbf{E}}$  term would only have  $\theta$  and  $\phi$  components. Assuming that any initial charge density would decay to zero,  $\nabla \sigma \times \bar{\mathbf{E}} = 0$  (Rikitake, 1966).

So, the final equation to consider is

$$\nabla^2 \bar{\mathbf{B}} = \mu \sigma \frac{\delta \bar{\mathbf{B}}}{\delta t} \quad (5.5)$$

A complete solution to (5.5) is composed of a toroidal field  $\bar{\mathbf{T}}$  which would be restricted to within the sphere, a poloidal field  $\bar{\mathbf{S}}$  which would be detected outside of the sphere, and an arbitrary scalar field  $W$  which can be assumed to be zero. Since the eventual goal is to determine the field measured outside of the sphere due to both (5.5) and (5.6), the only solution of interest is the poloidal field  $\bar{\mathbf{S}}$ :

$$\bar{\mathbf{S}} = -\nabla \times \nabla \times (\bar{r}_p) \quad (5.6)$$

So field equation (5.5) can be reduced to

$$\nabla^2 p = \mu \sigma \frac{\delta p}{\delta t} \quad (5.7)$$

where  $\nabla \times (\bar{r}_p)$  is the poloidal potential.

Outside of the conducting sphere, where no free currents exist

$$\nabla \times \vec{H} = 0 \quad (5.8)$$

Since (5.8) holds,  $\vec{E}$  can be represented by a scalar potential  $U$  such that

$$\vec{E} = -\nabla U \quad (5.9)$$

Since  $\vec{E}$  of eqn. (5.9) consists of field contributions both of internal and external origin (relative to the sphere of radius  $a$ ),  $U$  can be represented by

$$U = \sum_n a (e_n(t) \left(\frac{r}{a}\right)^n + i_n(t) \left(\frac{a}{r}\right)^{n+1}) P_n^0(\cos \theta) \quad (5.10)$$

where  $a$  is the radius of the sphere,  $r$  is the variable radius,  $\theta$  is the magnetic colatitude,  $e_n$  is the external coefficient,  $i_n$  is the internal coefficient, and  $P_n^0(\cos \theta)$  are the Legendre polynomials of degree  $n$ . Assuming that the dipole term is sufficient to represent the time-varying disturbing field used in this study,  $U$  can be simply represented by

$$U = a (e_1(t) \left(\frac{r}{a}\right) + i_1(t) \left(\frac{a}{r}\right)^2) P_1^0(\cos \theta) \quad (5.11)$$

Since the response function  $Q(\omega)$  is ideally

$$Q(\omega) = \frac{F(i_1(t))}{F(e_1(t))} \quad (5.12)$$

where  $F(i_1(t))$  and  $F(e_1(t))$  are the Fourier transforms of  $i_1(t)$  and  $e_1(t)$ , it is convenient to represent  $e_1$  and  $i_1$  in terms of a Fourier series

$$e_1 = \sum_n E_{1n} \cos \omega_n t + E_{2n} \sin \omega_n t \quad (5.13)$$

$$i_1 = \sum_n I_{1n} \cos \omega_n t + I_{2n} \sin \omega_n t$$

where  $e_1$  is the external field contribution and  $i_1$  is the induced field contribution to the potential.  $E_{1n}$ ,  $E_{2n}$ ,  $I_{1n}$ ,  $I_{2n}$  are the Fourier coefficients to the power series. Substituting (5.13) into (5.11) gives a simple power series representation to the potential  $U$ .

From the poloidal field (5.7),  $p$  can also be represented by a Fourier power series using the dipole term  $P_1^0(\cos \theta)$

$$p = r^{-1} \sum_n A_n(r) P_1^0(\cos \theta) \cos \omega_n t + C_n(r) P_1^0(\cos \theta) \sin \omega_n t \quad (5.14)$$

Substituting (5.14) into the differential equation (5.7) results in a coupled pair of equations

$$\begin{aligned} \frac{d^2 A_n}{dr^2} - 2 r^{-2} A_n &= \frac{1}{\rho} \omega_n C_n \\ \frac{d^2 C_n}{dr^2} - 2 r^{-2} C_n &= -\frac{1}{\rho} \omega_n A_n \end{aligned} \quad (5.15)$$

where  $\rho = \frac{1}{\sigma \mu}$ ,  $\sigma$  is resistivity and  $\mu = \mu_0$  is the free space permeability. (We assume  $\mu = \mu_0$  for the sphere.)

Using the conditions at the surface of the sphere ( $r = a$ ) for continuity of the B normal and H tangential components, we arrive at the boundary conditions at  $r = a$

$$a \frac{dA_n}{dr} \Big|_a + A_n(a) = \frac{3}{2} a^2 E_{1n} \quad (5.16)$$

$$a \frac{dC_n}{dr} \Big|_a + C_n(a) = \frac{3}{2} a^2 E_{2n}$$

Since these equations (5.15) to (5.16) are solved numerically, it is desirable to express them in nondimensional form; we make the following change of variables

$$\begin{aligned} r &= a - (1 - z) N\delta \\ A_n &= a^2 \hat{A}_n \\ C_n &= a^2 \hat{C}_n \end{aligned} \quad (5.17)$$

Substituting (5.17) into (5.15) yields (5.18) where  $c = N\delta/a$  and

$$\delta = (2/\mu\omega\sigma)^{1/2}$$

$$\frac{d^2 \hat{A}_n}{dz^2} - \frac{2c^2}{(c(z-1)+1)^2} \hat{A}_n = 2N^2 \hat{C}_n \quad (5.18)$$

$$\frac{d^2 \hat{C}_n}{dz^2} - \frac{2c^2}{(c(z-1)+1)^2} \hat{C}_n = -2N^2 \hat{A}_n$$

with boundary conditions at  $z = 1$

$$\begin{aligned} \frac{d\hat{A}_n}{dz} \Big|_{z=1} + c \hat{A}_n(1) &= c \frac{3}{2} E_{1n} \\ \frac{d\hat{C}_n}{dz} \Big|_{z=1} + c \hat{C}_n(1) &= c \frac{3}{2} E_{2n} \end{aligned} \quad (5.19)$$

where  $c = \frac{N\delta}{a}$ .

Examining the poloidal field,  $\bar{S}$  must go to zero at  $r = 0$ , so  $A_n(z=0)$  and  $C_n(z=0)$  goes to some small number as  $z \rightarrow 0$ , since the strength of the inducing field decreases with depth. By normalizing with "N" skin depths,  $z=0$  implies that the field is very small when it has penetrated N skin depths. So, additional boundary conditions at  $z = 0$  are

$$\begin{aligned}\hat{A}_n(0) &= \alpha \\ \hat{C}_n(0) &= \beta\end{aligned}\tag{5.20}$$

where  $\alpha$  and  $\beta$  are small and are assigned according to "N".

The actual solution of (5.18) is accomplished using a Runge-Kutta finite difference algorithm, for 4 simultaneous first order differential equations

$$\begin{aligned}Y_1 &= \hat{A}_n(z) \\ Y_2 &= \hat{A}'_n(z) \\ Y_3 &= \hat{C}_n(z) \\ Y_4 &= \hat{C}'_n(z)\end{aligned}$$

then (5.18) becomes

$$\begin{aligned}
 F_1 &= \frac{dY_1}{dz} = Y_2 \\
 F_2 &= \frac{2c^2 Y_1}{(c(z-1)+1)^2} + 2 N^2 Y_3 \\
 F_3 &= \frac{dY_3}{dz} = Y_4 \\
 F_4 &= \frac{dY_4}{dz} = \frac{2c^2 Y_3}{(c(z-1)+1)^2} - 2 N^2 Y_1
 \end{aligned} \tag{5.21}$$

where  $c = \frac{N\delta}{a}$  and  $z$  is radial distance.

A theorem for differential equations (Boyce and DiPrima, 1969) states that for a system of  $n$  first order, linear, homogeneous differential equations

$$\begin{aligned}
 x_1' &= p_{11}(t)x_1 + \dots + p_{1n}(t)x_n \\
 &\cdot \\
 &\cdot \\
 x_n' &= p_{n1}(t)x_1 + \dots + p_{nn}(t)x_n
 \end{aligned}$$

each solution  $\bar{x} = \tilde{\phi}(t)$  of this system can be expressed as a linear combination of  $\bar{x}^{(1)}, \dots, \bar{x}^{(n)}$ , with arbitrary coefficients  $c_n$

$$\bar{x} = c_1 \bar{x}^{(1)}(t) + \dots + c_n \bar{x}^{(n)}(t)$$

in exactly one way. Knowing this, 4 independent solutions to (5.20) are obtained using arbitrary  $\hat{A}_n(0), \hat{A}'_n(0), \hat{C}_n(0), \hat{C}'_n(0)$ . The final solution,  $c_1 \hat{A}_{n1}(z) + c_2 \hat{A}_{n2}(z) + c_3 \hat{A}_{ns}(z) + c_4 \hat{A}_{n4}(z)$ , must meet the four boundary conditions (5.19) and (5.20). This requires solution

to a set of four equations with four unknowns  $c_1, c_2, c_3, c_4$ :

$$\begin{aligned}
 c_1 \hat{A}_{n1}(0) + c_2 \hat{A}_{n2}(0) + c_3 \hat{A}_{n3}(0) + c_4 \hat{A}_{n4}(0) &= \alpha \\
 c_1 \hat{C}_{n1}(0) + c_2 \hat{C}_{n2}(0) + c_3 \hat{C}_{n3}(0) + c_4 \hat{C}_{n4}(0) &= \beta \\
 c_1 \hat{A}'_{n1}(1) + c_2 \hat{A}'_{n2}(1) + c_3 \hat{A}'_{n3}(1) + c_4 \hat{A}'_{n4}(1) &= \\
 c(3/2 E_{1n} - c_1 \hat{A}_{n1}(1) - c_2 \hat{A}_{n2}(1) - c_3 \hat{A}_{n3}(1) - c_4 \hat{A}_{n4}(1)) & \\
 c_1 \hat{C}'_{n1}(1) + c_2 \hat{C}'_{n2}(1) + c_3 \hat{C}'_{n3}(1) + c_4 \hat{C}'_{n4}(1) &= \\
 c(3/2 E_{2n} - c_1 \hat{C}_{n1}(1) - c_2 \hat{C}_{n2}(1) - c_3 \hat{C}_{n3}(1) - c_4 \hat{C}_{n4}(1)) &
 \end{aligned} \tag{5.22}$$

where  $c = \frac{N\delta}{a}$ ,  $E_{1n}$  and  $E_{2n}$  are input amplitude (eqn. 5.13) and " ' " denotes first derivative with respect to  $z$ .

Once the final solution for  $\hat{A}_n(z)$  and  $\hat{C}_n(z)$  is obtained, for particular conductivity profile and frequency  $\omega$ , the response function for the assumed  $E_{1n}$  and  $E_{2n}$  input (arbitrary since  $Q$  involves a ratio, so  $E_{1n} = E_{2n} = 1$ ) is computed

$$Q(\omega_n) = \frac{I_{1n}(\omega_n) - j I_{2n}(\omega_n)}{E_{1n} - j E_{2n}} \tag{5.23}$$

where  $j = \sqrt{-1}$  and  $I_{1n}$  and  $I_{2n}$  are derived from the boundary conditions (5.19). The response magnitude  $|Q|$  and the phase  $\phi(Q)$  can be expressed by

$$|Q| = \frac{(I_{1n}^2 + I_{2n}^2)^{1/2}}{(E_{1n}^2 + E_{2n}^2)^{1/2}}$$

and

$$\phi(Q) = \arctan \frac{(I_{1n} E_{2n} - I_{2n} E_{1n})}{(I_{1n} E_{1n} + I_{2n} E_{2n})} \tag{5.24}$$

Alternative methods for solving the forward problem involve solving the "R" part of the poloidal field equation (see eqn. 5.7) after separation of variables. One method requires a series of shells of constant conductivity where the analytical solution for each shell is known (Banks, 1969). The Runge-Kutta method can also be applied to the "R" equation in complex notation (Parker, 1970). Eckhardt (1963) transforms this same "R" equation into a nonlinear first order differential equation and solves it numerically.

#### V.2. Behavior of the Forward Problem Solution.

Response functions were calculated for periods  $10^4$  to  $10^6$  seconds, mantle conductivities .001 to 100 mho/m and an accepted core conductivity of  $3 \times 10^5$  mho/m (Stacey, 1977). This highly conducting core also insured that the boundary conditions at N skin depths would remain within the dimensions of the earth.

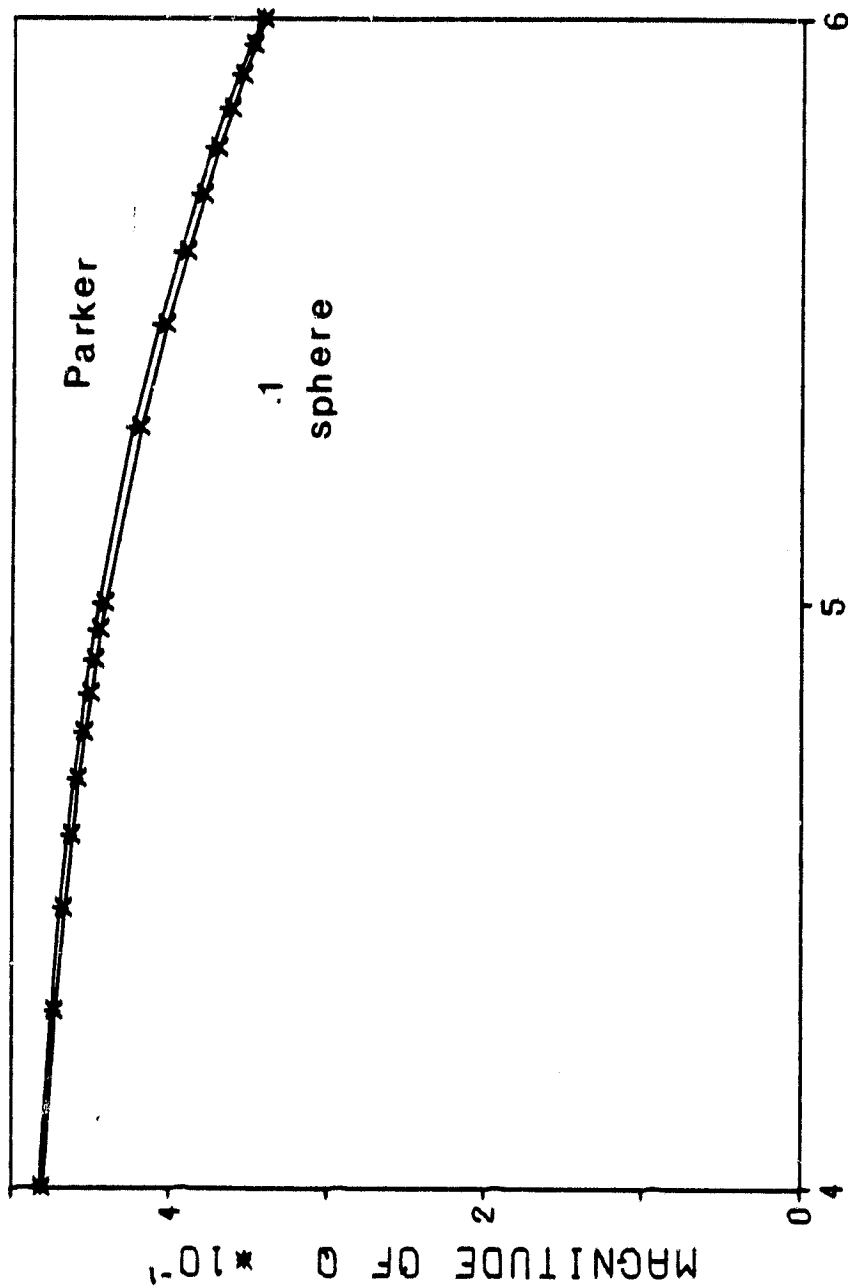
The response function for the range of periods considered is most sensitive to the upper regions of the earth. Further, the degree of sensitivity depends upon the conductivities involved and the rate of change of conductivity with depth. Large conductivities tend to hide variations in conductivity while lower conductivities are more transparent. Large changes in conductivity over small changes in depth are also more visible than gradual changes. For example, Parker's 1970 profile (fig. 1.2) compared to a homogeneous sphere of .1 mho/m shows only a small change in response function (fig. 5.1). Parker's profile is a smoothly varying model with the upper mantle having a conductivity of .1 mho/m. In contrast, Banks 1972 model (fig. 1.1) is

Figure 5.1: Parker's 1970 model compared to homogeneous sphere of

.1 mho/m.

(a) Magnitude of Q

MAGNITUDE OF Q VS PERIOD

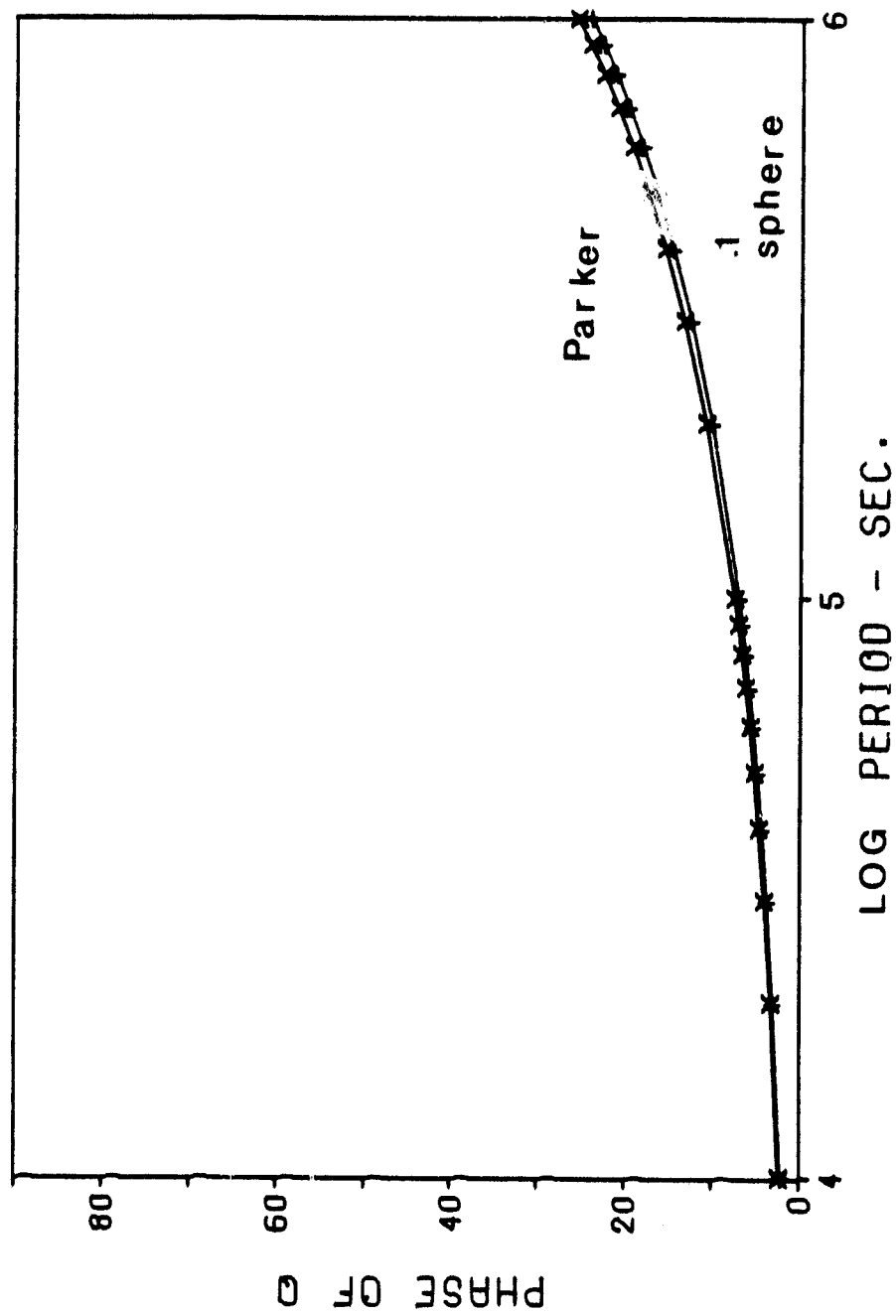


LOG PERIOD - SEC.

ORIGINAL PAGE 1  
OF POOR QUALITY

ORIGINAL PAGE 1  
OF POOR QUALITY

Figure 5.1: Parker's 1970 model compared to homogeneous sphere of  
.1 mho/m.  
(b) Phase of Q

PHASE OF  $Q$  VS. PERIOD

composed of a series of steps with large changes in conductivity and an upper mantle conductivity of .01 mho/m. Banks' model compared to a homogeneous sphere of .01 mho/m (fig. 5.2) shows a large contrast in response functions.

In assigning starting depths, it was found that the calculated response function was fairly insensitive to changes in  $N$  (number of skin depths) for  $N > 5$  and  $\alpha$  and  $\beta$  of order .001. This is particularly true for conductivity profiles with near surface values greater than .01 mho/m. Banks (1972) also calculated the response function for his conductivity profile and for Parker's (1970) using the analytical solutions for constant conductivity shells. Our response functions agree fairly well with Banks' calculation of Parker's profile, but disagree with Banks' calculation of phase for Banks' profile. Our phases for small conductivities tend to increase more rapidly with period than do Banks'. Low conductivities have large skin depths,  $\delta$ , so "c" (5.17) is greater than one. The phase is greatly affected by how much of the layer with  $c > 1$  is included in the finite difference calculation. The phases presented here are the largest allowable. However, the magnitude calculation is essentially exact.

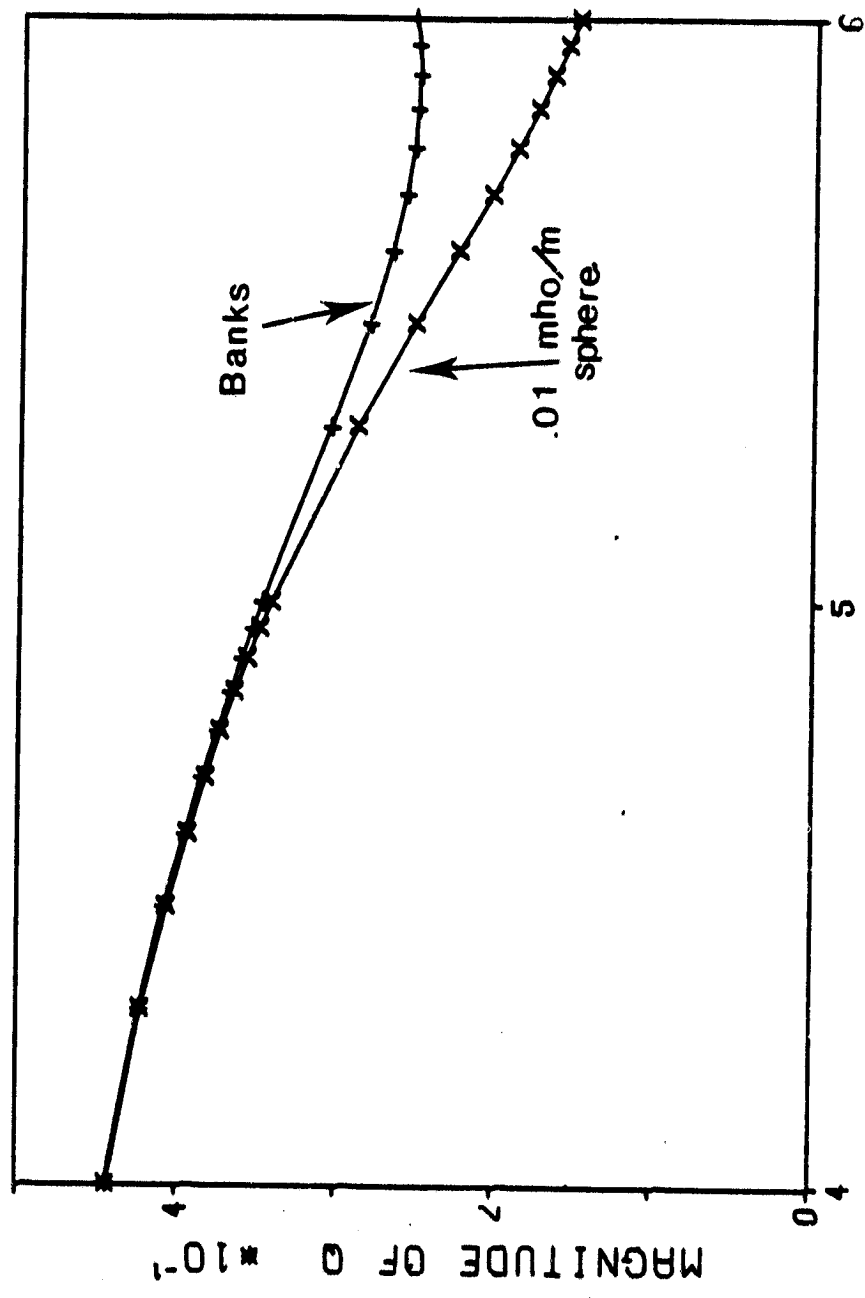
General behavior of the response functions is best illustrated by calculating  $Q$  for homogeneous spheres (fig. 5.3a,b). As conductivity increases, the magnitude of the response function,  $|Q|$ , increases while the phase,  $\phi$ , decreases as a function of period.

Figure 5.2: Banks' 1972 model compared to homogeneous sphere of

.01 mho/m.

(a) Magnitude of Q

MAGNITUDE OF Q VS PERIOD



LOG PERIOD - SEC.

ORIGINAL PAGE 1  
OF FOUR QUALITY

Figure 5.2: Banks' 1972 model compared to homogeneous sphere of  
.05 mho/m.

(b) Phase of Q

## PHASE OF Q VS. PERIOD

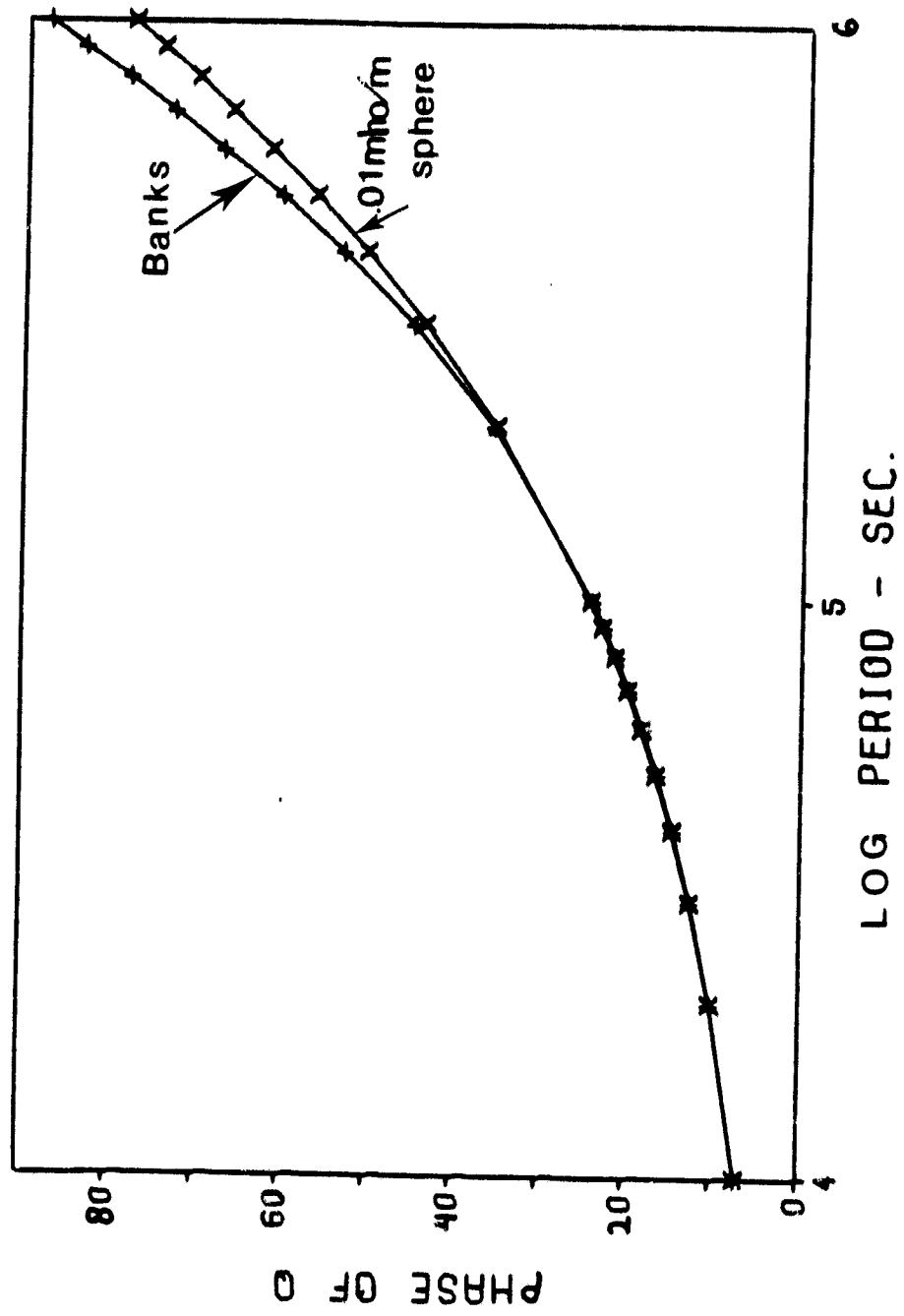


Figure 5.3: Response functions of homogeneous sphere of varying conductivity.

(a) Magnitude of  $Q$

MAGNITUDE OF Q VS PERIOD

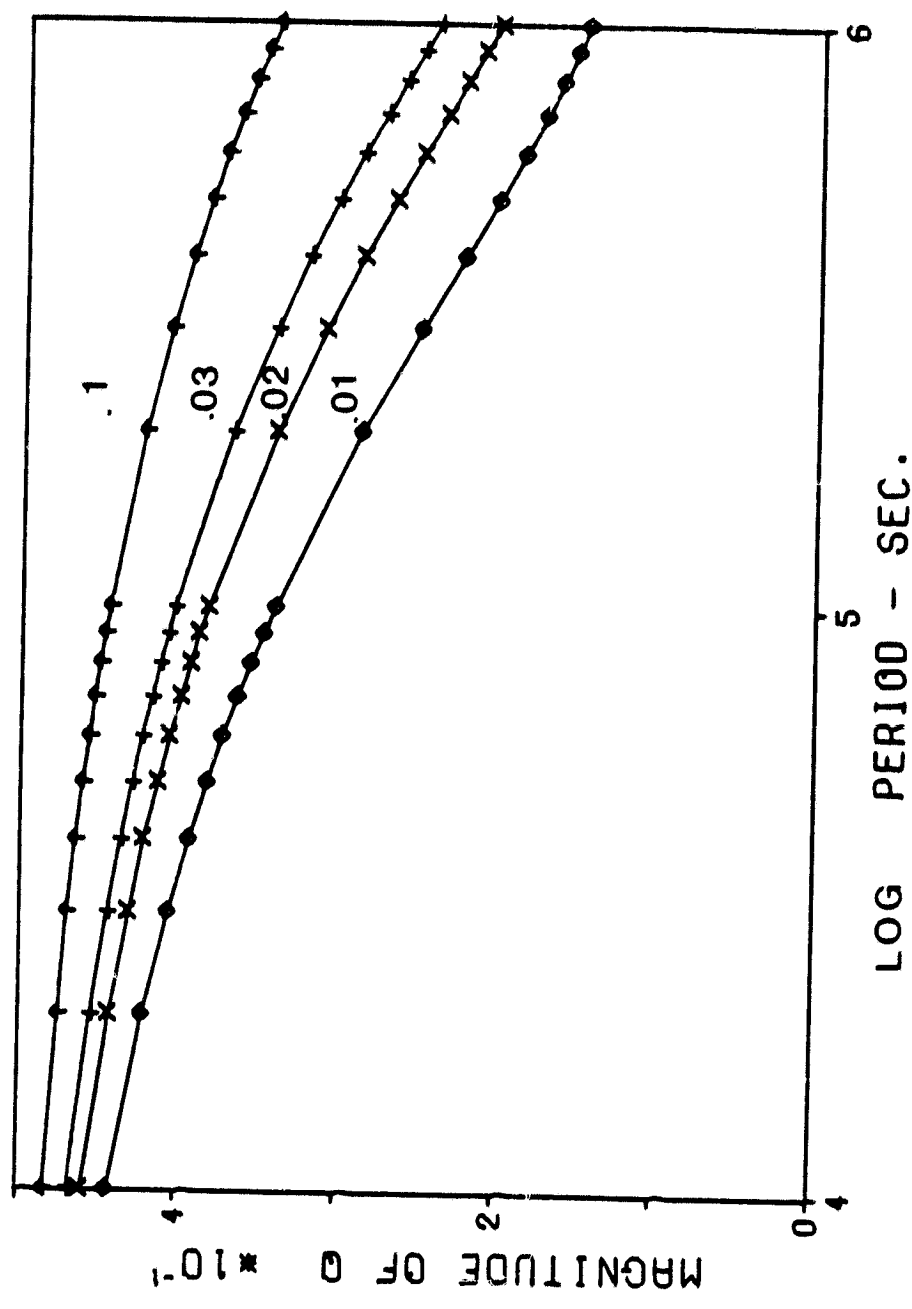
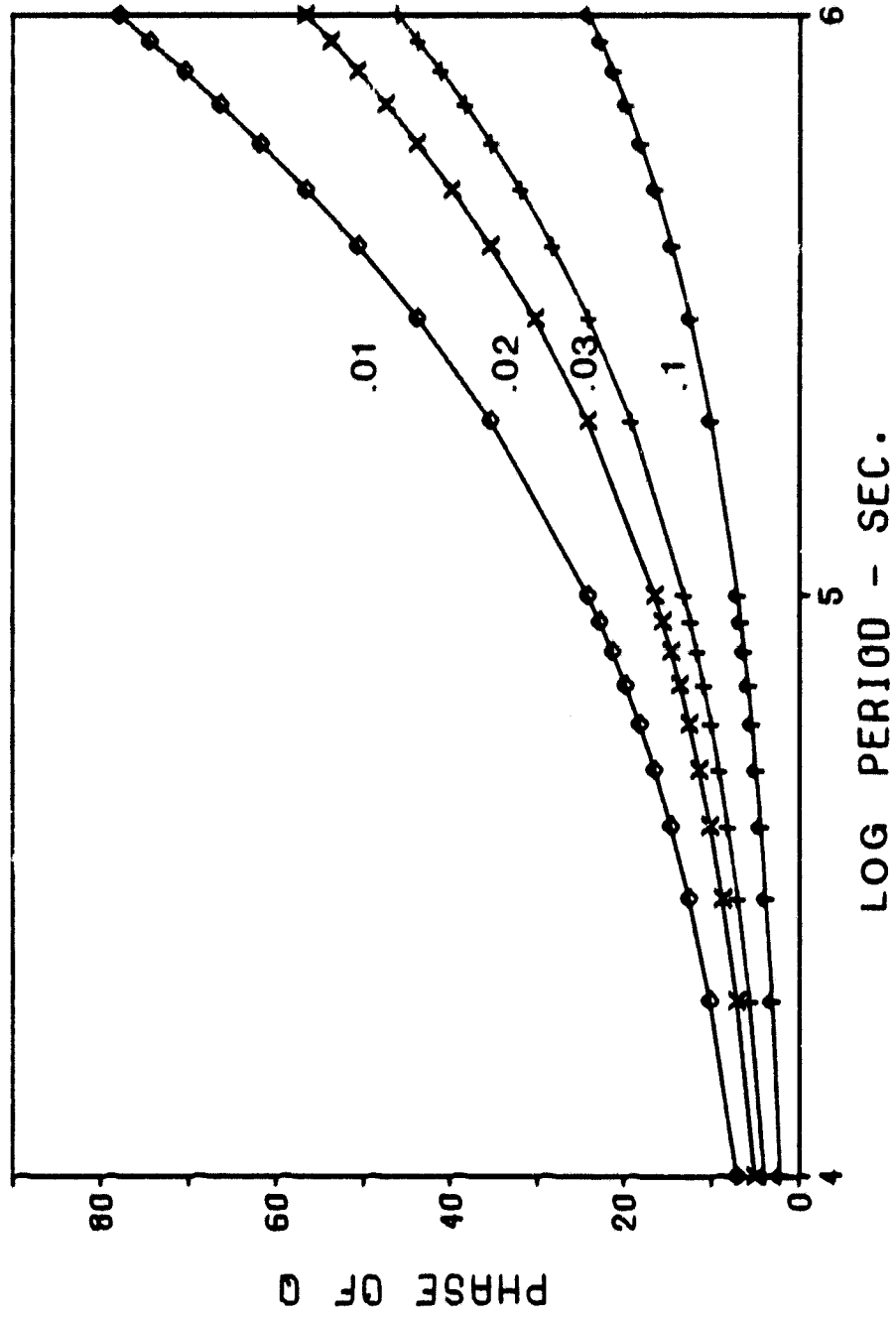


Figure 5.3: Response functions of homogeneous sphere of varying conductivity.

(b) Phase of  $Q$

PHASE OF Q VS. PERIOD



ORIGINAL PAGE 1  
OF POOR QUALITY

### V.3. Comparing Estimated Q to Calculated Q.

As a first step in interpreting the estimated values of Q, calculated response functions for simple conductivity profiles were compared to the estimated response. When response functions of homogeneous spheres are compared to estimated responses (fig. 5.4), the magnitudes lie in the vicinity of the .01 and .02 mho/m curves for periods greater than  $10^5$  seconds. For periods less than  $10^5$  seconds, the estimated magnitudes lie well below the .01 curve. For all periods considered, the phase lies below or within the 95% confidence interval of the .1 mho/m curve. Neither estimated magnitudes nor phase show the same monotonic shape as do the response function curves of homogeneous spheres. Clearly, a homogeneous sphere of any conductivity cannot explain this data.

Next, the estimated response function was compared to the response function for Banks' 1972 profile (fig. 1.1, fig. 5.5a) and Parker's 1970 profile (fig. 1.2, fig. 5.5b). The estimated magnitude (fig. 5.5c) is compatible with that of Banks' for periods greater than  $10^5$  seconds, but the phase is not (fig. 5.5d). The phase curve for Parker's model lies within the 95% confidence interval of the estimated phases but does not show the same monotonic shape. In all of the foregoing comparisons, the phase and magnitude estimates seem to indicate conductivities which are nearly an order of magnitude different from each other. Since the phase estimates contain non-physical negative values, more credence is given to the magnitude estimates. Modifications of Banks' conductivity profile (fig. 5.5a)

Figure 5.4: Comparison of best estimate of response function to those of homogeneous spheres.  
(a) Magnitude of  $Q$

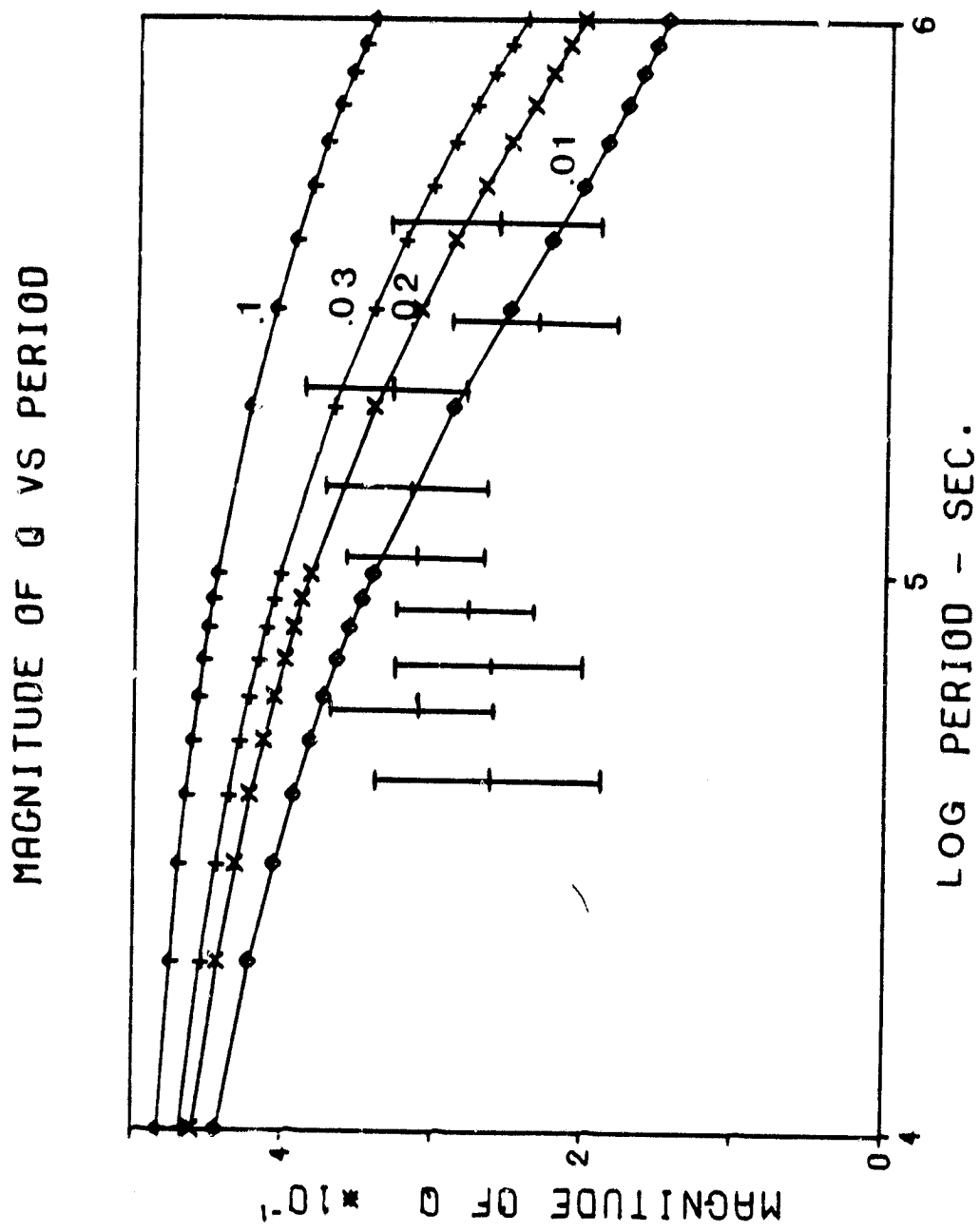
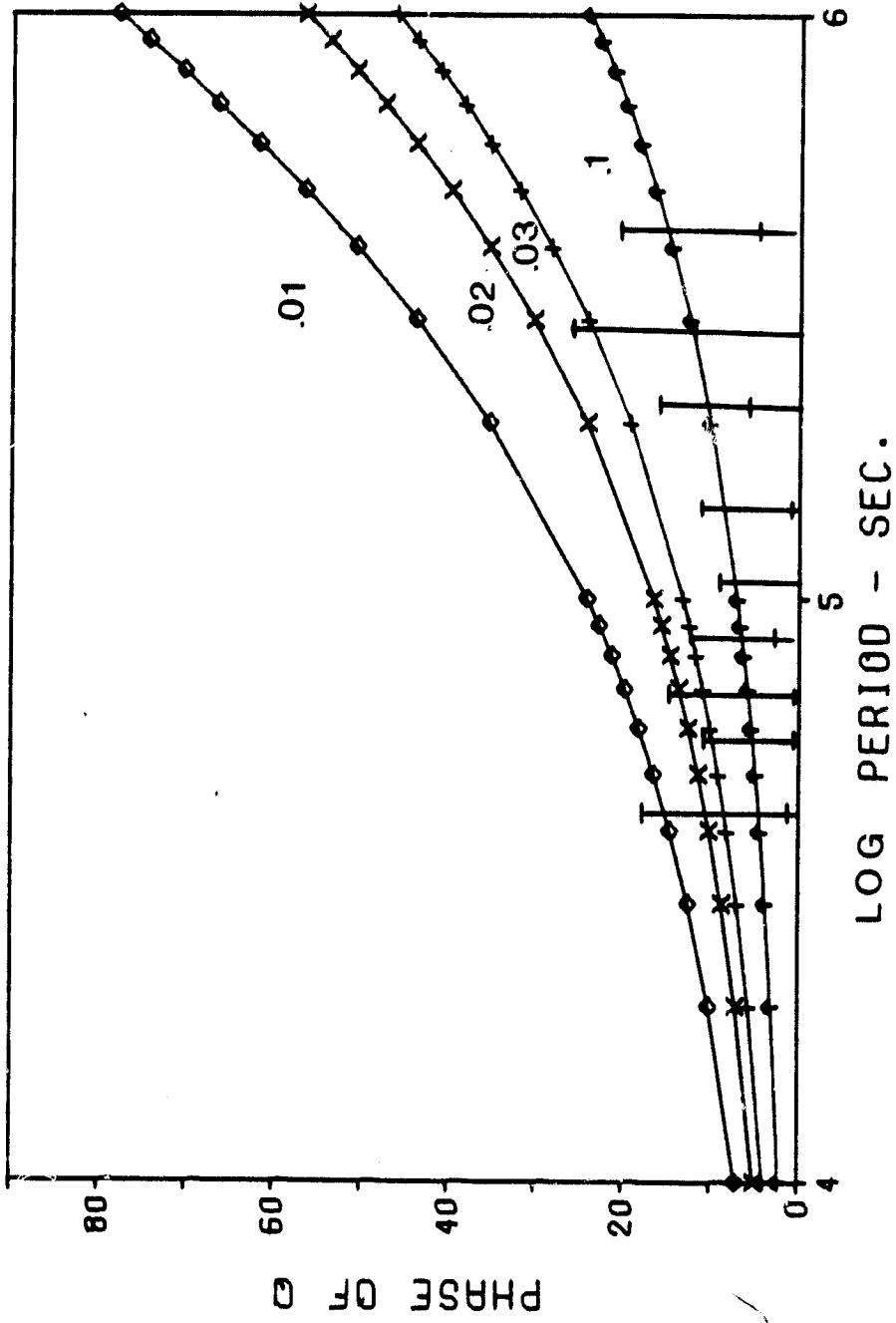


Figure 5.4: Comparison of best estimate of response function to those of homogeneous spheres.

(b) Phase of Q

PHASE OF  $\theta$  VS. PERIOD



ORIGINAL FILE  
PHASE OF  $\theta$

Figure 5.5(a): Banks' 1972 conductivity profile as used in this study.

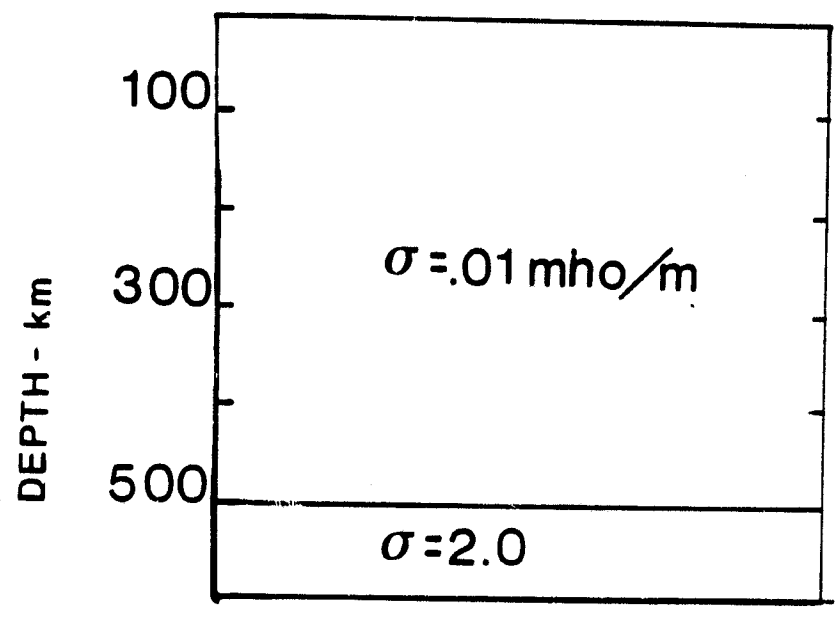
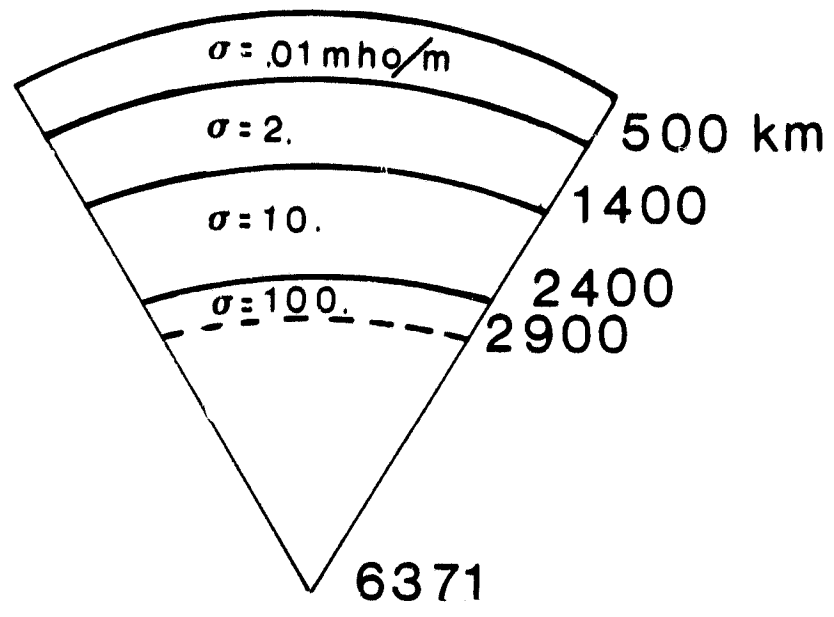


Figure 5.5(b): Parker's 1970 conductivity profile as used in this study.

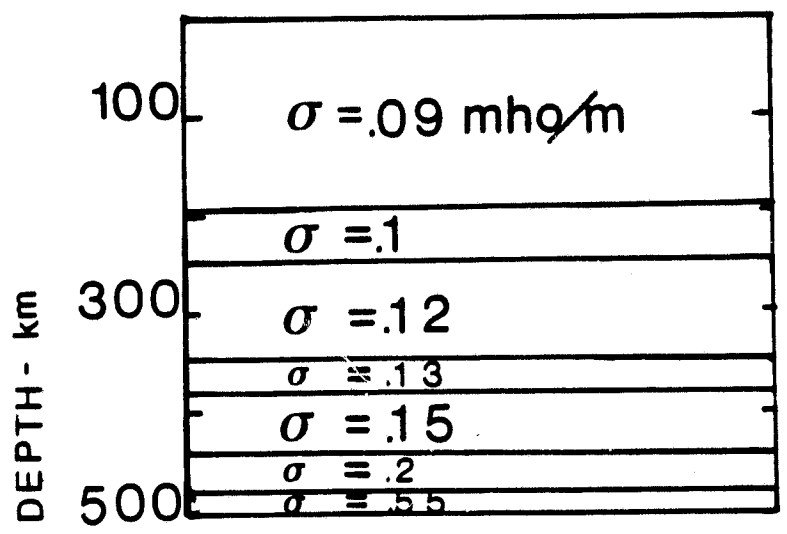
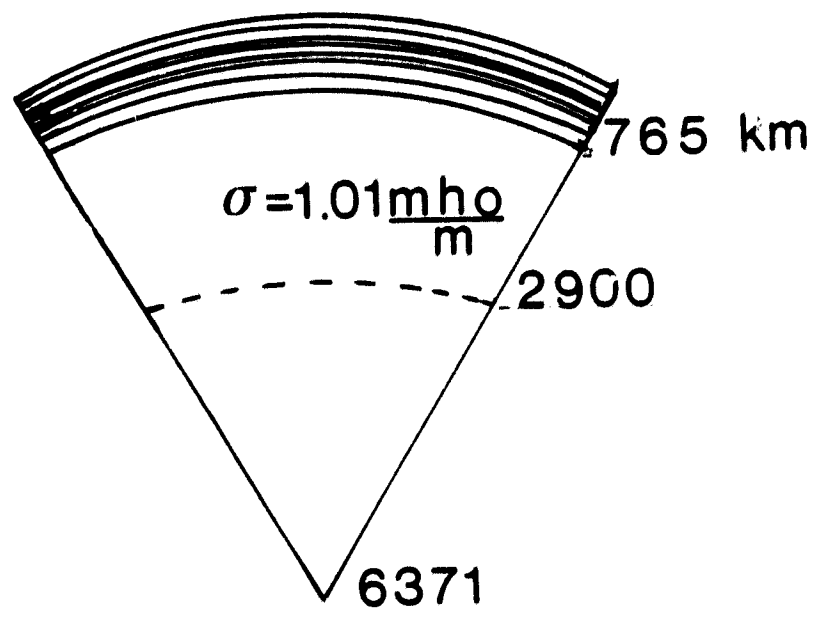
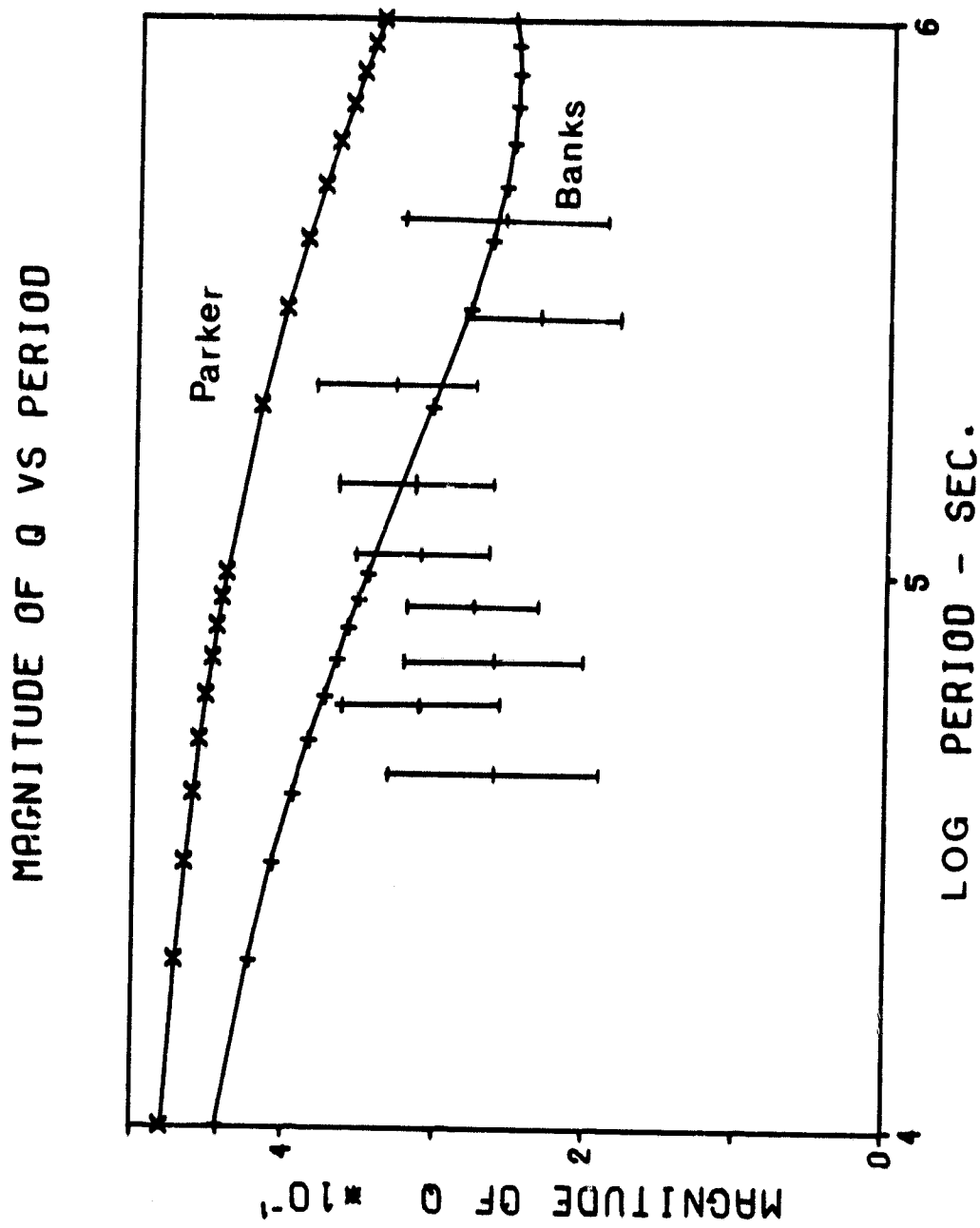


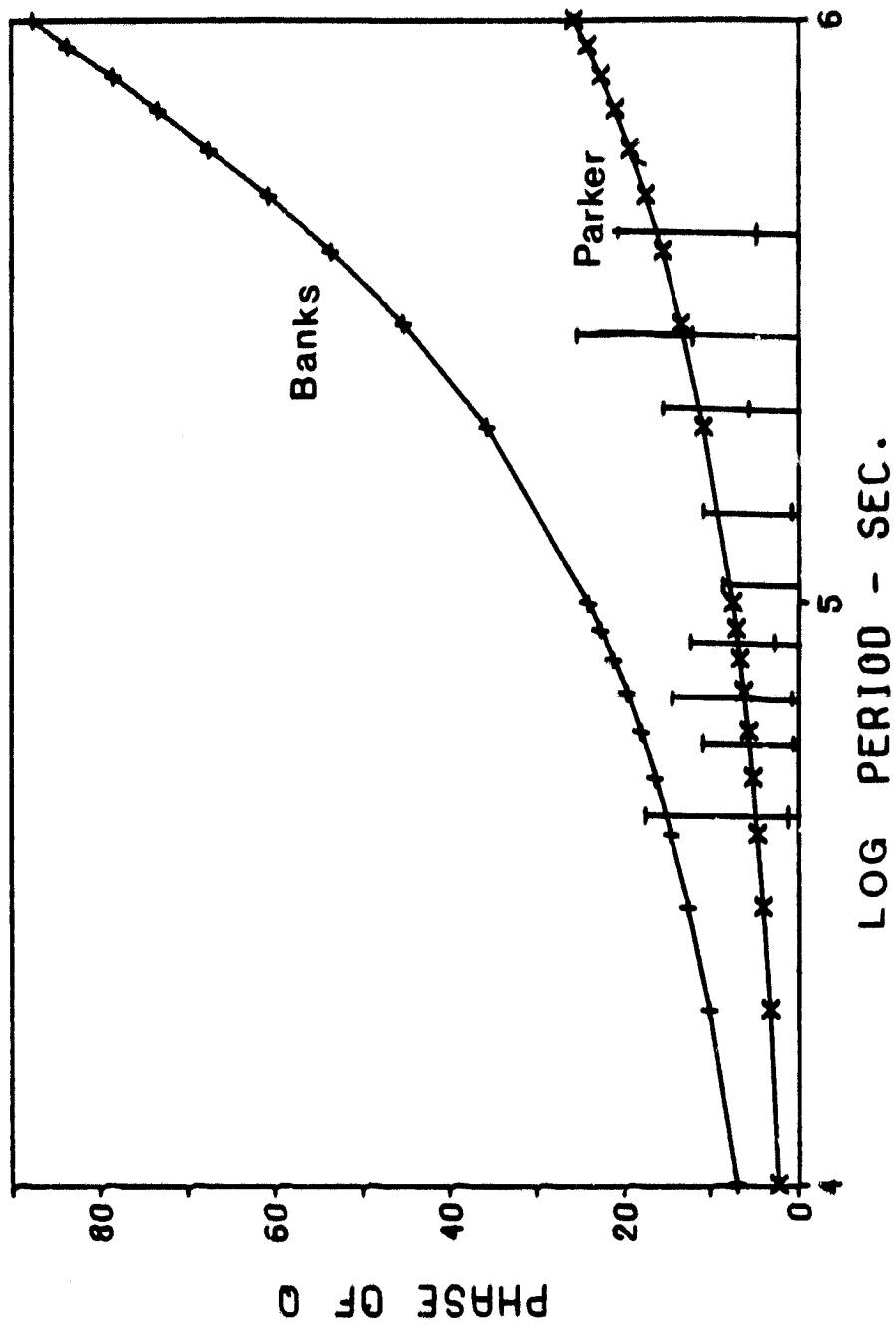
Figure 5.5(c): Comparison of magnitude estimates to those of Banks' and Parker.



ORIGINAL PAGE

Figure 5.5(d): Comparison of phase estimates to those of Banks and Parker.

PHASE OF Q VS. PERIOD



should yield response functions that are compatible with estimated magnitudes.

Since the frequency range considered should be sensitive to near-surface conductivity structures, layers of varying conductivity were superimposed onto the top 500 km of Banks' model. With a 30 km, .001 mho/m layer replacing the top 30 km of Banks' model, the calculated response magnitude agreed well with the estimated magnitude for periods less than  $10^5$  seconds (fig. 5.6, fig. 5.7a). Changing Banks' .01 mho/m layer to .02 mho/m, but maintaining the 500 km lower boundary (fig. 5.7) in this model, improved the agreement of estimated magnitude to the calculated magnitude in the vicinity of  $10^5$  seconds; the values for longer periods were too high. This establishes a conductivity range of .01 to .02 mho/m for depths just greater than 30 km (fig. 5.7). To test the sensitivity to layer thickness, the lower boundary of the .01 layer was varied from 500 km to 350 km (fig. 5.8); the magnitude shows very little change in this frequency range. Variance of conductivity from .01 to .02 mho/m with a lower boundary of 350 km (fig. 5.9) also shows very little change. Changing the conductivity from 2.mho/m to 1.mho/m for the layer below 500 km did not change the response function at all.

#### V.4. Ocean Effects on Response Function Q.

An electric current travelling a near-surface equatorial path would encounter continents with a lower conductivity than the oceans. The effective conductivity of an ocean-continental medium can be considered as a simple model in which the oceans and continents

are slabs of uniform cross-section but have a variable thickness.

From Ohm's law one can calculate the effective conductivity of a medium made up of slabs of varying thickness and two conductivities  $\sigma_1$  and  $\sigma_2$ :

$$\sigma = \frac{\sigma_1 \sigma_2}{\frac{\sum_i t_{1i}}{T} \sigma_2 + \frac{\sum_j t_{2j}}{T} \sigma_1} \quad (5.25)$$

where  $t_{1i}$  is the thickness of the  $i^{\text{th}}$  slab of conductivity  $\sigma_1$  and  $t_{2j}$  is the thickness of the  $j^{\text{th}}$  slab of conductivity  $\sigma_2$ .  $T$  is the total thickness and all slabs have the same cross-section area.

Applying equation 5.25 to an ocean-continental medium, surface area fractions of ocean ( $\sum_i t_{1i}/T$ ) and continent ( $\sum_j t_{2j}/T$ ) were estimated along the equator between  $30^\circ$  N and  $30^\circ$  S latitude. Using a  $5^\circ \times 5^\circ$  grid, estimates were made for each  $30^\circ$  longitude spread along the equator. Using typical continental conductivities of  $10^{-3}$  to  $10^{-1}$  mhos/m derived from magnetotelluric data (Gough, 1974), effective oceanic conductivities were calculated. For an ocean of 3.3 mho/m, these values are:

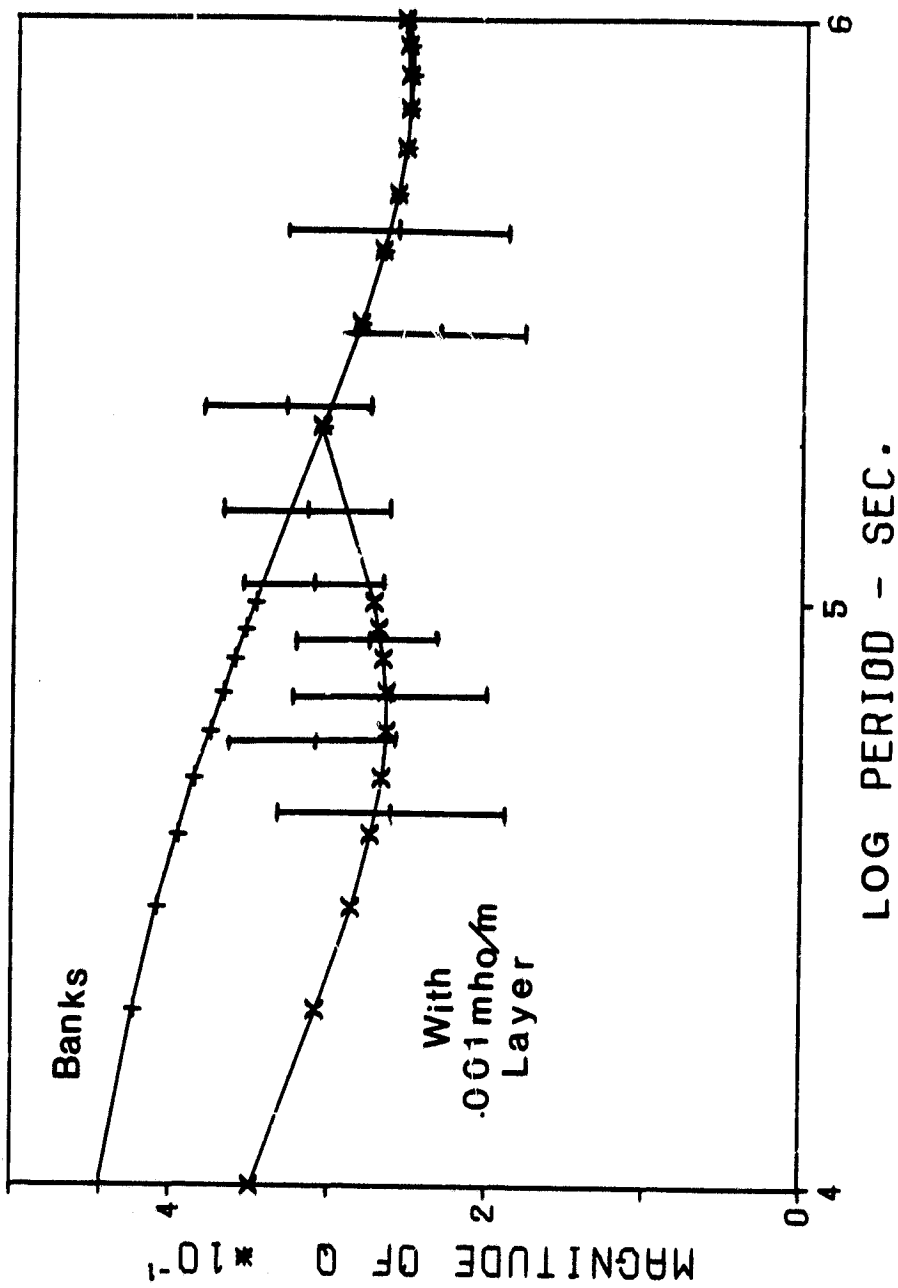
$$\begin{aligned} 3.78 \times 10^{-3} \text{ mhos/m for } 10^{-3} \text{ crust} \\ 3.76 \times 10^{-2} \text{ mhos/m for } 10^{-2} \text{ crust} \\ 3.49 \times 10^{-1} \text{ mhos/m for } 10^{-1} \text{ crust} \end{aligned}$$

The above relationships indicate that the effective conductivity is dominated by the continental conductivity.

Response functions were calculated for effective ocean

Figure 5.6: Comparison of estimated magnitudes to calculated magnitudes for Banks' 1972 profile and for Banks' profile with a 30 km surface layer at .001 mho/m.

MAGNITUDE OF Q VS PERIOD



LOG PERIOD - SEC.

C-2

Figure 5.7: Effects of variation of second layer (lower boundary at 500 km) from .01 mho/m to .02 mho/m.

(a) with .01 mho/m layer

(b) with .02 mho/m layer.

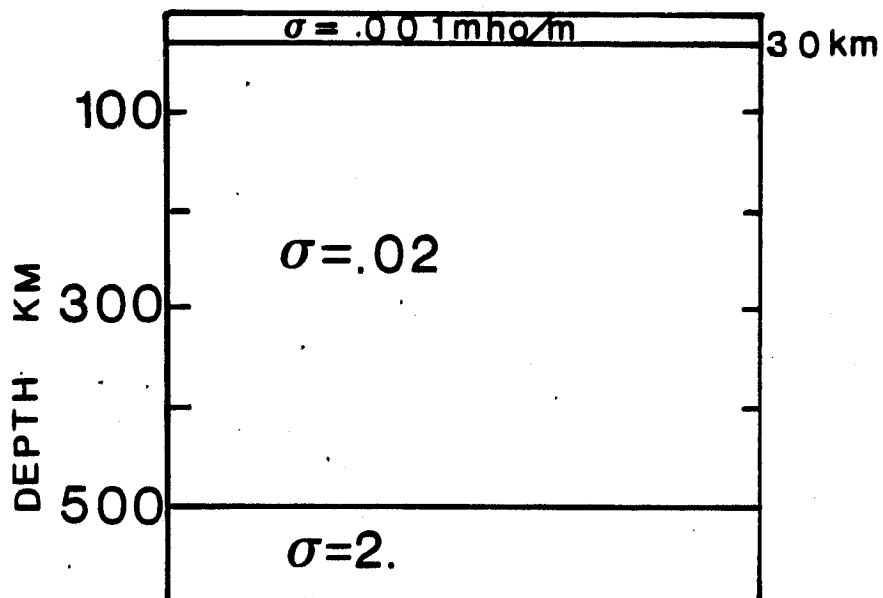
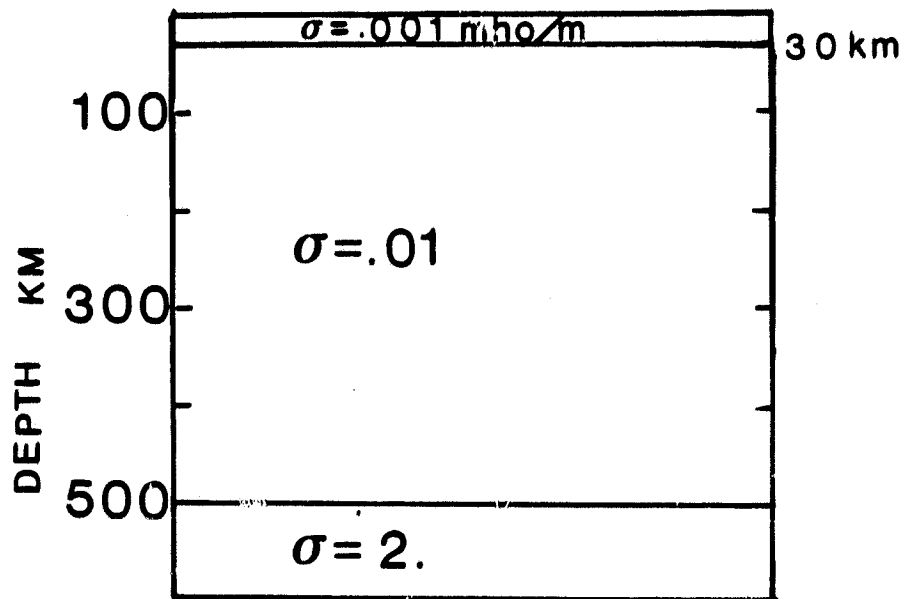


Figure 5.7: Effects of variation of second layer (lower boundary at 500 km) from .01 mho/m to .02 mho/m.

(c) Response magnitude estimates compared to calculated response magnitudes.

MAGNITUDE OF Q VS PERIOD

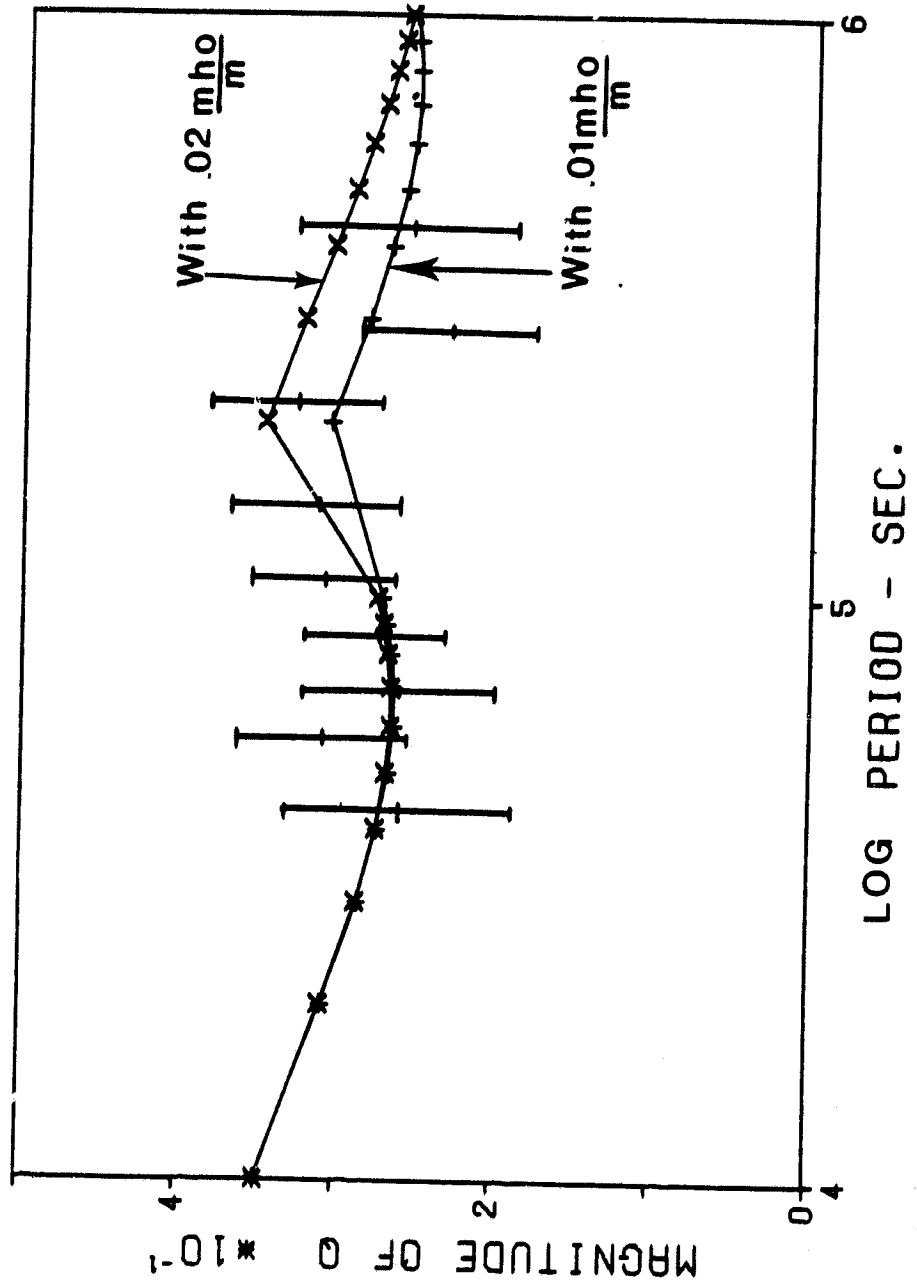
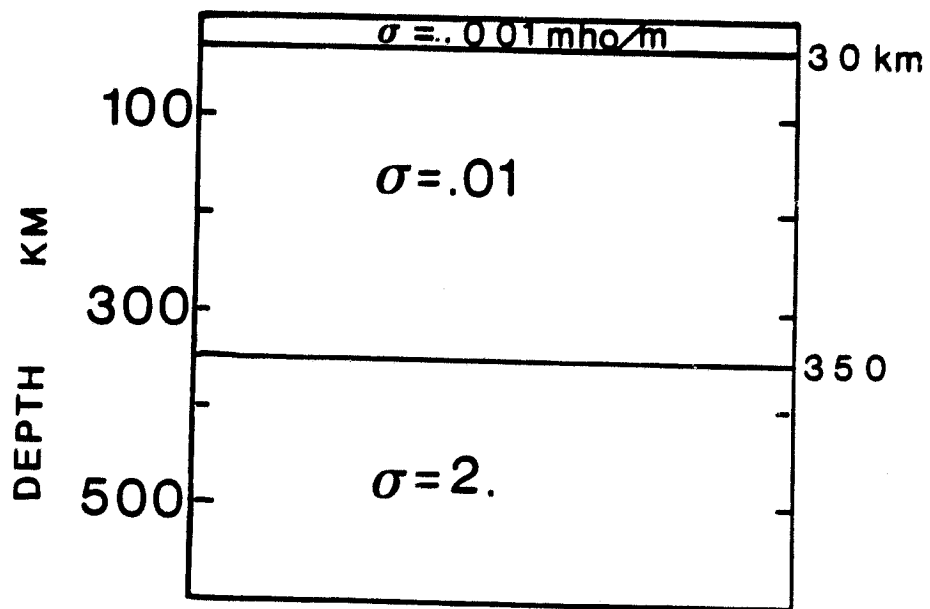
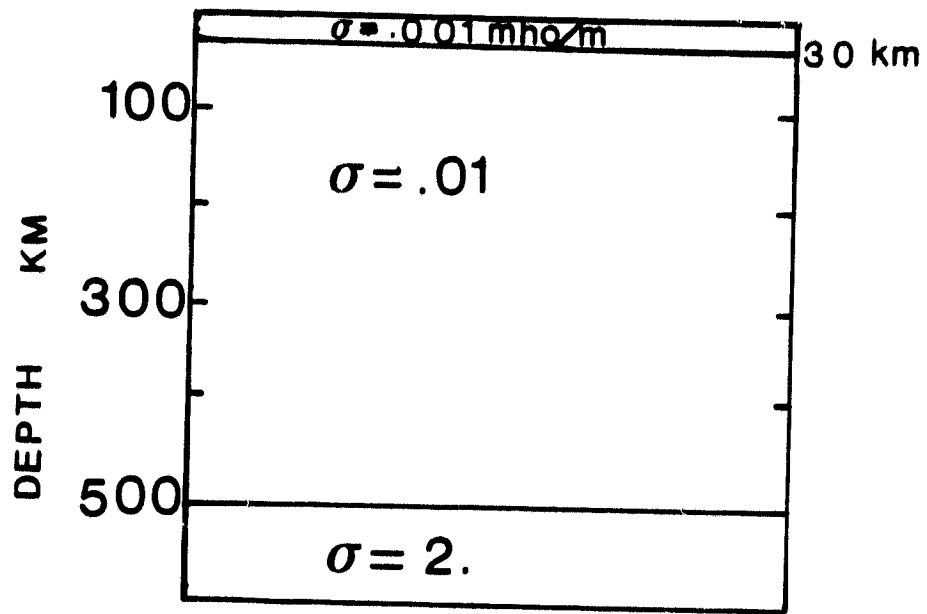


Figure 5.8: Effects of variation of second layer thickness.

(a) Lower boundary of .01 mho/m layer at 500 km.

(b) Lower boundary of .01 mho/m layer at 350 km.



**Figure 5.8: Effects of variation of second layer thickness.**

**(c) Response magnitude estimates compared to calculated  
response magnitudes.**

# MAGNITUDE OF Q VS PERIOD

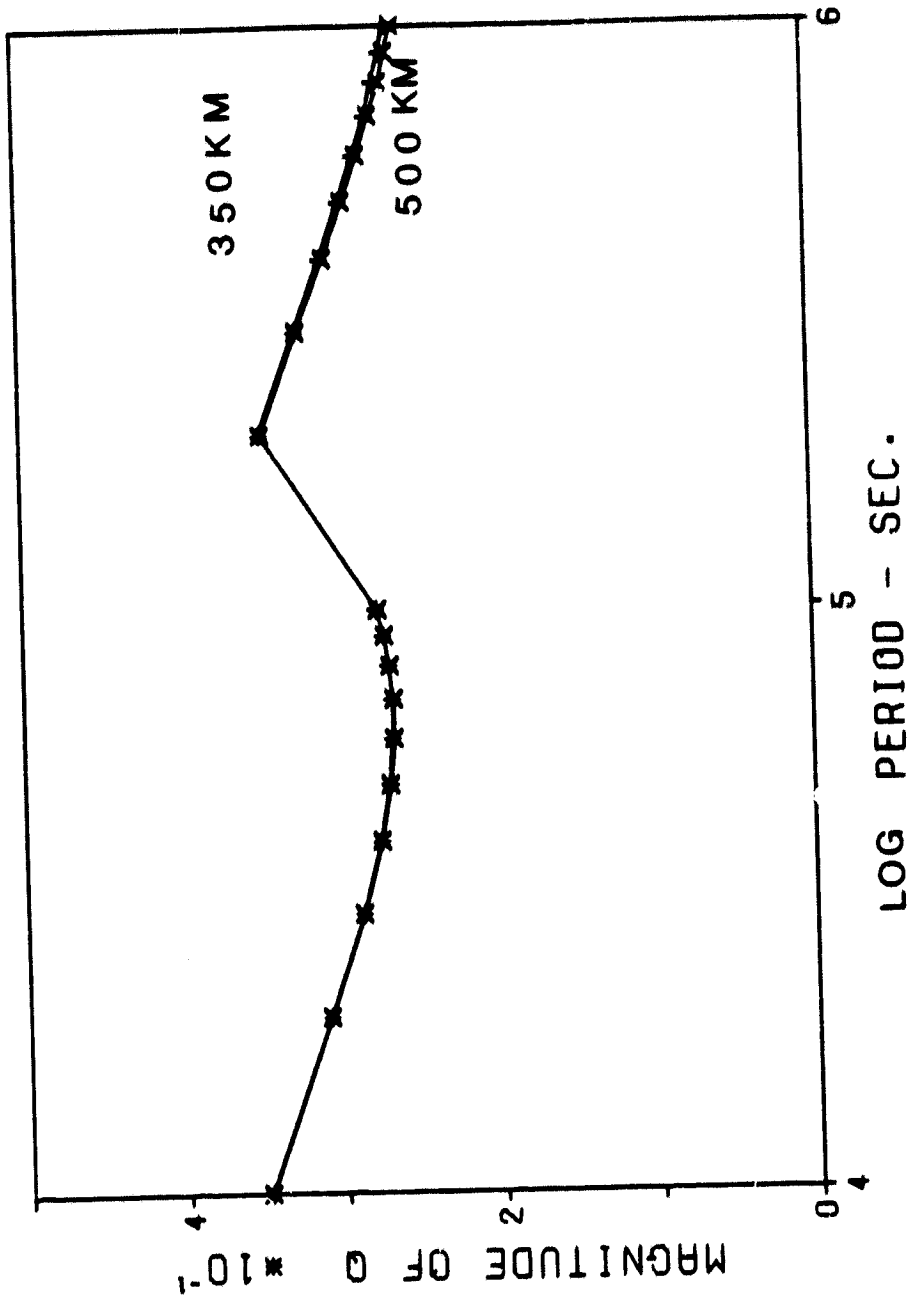
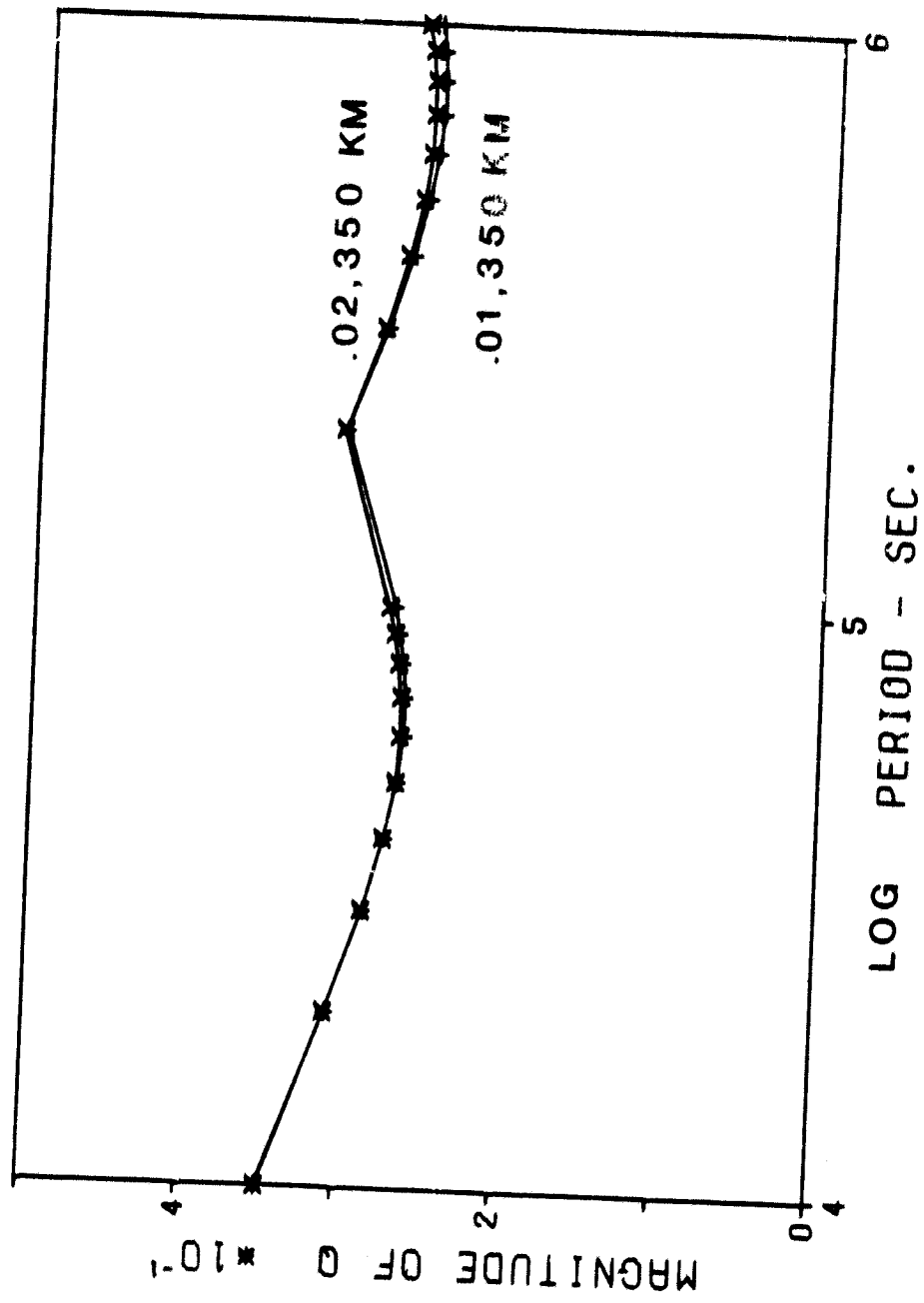


**Figure 5.9: Effects of variation of second layer (lower boundary at 350 km) from .01 mho/m to .02 mho/m.**

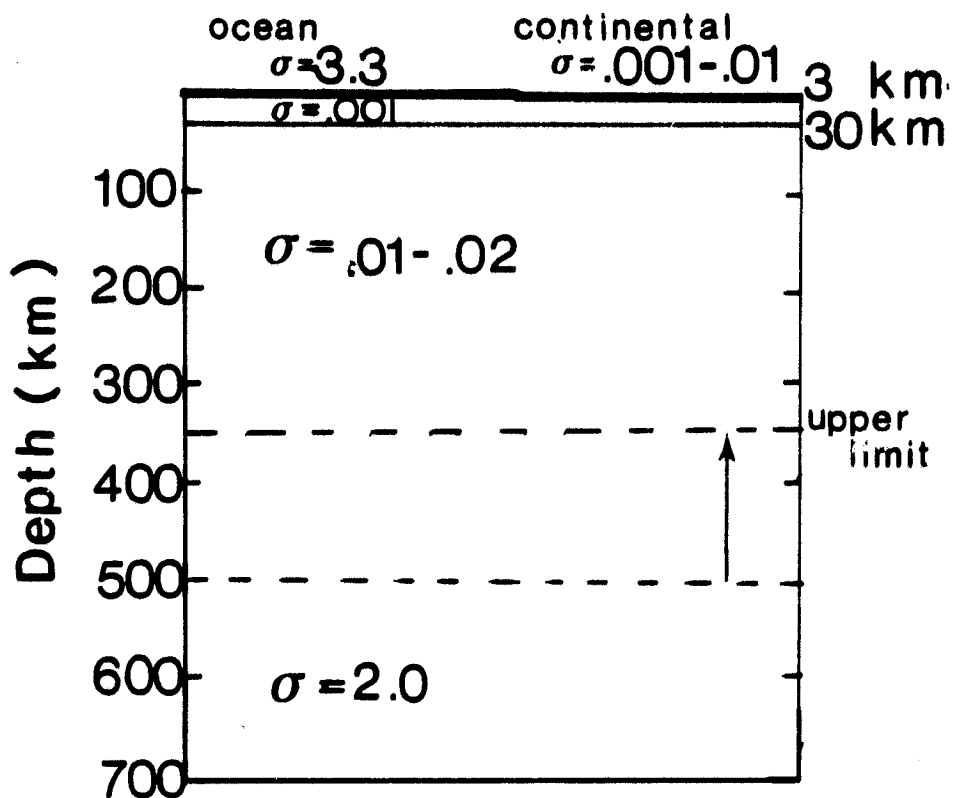
# MAGNITUDE OF Q VS PERIOD



conductivities superimposed onto the model (fig. 5.7). The .00378 mho/m ocean of 3 km thickness made virtually no difference in calculated response function when compared to the original model. The .0376 mho/m ocean raised the response function magnitude for periods just below the data range. For effective ocean conductivities greater than .0376 mho/m, the response function magnitude is significantly raised in the frequency range of interest. Since our estimated magnitudes are much lower than these values, an upper bound of .01 mho/m is placed on continental conductivity for the top 3 km (fig. 5.10).

**Figure 5.10: Conductivity profile for estimated response function.**

## Conductivity (mho/m)



## CHAPTER VI: TEMPERATURE IN THE MANTLE

VI.1. Relation of temperature to conductivity

Electrical conductivity estimates for the earth are often related to temperature. This is a valid relation if the conductivity is intrinsically controlled by temperature and if the composition is known. Estimated electrical conductivity for the upper mantle and the crust is within the range of semiconductors ( $10^{-9}$  to  $10^2$  mho/m). For these materials, conductivity depends upon populating the "conduction band" (fig. 6.1) with electrons from the "valence band". In the intrinsic temperature range, electrons are thermally activated into the conduction band, where they become mobile and contribute to the conductivity. This temperature dependence is expressed by

$$\sigma = \sigma_0 \exp (-E_g/2kT) \quad (6.1)$$

where  $k$  is Boltzman's constant,  $T$  is temperature,  $\sigma_0$  is a constant characteristic of the semiconductor, and  $E_g$  is the activation energy or "gap energy". A plot of the logarithm of resistivity vs  $1/T$  reveals a straight line (fig. 6.2) if the semiconductor is intrinsically controlled.

At higher temperatures, a semiconductor may become an "ionic conductor". Here, the charge carriers are ions (lattice defects) rather than electrons (electron-hole pairs). Conductivity is controlled by the rate of diffusion of the ions. For sufficiently high temperatures, ion diffusion is also temperature controlled, implying that conductivity can be represented by

Figure 6.1: In an intrinsic semiconductor, electrons are thermally excited from the valence band into the conduction band, where they become mobile. (Kittel, 1971)

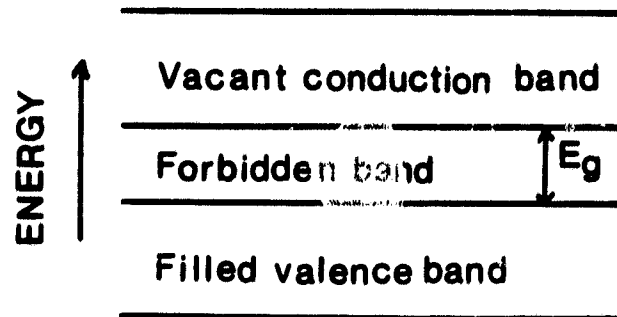
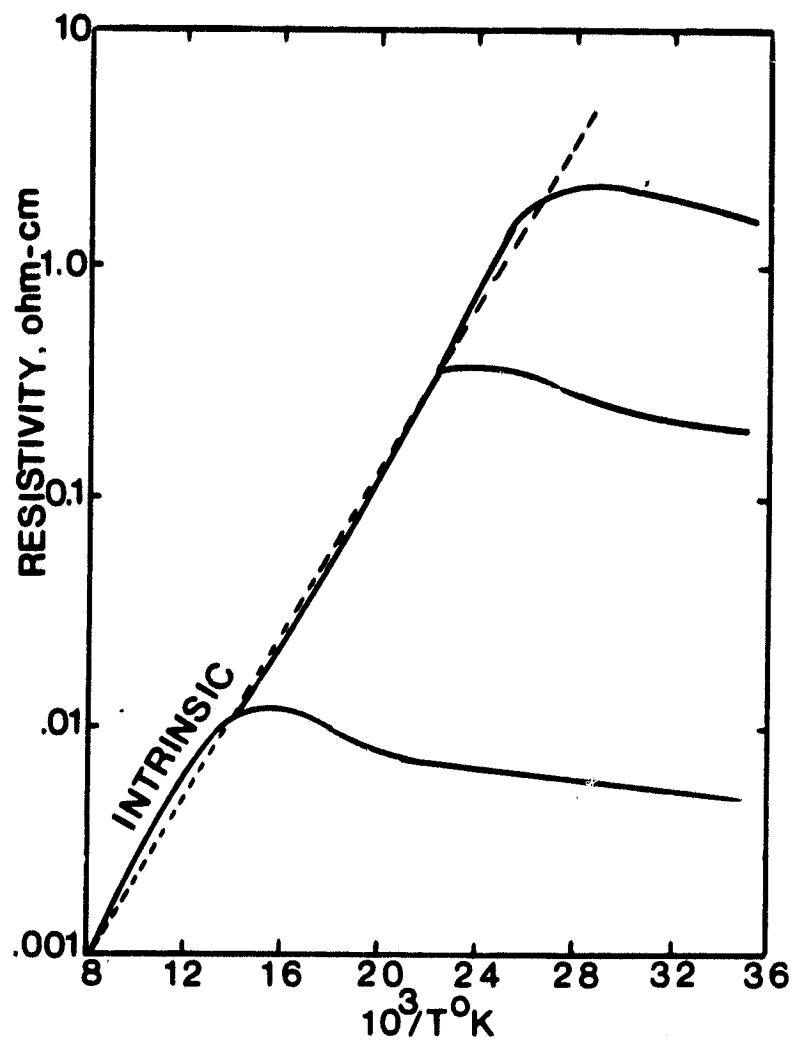


Figure 6.2: A material may be an extrinsic semiconductor at low temperatures and an intrinsic semiconductor at higher temperatures. Here, germanium is doped with varying amounts of gallium resulting in different temperatures for intrinsic semiconduction to occur. (Kittel, 1971)



ORIGINAL PAGE 1  
OF FOUR

$$\sigma = \sigma_0 \exp(-E/kT) = Nq\mu \exp(-E/kT) \quad (6.2)$$

where  $\sigma_0 = Nq\mu$ ,  $N$  is ion concentration,  $q$  is charge,  $\mu$  is ion mobility, and  $E$  is the activation energy for an ion to move from one location to a similar one.

Pressure effects probably have little or no influence on intrinsic semiconduction where the charge carriers are electrons. Experimental results for pressures up to 8 kb indicate that conductivity is weakly affected (Duba, et. al., 1974). Pressure effects might become more significant where ionic conduction is the dominant mechanism since lattice compaction may affect ion mobility. However, it is difficult to say what such pressure effects might be (Misener, 1973). In any case, it is probably safe to assume that temperature effects will dominate over pressure effects.

## VI.2 Composition of the mantle

The velocity of the seismic P-wave in the upper mantle is  $8.2 \pm 0.2$  km/sec which indicates a density of  $3.3 \text{ g/cm}^3$ . This observation along with petrological considerations, suggests an upper mantle composition of peridotite (olivine + pyroxene  $\pm$  spinel) and/or eclogite (pyroxene + garnet  $\pm$  quartz). Eclogites, which are thought to be of mantle origin, tend to have slightly higher density than expected for the mantle. Peridotite is generally considered the more likely mantle material.

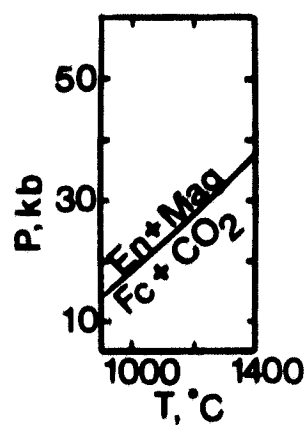
A peridotite mantle is also suggested by the common occurrence of peridotite inclusions found in Kimberlite pipes. Among these xenoliths, olivine ( $\text{Fo}_{88-94}$ ) is the principal mineral,

with an average olivine/orthopyroxene ratio of 2/1 (Ringwood, 1975). Garnet lherzolite -- the most common peridotitic inclusion -- is composed of olivine 64%, orthopyroxene 27%, clinopyroxene 3%, pyrope - rich garnet 6% (Ringwood, 1975). Such petrological observations lead to the assumption that the properties of the upper mantle can be approximated by the properties of olivine ( $Fe_{88-94}$ ). This single mineral model is further supported by Birch (1969), who concluded that the elastic properties of the upper 200 km of the mantle could be represented to first order approximation by a homogeneous layer of olivine.

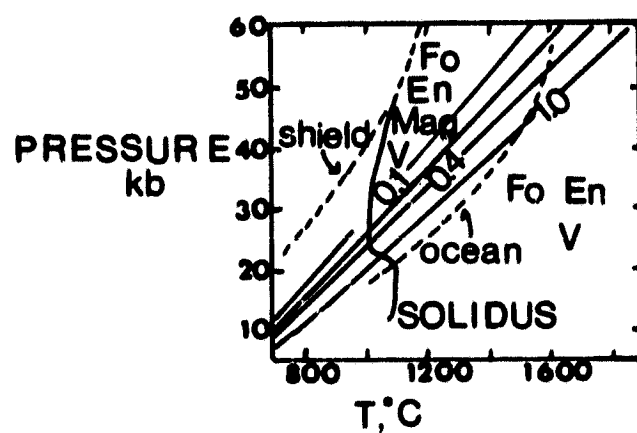
A peridotitic mantle, composed mainly of olivine, is also a convenient model for explaining various seismological occurrences. First, the almost worldwide increase in seismic velocity at the Mohorovičić boundary could be attributed to the transition from a gabbroic lower crust to a peridotitic upper mantle. Secondly, the increment in seismic velocity observed at 420 km could be explained by a phase transition of olivine from a low-pressure orthorhombic form to a high pressure spinel structure. Finally, the low-velocity zone, occurring between 60 and 150 km beneath the oceans and in the vicinity of 200 km under shield areas, is believed to be due to incipient partial melting. This localized phenomenon could be the result of the depressed melting temperature of peridotite at 20-30 kb in a  $CO_2$  and  $H_2O$  environment (Eggler and Kushiro, 1979; Fig. 6.3).

Alternative mantle models have included an eclogite mantle and an eclogite + peridotite mantle. As already mentioned, an eclogite mantle would have a higher density than would be expected from seismic observations. Also, an eclogitic mantle would require an intermediate

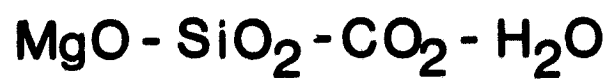
Figure 6.3: P-T diagram for the reaction  $\text{En} + \text{Mag} = \text{Fo} + \text{CO}_2$ .  
(A) Calculated boundary for the reaction. (B) Shown are the phase assemblages for a peridotite composition in the system  $\text{MgO-SiO}_2\text{-CO}_2\text{-H}_2\text{O}$  containing less than 20 weight percent  $\text{CO}_2$ . The solidus is for peridotite with amounts of  $\text{H}_2\text{O}$  and  $\text{CO}_2$  small enough to be buffered within the system. (Eggler and Kushiro, 1979)



A



B



step between the gabbroic crust at 15 kb and the eclogite mantle at pressures above 20 kb (Carmichael, Turner, Verhoogen, 1974). A garnet-granulite assemblage (garnet + pyroxene + plagioclase) could exist at the 20 + 3 kb pressure regime but, the complex "phase transition" of gabbro-granulite-eclogite is incompatible with the sharp Moho discontinuity. Although an eclogite mantle is favored by some for its compatibility with certain magma genesis models, a peridotitic mantle seems the preferred model.

### VI.3 Electrical conductivity of olivine (Fo<sub>88-94</sub>)

Early investigations (Misener, 1973) indicated that olivine (Fo<sub>88-94</sub>) is an extrinsic (impurity controlled) semiconductor below 800°C. Later measurements (Duba, 1974) showed the expected temperature dependence for temperatures greater than 800°C. Because of kinetic effects and apparatus problems, accurate measurements of conductivity is limited to temperatures below 1500°C.

A necessary condition in all high temperature experiments is to have controlled oxygen fugacity ( $f_{O_2}$ ). Nitsan (1974) showed that olivine (herein chosen to be the representative case of Fo<sub>90</sub>) is stable over a limited range of oxygen fugacities. Outside of the stability field, olivine will oxidize or reduce to other minerals. Duba (1976) found that electrical conductivity varies less than 1/3 of a magnitude for changes of  $f_{O_2}$  within the stability field. However, for  $f_{O_2}$  variations outside of the stability field, conductivity can change by several orders of magnitude (fig. 6.4). These reaction products apparently provide better electrical pathways.

Figure 6.4: Stability field of olivine ( $Fo_{90}$ ) is defined with regard to temperature and pressure (Nitsan, 1974). Also included are buffers OQPM (fayalite-quartz-pyroxene-magnetite), OQM (fayalite-quartz-magnetite), MW (magnetite-wustite), and WI (magnetite-iron). "Error bars" are the region where Duba (1976) tested the variation of conductivity with variation in  $f_{O_2}$  within the stability field and found that conductivity varied less than 1/3 magnitude.

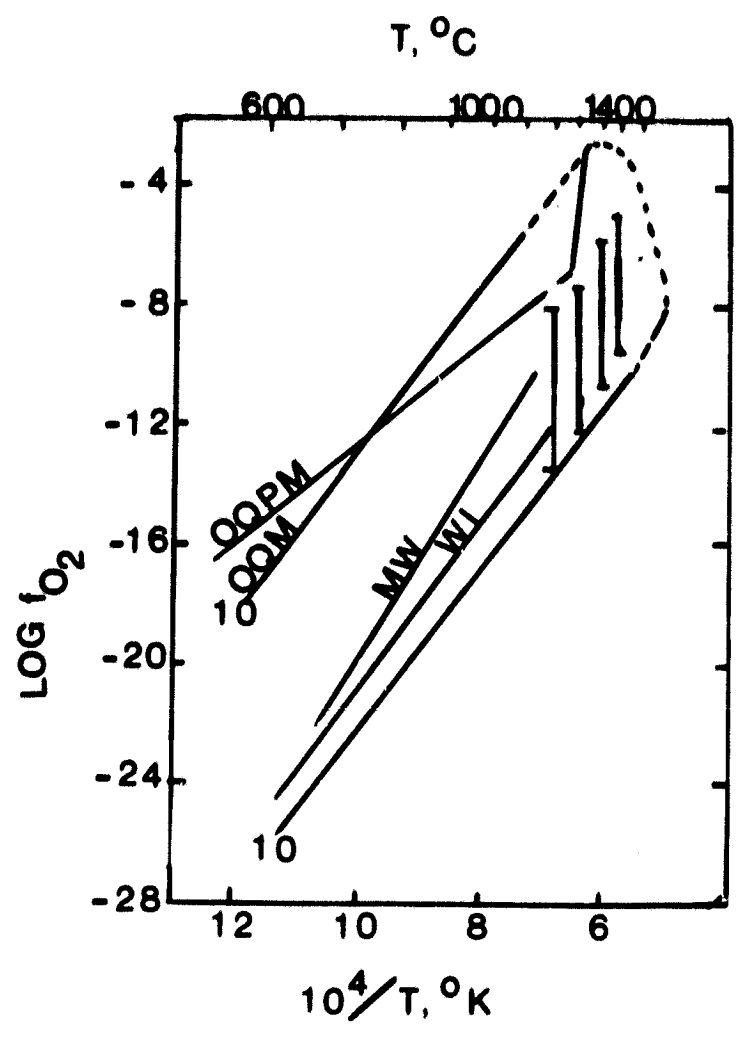




Figure 6.5: Variation of conductivity as a function of temperature for single crystal olivine ( $\sim\text{Fo}_{90}$ ). (a) Olivine from San Carlos Indian Reservation (Duba and Nicholls, 1973; Duba, 1976) (b) Olivine from St. John's Island (Duba, et.al., 1974; Duba, 1976) All are under controlled oxygen fugacity.

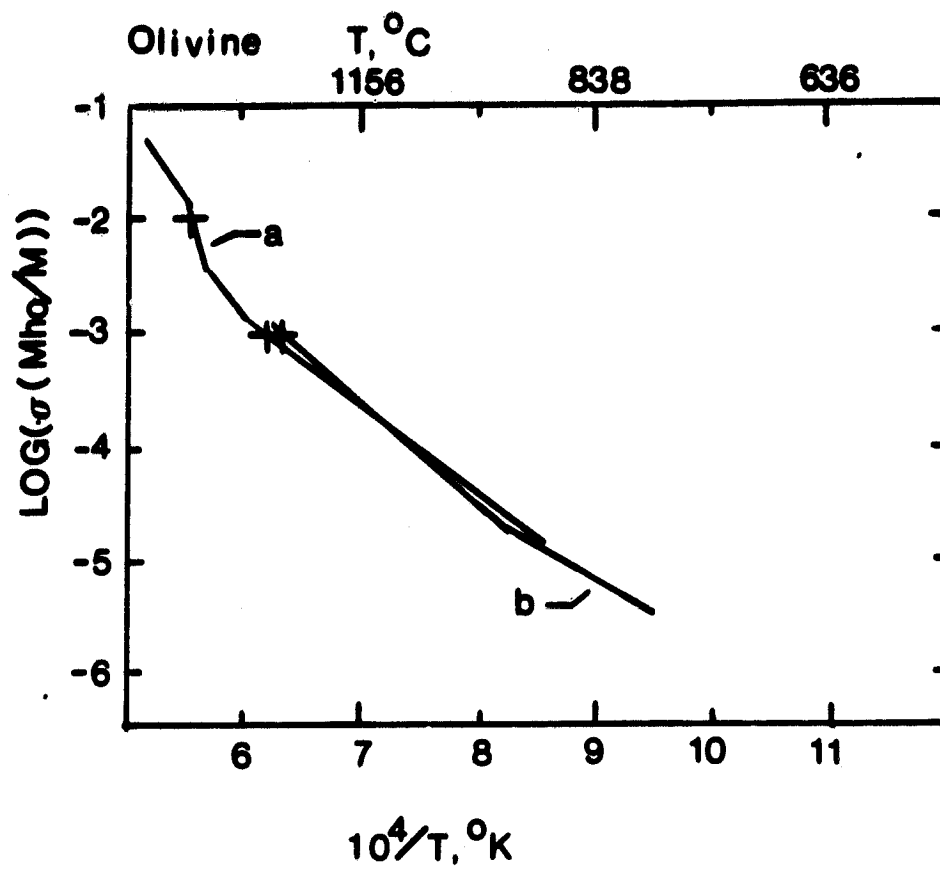
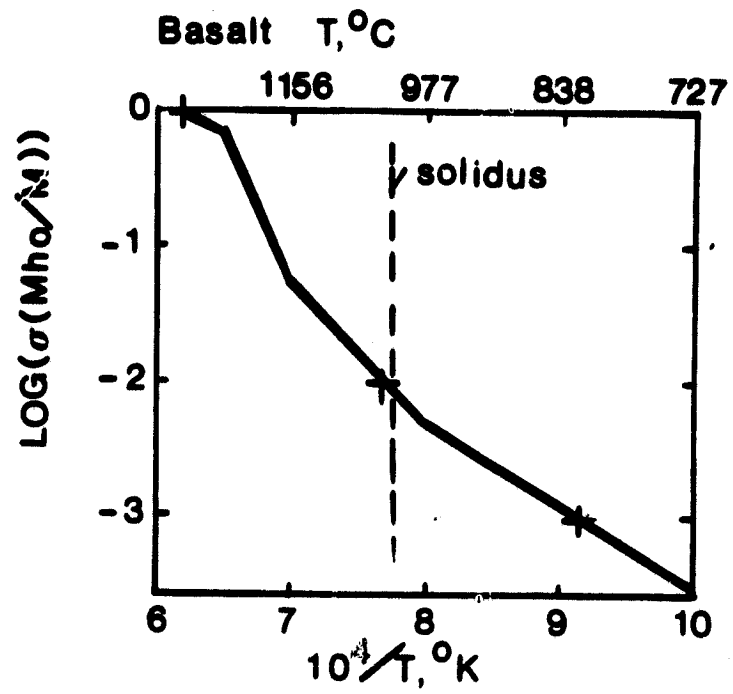


Figure 6.6: Electrical conductivity as a function of temperature for basalt at controlled oxygen fugacity (Duba, et. al., 1975).

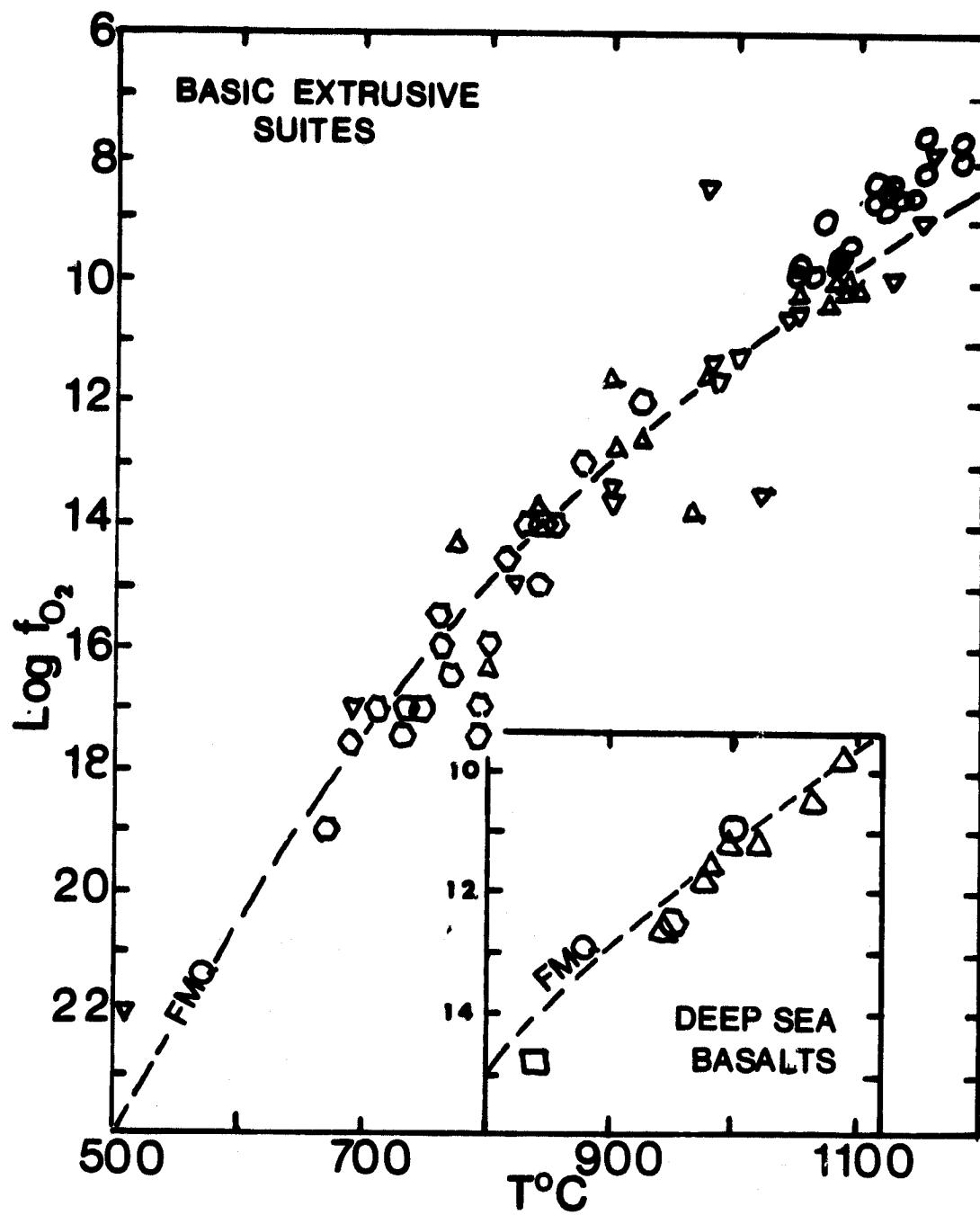


become  $\log(f_{O_2}) = -7.94$  at 32 kb and  $\log(f_{O_2}) = -6.02$  at 124 kb. The rate of change of  $\log(f_{O_2})$  with pressure is different for different reactions, so the overall shape and location of the stability field will change with pressure. Compared to the stability field at 1 bar, there will be little change at shallow depths (100 km, 32 kb) and some change before the transition zone (400 km, 124 kb). Still, since the electrical conductivity does not change drastically for  $f_{O_2}$  within the stability field, this pressure effect is of minor importance in this study.

#### VI.4 Temperature as a function of depth

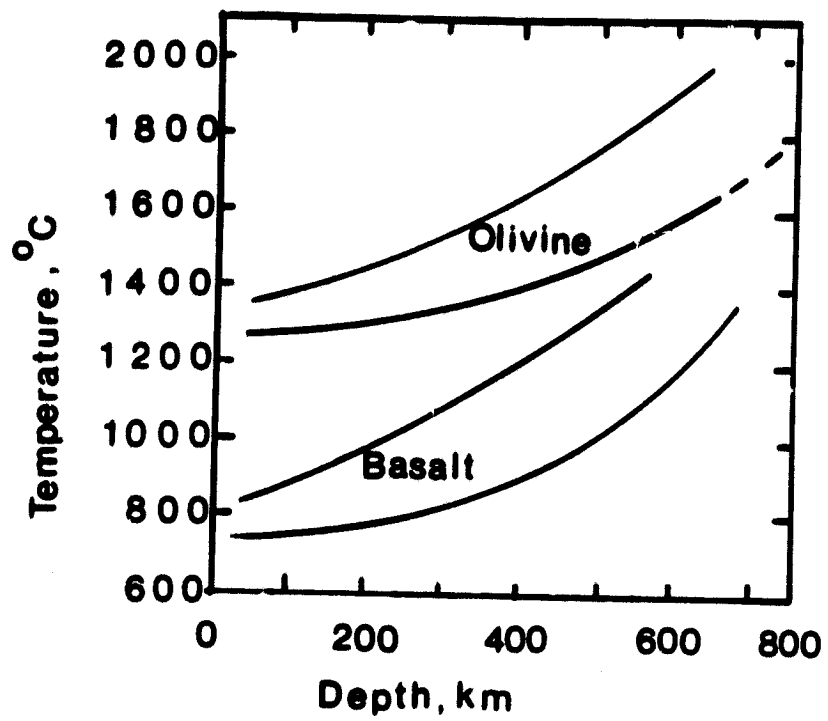
Numerous chemical analysis of basalts from around the world imply that the  $f_{O_2}$  within the mantle should be near the fayalite-magnetite-quartz buffer (fig.6.7). The olivine conductivities (fig.6.5) used here are at controlled  $f_{O_2}$ 's within the stability field of olivine ( $Fe_{90}$ ) but vary from the oxidizing side to the reducing side as a function of temperature (Duba, 1976). Knowing that variations in  $f_{O_2}$  within the stability field result in changes of conductivity up to 1/3 magnitude, a certain amount of error is allowed for  $f_{O_2}$ . Also, knowing that the depths obtained in the estimated conductivity profile (fig.5.10) derived from "Q" are upper limits, error is allowed for location. Considering these error contributions, a temperature profile based on the conductivity of olivine ( $Fe_{90}$ ) and basalt is presented (fig.6.8). The two profiles differ a great deal, but this difference may largely be due to experimental errors in the determination of conductivity in basalts.

**Figure 6.7: Oxygen fugacity calculations for basalts from around the world. There is a strong tendency to follow the fayalite-magnetite-quartz (FMQ) buffer (Haggerty, 1976).**



ORIGINAL PAGE IS  
OF POOR QUALITY

Figure 6.8: Temperature profiles estimated from response function  $\hat{Q}$  and associated conductivity. Conductivity-temperature relation for olivine is from fig.6.6. Conductivity-temperature relation for basalt is from fig.6.7.



Temperature estimates for depths down to 200 km were made using detailed compositional analysis of kimberlites (Boyd, et. al., 1973; fig. 6.9). The resulting temperature profiles (fig. 6.10) intersect the "Q" profile (based on electrical conductivity of olivine) in the 150 to 200 km range. For shallower depths, the geochemical geotherms are much lower than what is indicated by Q. This disagreement may be due to several factors. One very likely error is in assuming that olivine is the controlling agent for shallow conduction. Other materials are probably controlling conductivity at shallow depths. At temperatures below 800°C, conductivity is impurity controlled rather than temperature controlled -- leading to conductivity values higher than would be expected. Finally, very low conducting surface layers ( $10^{-4}$  mho/m or less) would not be seen by the induction method employed here for frequencies of 0.2 to 2.0 cycles/day (according to tests employing the forward problem calculation for Q). The pyroxene geotherm combined with the olivine measurements indicate a conductivity of  $10^{-5}$  mho/m near the surface -- this value is too low to be detected.

**Figure 6.9: Geotherm estimates based on detailed compositional analysis of lherzolite nodules from kimberlites. Slight differences in geotherm will occur depending on how pressure is calculated (Boyd and Nixon, 1973).**

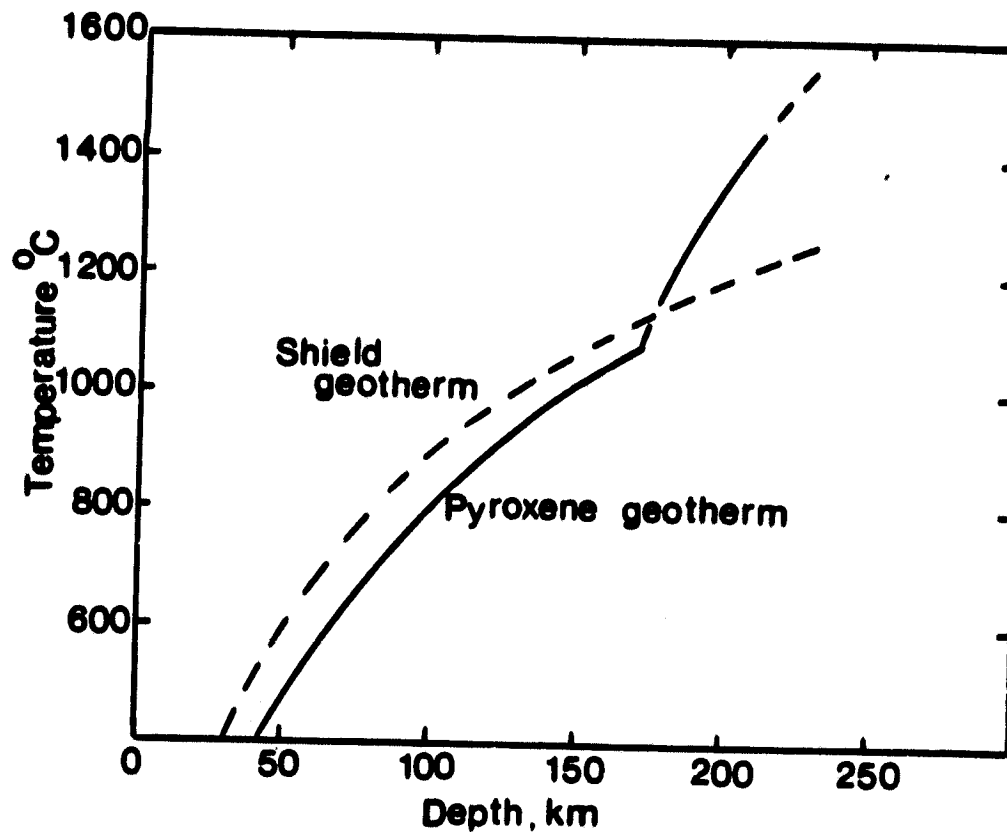


Figure 6.10: Comparison of "Q" geotherm to pyroxene geotherm of Boyd and Nixon (fig.6,9). Q geotherm is based on electrical conductivity of olivine (fig.6.5).

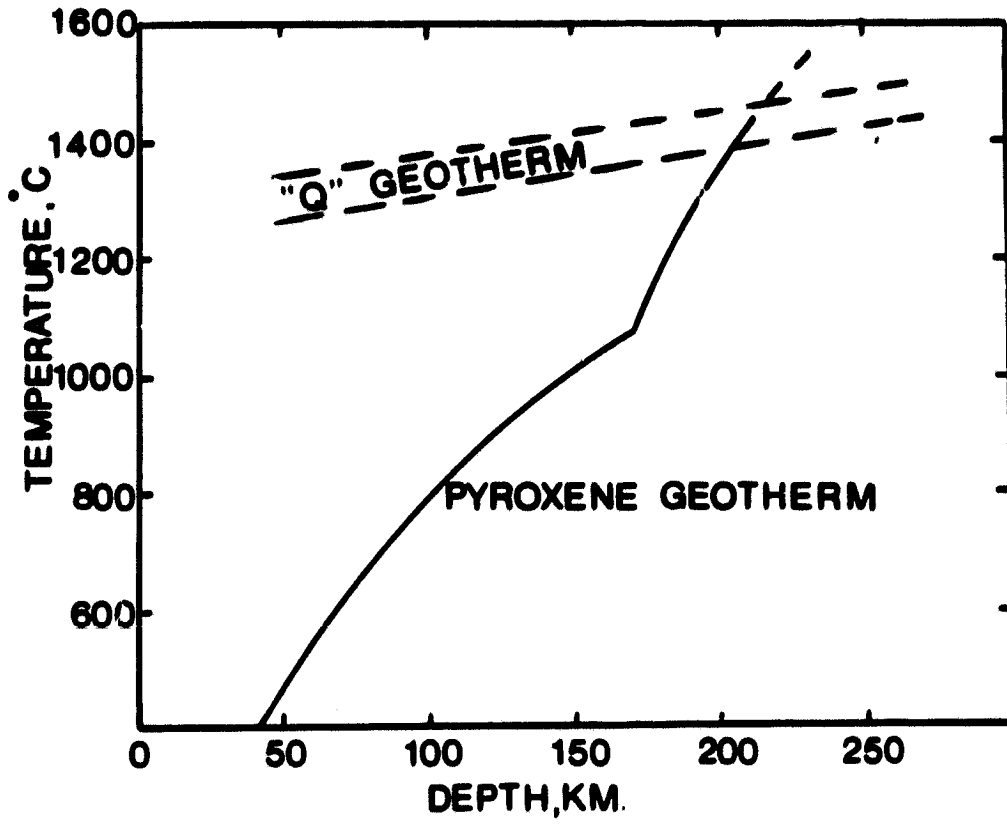
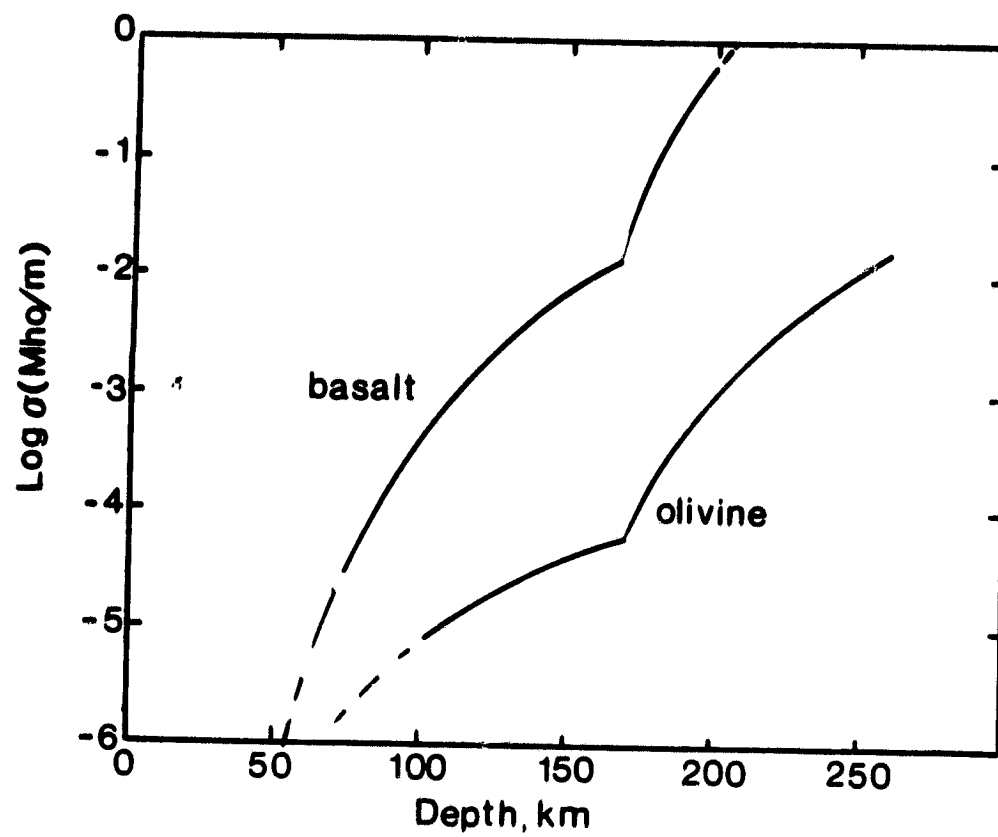


Figure 6.11: Expected electrical conductivity profiles for the upper 250 km if pyroxene geotherm is correct (fig.6.9). Conductivity estimates are based on olivine (fig.6.5) and basalt(fig.6.6).



## CHAPTER VII: CONCLUSION

A global electrical conductivity profile for the upper mantle and crust is obtainable through analysis of satellite magnetic field data. The resulting profile is based on estimates of  $Q(\omega)$  for frequencies of 0.2 to 2.0 cycles/day. This range is higher than that generally used in global induction studies using land observatory data.

The upper mantle has a characteristic conductivity of order  $10^{-2}$  mho/m. This result is compatible with Banks' (1972) model but is not compatible with Parker's (1970) values of order  $10^{-1}$  mho/m. Considering laboratory measurements of conductivity of olivine (Duba, 1976), Parker's conductivity would correspond to temperatures that would melt the mantle.

Shallow structures are indicated by the response function  $\hat{Q}(\omega)$ . An upper limit of  $10^{-2}$  mho/m is placed on the top 3 km of crust. Beneath this, a conductivity of  $10^{-3}$  mho/m extends downward to at least 30 km depth before increasing to values of order  $10^{-2}$  mho/m. The bottom of the  $10^{-2}$  mho/m layer is difficult to define because of the limited range of frequency, but the lower boundary has an upper limit of 350 km.

In relating temperature to conductivity, the temperature profile derived from conductivity estimates is acceptable for depths greater than 150 - 200 km. For shallower depths, temperatures based on olivine conductivity are too high for a peridotitic mantle.

This disagreement between the "Q" geotherm and the pyroxene geotherm leads to several possible problems. One is in assuming that olivine is the controlling agent in shallow conduction. We know from numerous geological studies that it is not the main material in very shallow depths. Basalt conductivity measurements may be more appropriately applied to this study, but laboratory measurements tend to be unreliable. Another problem concerns the sensitivity of this induction method to shallow, low conducting layers. The pyroxene geotherm combined with the olivine measurements would indicate conductivities of order  $10^{-5}$  mho/m -- such conductivities would not be seen by Q estimates for frequencies 0.2 to 2.0 cycles/day. Whether or not the surface conductivity is  $10^{-4}$  or  $10^{-5}$  is a moot point with regards to temperature since at such low temperatures, the conductivity is impurity controlled.

As for the conductivity profile itself, magnetotelluric measurements are compatible with the shallow structure -- but local field measurements also indicate values both higher and lower than estimated from Q. However, the upper mantle value of  $10^{-2}$  mho/m seems quite reliable.

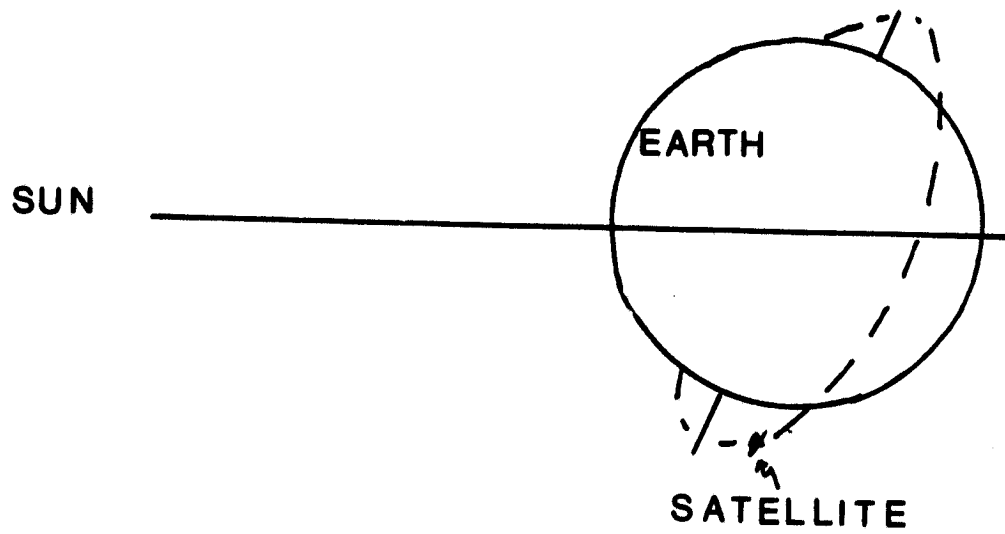
## Appendix A: Polar Orbit

(illustration on next page)

Characteristics of satellite orbits:

Satellite	launch date	inclination	perigee	apogee
OGO 2	Oct.14,1965	87.3 <sup>o</sup>	410 km	1510km
OGO 4	July 28,1967	86.0 <sup>o</sup>	410 km	910 km
OGO 6	June 5,1969	82.0 <sup>o</sup>	400 km	1100km

(Langel,1979)



**POLAR ORBIT**

Appendix B: Main program for finding  $e(t)$  and  $i(t)$

```

C      PROGRAM NAME IS 'FIFIO'
C      ** AS OF MARCH 7, 1980
C      ATTEMPTS TO WRITE ON TEMPORARY DISK FILE.
C      NOTE: ICL
C      CALLS GUESS5 FOR INTERPOLATION
C      CALLS ECMP FOR ANOMALY CORRECTION
C
C      PURPOSE IS TO CALCULATE E(T), I(T).
C      ORIGINAL PROGRAM WAS 'TS?' WHICH CALCULATES
C      E(F), I(F), RATIO, AND PLOTTING ROUTINES.
C      *****
C      INTEGER*2 IN(10,50), IPASS
C      DIMENSION AREA(301), MSIN(50)
C      DIMENSION EIMAT(150,3)
C      DIMENSION OUT2(150,4)
C      COMMON /FLDCOM/ST,CT,SPH,CPH,R,NMAX,RT,RP,RR,H
C      DATA RATIO/.10/,RAD/57.295779/
C      DIMENSION PDT(5,150)
C      REAL*8 DTAPE
C      DATA DTAPE/'0F4206'/.SEAS/1./, IOTYPE/1/, NUNIT/R/, IPASS/ 0/
C      DATA IO/O/, NFILE/1/ , IX/O/
C      EQUIVALENCE(IN(1,1), AREA(52)) , (MJD, AREA(1)), (MSIN(1), AREA(2))
C      COMMON /CAL SWITCH
C      BARHEIMAT FOR E AND I:
C      SWITCH=0.0
C      SWITCH=1.0 INDICATES CALCOMP PLOTS
C      ITEST=0
C      IE=0
C      L=1
C      CALL FIELDG(0.,0.,0.,)96R.,.18,L,A,D,C,F)
C      REWIND 5
C      READ (15,400) NJDS,NJDE,MSS,MSE,IPR
C      WRITE(7,400) NJDS,NJDE,MSS,MSE,IPR
400  FORMAT (2I5,3I10)
C      WRITE (6,501) NJDS,NJDE,MSS,MSE ,IPR
501  FORMAT (2X,2I5,3I10)
C      TM=CNVJUL(NJDS)
C      LREAD = 1
C      LPRINT=1

```

	NMX = 14	0000041
	CALL MOUNT(IOTYPE,NUNIT,DTAPE)	0000042
1	INC=0	0000043
	DBM = 0.	0000044
	IFS = 0	0000045
	INL=0	0000046
	IPC=0	0000047
	TT=0.0	0000048
	RA=0.0	0000049
	IC=0	0000050
C	DUMMY VARIABLE IC USED FOR PLOT SUBROUTINE. HAVE	0000051
C	MODIFIED ORIGINAL PROGRAM BY ADDITIONS AND BY	0000052
C	CALLING OTHER SUBROUTINES AT NUMBER 500 INSTEAD OF STOP2.	0000053
	READ (15,450) TU	0000054
	WRITE(7,450) TU	0000054
450	FORMAT(1X,F5.2)	0000055
	WRITE(6,470) TU	0000056
470	FORMAT(1X,'LOCAL TIME USED:',2X,F5.2)	0000057
	A=TU+ 1.0	0000058
	BA=TU-1.0	0000059
4	CALL POSN(IOTYPE,NUNIT,NFILE)	0000060
5	CALL FREAD(AREA,NUNIT,LEN,6500,65)	0000061
	IF(LEN.NE.1204) CALL ABEND(5)	0000062
	IF(MJD.LT.NJDS) GO TO 5	0000063
	IF(MJD.GT.NJDE) GO TO 500	0000064
	INC = INC + 1	0000065
6	DO 50 I= 1,50	0000066
	IF(MSIN(I).EQ.-999) GO TO 5	0000067
	IF(MSIN(I).LT.0) GO TO 50	0000068
	IF(MJD.GT.NJDS.AND.MJD.LT.NJDE) GO TO 8	0000069
	IF(MJD.EQ.NJDS.AND.MSIN(I).LT.MSS) GO TO 50	0000070
	IF(MJD.EQ.NJDE.AND.MSIN(I).GT.MSE) GO TO 500	0000071
8	IF(IPASS.EQ.0) GO TO 9	0000072
	IF(IPASS.EQ.IN(8,1)) GO TO 10	0000073
	IF(IP.LT.20) GO TO 9	0000074
	IF(DPH.GT.5.) GO TO 9	0000075
	IF(A.LT.24.0.AND.BA.GE.0.0) GO TO 12	0000076
C	I HAVE REPLACED .OR. WITH .AND. IN THE ABOVE STATEMENT!!	0000077
C	LOCAL TIME CHOICE CORRECTED HERE. I HOPE!!!!!!	0000078
	IF(TML.GT.0.0.AND.TML.LT.1.0) GO TO 2	0000079
	IF(A.GE.24.0) GO TO 3	0000080
	BA= BA+ 24.0	0000081
	RA=ABS(TML-BA)	0000082
	BA=BA-24.0	0000083
	IF(RA.GT.1.0) GO TO 9	0000084

	GO TO 15	0000085
3	RA=ABS(A-TML)	0000086
	IF(RA.GT.2.0) GO TO 9	0000087
	GO TO 15	0000088
2	IF(A.GE.24.0) GO TO 16	0000089
	RA=ABS(TML-BA)	0000090
	IF(RA.GT.2.0) GO TO 9	0000091
	GO TO 15	0000092
16	A=A-24.0	0000093
	RA=ABS(A-TML)	0000094
	A=A+24.0	0000095
	IF(RA.GT.1.0) GO TO 9	0000096
	GO TO 15	0000097
12	IF(TML.LT.9A.OR.TML.GT.A) GO TO 9	0000098
15	FMS=MS	0000099
	UTMR = FMS/3600000.	0000100
	ISW = 1	0000101
13	DO 100 K=1,IP	0000102
	IF(PDT(J,K).LT.45.0.OR.PDT(1,K).GT.135.) GO TO 100	0000103
14	K = PDT(2,K) + 6371.	0000104
	TH = (90. - PDT(4,K)) / RAD	0000105
	ST = SIN(TH)	0000106
	CT = COS(TH)	0000107
	PH = PDT(5,K) / RAD	0000108
	SPH = SIN(PH)	0000109
	CPH = COS(PH)	0000110
	CALL FIELD	0000111
	ADR = 6371./K	0000112
	ADR3 = ADR**3	0000113
	THD = PDT(1,K) / RAD	0000114
	STD = SIN(THD)	0000115
	CTD = COS(THD)	0000116
	CHSA = (1.98027 - CT*CTD) / STD / ST	0000117
	IF(CHSA.GT.1.) COSA = 1.	0000118
	IF(COSA.LT.-1.) COSA = -1.	0000119
	SINA = SQRT(1. - COSA**2)	0000120
	RTD = HT*COSA - RP*SINA	0000121
	RPD = RP*COSA + HT*SINA	0000122
	IF(ISW.EQ.1) GO TO 18	0000123
	DH = -(E + ADR3*FI)*STD	0000124
	DZ = (E - 2.*ADR3*FI)*CTD	0000125
	RD = SQRT((DH-BTD)**2 + (DZ-RR)**2 + 4RPD**2)	0000126
	DR = RD - R	0000127
	IF(IPR.EQ.1) WRITE(6,95)(PDT(J,K),J=1,5),DR,DZ,DR,RD,R	0000128
95	FORMAT(//,2X,10F12.3)	0000129

```

SC1 = SC1 + (DM-PDT(3,K))*F2
GO TO 100
1* F1 = MTO*ST)
F2 = MR*CTD
MFTA = F1 + 2.*F2
ALPHA = F1 - F2
F1 = ALPHA/4
F2 = (META*ADR3)/K
SC1 = SC1 + PDT(3,K)*F1
SC2 = SC2 + PDT(3,K)*F2
S11 = S11 + F2*F1
S12 = S12 + F2*F2
SE1 = SE1 + F1*F1
100 CONTINUE
IF (ISW.EQ.1) GO TO 25
E = (SC1*S12-SC2*S11)/(SE1*S12-S11*S11)
F1 = -(E*SE1-SC1)/S11
RATIO = F1/E
TT=UTHR +(KDY-NJOS)*24.0
IC=IC+1
IF (IC.LE.150) GO TO 45
WRITE(6,80)
40 FOR AT(1X,'FROM HERE HAVE MORE THAN 150 POINTS',//)
IF (IC.EQ.151) IC=150
IF (IC.EQ.150) GO TO 500
45 EIMAT(10,1)=TT
EIMAT(10,2)=E
EIMAT(10,3)=F1
46 WRITE(6,90)
90 FORMAT(2X,'THIS IS MJD,UTHR,TOTAL TIME,DM,LOCAL T,E,1')
WRITE(6,97) KDY,UTHR,TT,DM,TML,E,F1
97 FORMAT(2X,15.6FH,2)
ISW = 2
SC1 = 0.
GO TO 13
25 AP = IP
SC1 = SORT(SC1/AP)
WRITE(6,98)
98 FORMAT(2X,'DM,E,FI,RATIO,AND SIGMA')
WRITE(6,96) DM,E,FI,RATIO,SC1
96 FORMAT(5X,5F12.5)
ISW = 1
IPASS = IN(4,1)
9 SC1 = 0.
SC2 = 0.

```

```

0000131
0000132
0000133
0000134
0000135
0000136
0000137
0000138
0000139
0000140
0000141
0000142
0000143
0000144
0000145
0000146
0000147
0000148
0000149
0000150
0000151
0000152
0000153
0000154
0000155
0000156
0000157
0000158
0000159
0000160
0000161
0000162
0000163
0000164
0000165
0000166
0000167
0000168
0000169
0000170
0000171
0000172
0000173
0000174

```

	S11 = 0.	0000175
	S12 = 0.	0000176
	SF1 = 0.	0000177
	DMM = 100.	0000178
	DPM = 20.	0000179
	IP = 0	0000180
10	DPLAT = IN(9,1)	0000181
	DPLAT=DPLAT/100.	0000182
	ADP = ABS(DPLAT)	0000183
	DM = IN(6,1)	0000184
	DM = DM/10.	0000185
	IF(ADP.GT.20.) GO TO 40	0000186
	IF(ADP.GT.DPM) GO TO 20	0000187
	DMM = ADP	0000188
	ALSNV = IN(5,1)/100	0000189
20	IF(DM.GT.DMM) GO TO 40	0000190
11	DMM = DM	0000191
	ALT = IN(4,1)*1.	0000192
	DPL = DPLAT	0000193
	TAL = IN(7,1)	0000194
	TIL = TAL/1000.	0000195
	MS = MSTP(1)	0000196
	KOV=ALN	0000197
40	IP = IP + 1	0000198
	IF(IP.GT.150) CALL ABEND(40)	0000199
	HT = IN(4,1)	0000200
	ALON = IN(3,1)	0000201
	ALAT = IN(2,1)	0000202
	PDT(1,IP) = 90. - DPLAT	0000203
	PDT(2,IP) = HT/10.	0000204
	PDT(3,IP) = DM	0000205
	PDT(4,IP) = ALAT/100.	0000206
	PDT(5,IP) = ALON/100.	0000207
	IF(ITEST.NE.0) GO TO 610	0000208
-600	WRITE(6,600) ALT,PDT(2,IP),PDT(3,IP),PDT(4,IP),PDT(5,IP)	0000209
	FORMAT(1X,'ALT= ',E10.3,' HT=',E10.3,' DM= ',E10.3,' LAT=',	0000210
	1E10.3,' LONG=',E10.3)	0000211
	ITEST=ITEST+1	0000212
- 610	CONTINUE	0000213
	IRTP=0	0000214
	XLAT=PDT(4,IP)	0000215
	HEIGHT=PDT(2,IP)	0000216
	XLONG=AKND(PDT(5,IP)+360.,360.)	0000217
	IF(XLAT.LE.-50..OR.XLAT.GE.50.) GO TO 460	0000218
	CALL ECOMP(XLAT,XLONG,HEIGHT,IRTP,DMA)	0000219

C		0000210
C	DHA IS AN ANOMOLY CORRECTION	0000211
C	LET DH = DH - DHA IN PDT(3,IP)	0000212
C		0000213
	IF(DHA.GT.-50.)PDT(3,IP)=PDT(3,IP)-DHA	0000214
640	CONTINUE	0000215
	IF(ITEST.NE.1) GO TO 620	0000216
	WRITE(6,60)PDT(3,IP)	0000217
620	ITEST=ITEST+1	0000218
601	FORMAT(5X,'FINAL DH IS ',E10.3)	0000219
50	CONTINUE	0000220
	GO TO 5	0000221
500	WRITE(6,650)	0000222
650	FORMAT(7,5X,'EIMAT(I,J) AS GUESS5 SEES IT',/)	0000223
	WRITE(6,700)((EIMAT(I,J),J=1,3),I=1,IC)	0000224
700	FORMAT(1X,3E12.3)	0000225
	CALL GUESS5(EIMAT,IC,OUT2,IE,AVE)	0000226
	STOP	0000227
	END	0000228

Appendix C: Data reduction programs for estimating  $\hat{Q}(\omega)$

includes:

Mad

INT3

Stack

Imsl and system library functions are also required.

Unlisted subroutines in Mad are listed in thesis by (Thayer, 1975)

FILE: MAD            FORTRAN A1            \*\*\* Brown University Computer Cen'

```

C   MAGNETIC ANALYSIS PROGRAM
C   OCTOBER 1979
C
  DIMENSION PERIOD (25), Q(500), WINDOW(500), TITLE(15), C(2)
  DIMENSION CONSQ(25), CON(25), QNAG1(25), QNAG2(25)
  DIMENSION QPHAS1(25), QPHAS2(25)
  COMPLEX C1(1000), C2(1000), P(2,2,25), X1Q(1000), X2Q(1000)
  COMPLEX Q1(25), Q2(25), ENERGY(500)
  DATA NAXN/1000/, NAXPER/25/
  RADDEG=57.295780
1  READ (5,1000,END=111) INPUT,NPER,INAX,LADD,MNIN,SEL,EXTENT
1000  FORMAT (5I5,2F10.0)
  READ (5,2000) (PERIOD(I),I=1,NPER)
2000  FORMAT (8F10.0)
  WRITE (6,3000)
3000  FORMAT (1H1,13(' ')//1X,'*',11X,'*'//1X,'*' MAGSAT '*'//1X,
1  '*',11X,'*'//1X,13('')////1X,
2  'THE INPUT DATA SERIES: '//)
C
C   FFT COEFFICIENTS ARE READ IN
C
  CALL IOPFT (INPUT,TITLE,N,NCOEPP,NAXN,DT,C1,C(1))
  CALL IOPFT (INPUT,TITLE,N,NCOEPP,NAXN,DT,C2,C(2))
C
  IF (INAX.EQ.0) INAX=N
  WRITE (6,4000) (C(I),I=1,2),SEL,LADD,INAX,MNIN,NPER,
1 (PERIOD(I),I=1,NPER)
4000  FORMAT (////1X,'THE COMPONENTS USED IN THIS ANALYSIS ARE:   X1=',
1A4,'   X2=',A4////1X,'GAUSSIAN SPECTRAL WINDOWS: '//1X,
2'SELECTIVITY IS',F8.4/1X,
3'NUMBER OF INTERPOLATIONS BETWEEN EACH PAIR'/1X,
*'OF ADJACENT ',
4'HARMONICS IS SPECIFIED AS',I3/1X,
5'THE NUMBER OF HARMONICS USED ON EACH SIDE OF EACH INTERPOLATION',
6' IS',I4/1X,
7'FEWEST TOTAL ENERGY DENSITY VALUES ALLOWED IN EACH SPECTRAL',
8' WINDOW IS',I4/1X,
9'THERE ARE',I3,' PERIODS ANALYZED: '(1X,10F12.2)
  TO=N*DT
  WRITE (7,7000) (TITLE(I),I=2,15)
7000  FORMAT (14A4)
C
C   TRANSIENT SPECTRA IN THE FREQUENCY BANDS ARE CALCULATED
C
  DO 10 L=1,NPER
  WRITE (6,17000)
17000  FORMAT (1H1,72(' ')//1X,72(' ')//1X,20X,'**** BAND ANALYSIS ****'
1////)
  WRITE (6,13000) (TITLE(I),I=1,15),PERIOD(L),SEL
13000  FORMAT (1H ,15A4//1X,5X,'PERIOD=',F12.2,' SEC.',5X,
1'SELECTIVITY=',F7.4)
  CALL PPARHT (N,DT,MNIN,LADD,INTERP,PERIOD(L),SEL,N,
1 ILOW,IHIGH,NPFT,BELOW,ABOVE,EXTENT)
  CALL HCOV (C1,C2,ENERGY,ILOW,IHIGH,B)
C

```

FILE: MAD            FORTRAN A1            \*\*\* Brown University Computer Cen:

```

C     EQUATION (7), PAGE 229 R.E. THAYER PH.D. THESIS, 1975            H
C            NU=IFIX (5.0132565*SEL*N*DT/PERIOD(L)+1.)            H
          NU=IFIX (FLOAT(NU) / N)            H
          CALL BAND (N,DT,INAX,N,Q,ILOW,INIGH,NPPT,INERF,NBELOW,NABOVE,            H
          1 C1,C2,X1Q,X2Q)            H
C            SMOOTHED ENERGIES ARE CALCULATED            H
C            Q0=T0/PERIOD(L)            H
          CALL FWINDOW (Q,N,Q0,SEL,WINDOW,WEIGHT)            H
          CALL FENGRY (X1Q,X1Q,WINDOW,WEIGHT,N,P(1,1,L),ENERGY)            H
          CALL FENGRY (X1Q,X2Q,WINDOW,WEIGHT,N,P(1,2,L),ENERGY)            H
          P(2,1,L)=CONJG (P(1,2,L))            H
          CALL FENGRY (X2Q,X2Q,WINDOW,WEIGHT,N,P(2,2,L),ENERGY)            H
C            CALCULATE ESTIMATES FOR Q = I/E            H
C            Q1(L)=P(1,2,L)/P(1,1,L)            H
          Q2(L)=P(2,2,L)/P(2,1,L)            H
          CONSQ(L)=REAL( (P(2,1,L)*P(2,1,L))/(P(1,1,L)*P(2,2,L)) )            H
          COH(L)=SQRT(CONSQ(L))            H
          QHAG1(L)=SQRT( REAL( Q1(L)*CONJG(Q1(L)) ) )            H
          QPHAS1(L)=ATAN2( AINAG(Q1(L)) , REAL(Q1(L)) ) * RADDEG            H
          QHAG2(L)=SQRT( REAL( Q2(L)*CONJG(Q2(L)) ) )            H
          QPHAS2(L)=ATAN2( AINAG(Q2(L)) , REAL(Q2(L)) ) * RADDEG            H
          WRITE (6,14000) NU,N            H
14000     FORMAT (///1X,'THERE ARE ',I4,' DEGREES OF FREEDOM',3X,            H
          1 '(N = ',F8.4,')')            H
          WRITE (6,14500) COH(L)            H
14500     FORMAT (/1X,'COHERENCY: ',F12.4)            H
          WRITE (6,17000)            H
          WRITE (6,2005) NU            H
2005     FORMAT (////1X,'SMOOTHED SPECTRAL ENERGY MATRIX',5X,'(',I4,            H
          1 ' DEGREES OF FREEDOM) '///26X,'EXT',27X,'INT'/9X,'.',60(' ') /            H
          29X,' ')            H
          WRITE (6,2001) P(1,1,L),P(1,2,L)            H
          WRITE (6,2002) P(2,1,L),P(2,2,L)            H
2001     FORMAT (5X,'EXT ',2(2X,2E14.5)/9X,' ')            H
2002     FORMAT (5X,'INT ',2(2X,2E14.5)/9X,' ')            H
          NU2=2*NU            H
          CALL CONFID (NU2,CONSQ(L),P(1,1,L),P(1,2,L),P(2,1,L),P(2,2,L),            H
          1 QHAG1(L),QPHAS1(L),DELO,DELP)            H
          WRITE (6,2004) Q1(L),QHAG1(L),DELO,QPHAS1(L),DELP            H
2004     FORMAT (///1X,'RESPONSE FUNCTION ESTIMATES: '//1X,            H
          1 'Q1 = (' ,2E14.5,')'/20X,'MAGNITUDE = ',F12.4,1X,'+/- ',F12.4/20X,            H
          2 ' PHASE = ',F12.2,1X,'+/- ',F5.2,' DEGREES')            H
          CALL CONFID (NU2,CONSQ(L),P(1,1,L),P(1,2,L),P(2,1,L),P(2,2,L),            H
          2 QHAG2(L),QPHAS2(L),DELO,DELP)            H
          WRITE (6,2006) Q2(L),QHAG2(L),DELO,QPHAS2(L),DELP            H
2006     FORMAT (1H0,'Q2 = (' ,2E14.5,')'/20X,'MAGNITUDE = ',F12.4,            H
          1 1X,'+/- ',F12.4/20X,            H
          1 ' PHASE = ',F13.2,1X,'+/- ',F5.2,' DEGREES')            H
          WRITE (7,7001) PERIOD(L),SEL,NU,CONSQ(L)            H
          WRITE (7,7002) P(1,1,L),P(1,2,L)            H

```

FILE: MAD

FORTRAN A1

\*\*\* Brown University Computer Cent

```
7001 WRITE (7,7002) P(2,1,L),P(2,2,L)      H:  
      FORMAT (F10.1,F10.2,I10,F10.5)      H:  
7002 FORMAT (2(2X,2E14.5))                H:  
10    CONTINUE                             H:  
      GO TO 1                              H:  
111  STOP                                  H:  
      END                                  H:
```

```

1 READ INT3      FORTMAN C1 TEST      6/16/80 21:26
C   TO APPLY LINEAR INTERPOLATION TO MISSING DATA POINTS
C   JUNE 16, 1980
C
  DIMENSION T(124),E(124),F1(124),CODE(124)
  DIMENSION E3(124),F13(124)
  DIMENSION T1(15),T2(15)
  READ (5,100) (T1(I),I=1,15)
  READ (5,100) (T2(I),I=1,15)
  READ (5,200) N
100  FORMAT (15A4)
200  FORMAT (I3)
 250  READ (5,250) (T(I),E(I),F1(I),CODE(I),E3(I),F13(I),I=1,N)
  FORMAT(1X,4E10.3)
  DO 10 I=2,N
  IF (CODE(I).EQ.0.) GO TO 10
  IF (CODE(I-1).EQ.1.) GO TO 10
  DO 20 J=1,N
  IF (CODE(I+J).EQ.0.) GO TO 30
  CONTINUE
 30  A1=(E(I+J)-E(I-1))/(T(I+J)-T(I-1))
  A3=(F3(I+J)-F3(I-1))/(T(I+J)-T(I-1))
  A2=(F1(I+J)-F1(I-1))/(T(I+J)-T(I-1))
  A4=(F13(I+J)-F13(I-1))/(T(I+J)-T(I-1))
  R1=E(I-1)-A1*T(I-1)
  R3=E3(I-1)-A3*T(I-1)
  R2=F1(I-1)-A2*T(I-1)
  R4=F13(I-1)-A4*T(I-1)
  DO 40 K=1,J
  E(I-1+K)=A1*T(I-1+K)+R1
  E3(I-1+K)=A3*T(I-1+K)+R3
  F1(I-1+K)=A2*T(I-1+K)+R2
  F13(I-1+K)=A4*T(I-1+K)+R4
 40  CONTINUE
 10  CONTINUE
  WRITE (4,100) (T1(I),I=1,15)
  WRITE (4,100) (T2(I),I=1,15)
  WRITE (4,200) N
  WRITE (4,300) (T(I),E(I),F1(I),CODE(I),E3(I),F13(I),I=1,N)
300  FORMAT (4E10.3)
  STOP
  END

```

```

:READ) STACK FORTRAN C1 TEST 3/24/80 9:39
C STACK STA0001
C OCT 24, 1979 STA0002
C TO SELECTIVELY STACK ENERGIES FOR A GIVEN PERIOD OR STA0003
C FREQUENCY AND WEIGHT EACH ENTRY BY ITS NO. OF DEGREES OF FREEDOM STA0004
C NX=NO. OF PERIODS CONSIDERED STA0005
C NSET=NO. OF DATA SETS CONSIDERED STA0006
C NORM(I)=NO. OF DATA SETS STACKED AT PERIOD PER(I) STA0007
C C11(I),C12(I),C21(I),C22(I) ARE 4 SEPARATE ENERGY FUNCTIONS STA0008
C AT PER(I) STA0009
C N=NO. OF DEGREES OF FREEDOM FOR SPECTRAL ESTIMATES AT SOME PER(I) STA0010
C I) STA0011
C N= NO. OF DEGREES OF FREEDOM FOR PER(I) STA0012
C NDEG(I)=FINAL NO. OF DEGREES OF FREEDOM FOR PER(I) STA0013
C ** IF WISH A SPECTRAL ELEMENT NOT TO BE INCLUDED IN STACKING STA0014
C AT THAT PER(I), SET N=0 STA0015
C DIMENSION PER(25),NORM(25),NDEG(25) STA0016
C DIMENSION SUM1(25),SUM2(25),SUM3(25),SUM4(25) STA0017
C DIMENSION SEL(25) STA0018
C COMPLEX SC11(25),SC12(25),SC21(25),SC22(25) STA0019
C COMPLEX C11(25),C12(25),C21(25),C22(25) STA0020
C DATA SC11/25*(0.0,0.0)/,SC12/25*(0.0,0.0)/,SC21/25*(0.0,0.0)/, STA0021
C SC22/25*(0.0,0.0)/ STA0022
C DATA SUM1/25*0.0/,SUM2/25*0.0/,SUM3/25*0.0/,SUM4/25*0.0/ STA0023
C DATA NDEG/25*0/,NORM/25*0/ STA0024
C NX=4 STA0025
C NSET=8 STA0026
C RADDEG=180./3.1415 STA0027
C DO 20 IX=1,NSET STA0028
C DO 10 I=1,NX STA0029
C READ(5,100) PER(I),SEL(I),N STA0030
100 FORMAT(F10.1,F10.2,I10) STA0031
C READ(5,200) C11(I),C12(I) STA0032
200 FORMAT(2(2X,2E14.5)) STA0033
C READ(5,200) C21(I),C22(I) STA0034
C IF(N.NE.0)NORM(I)=NORM(I)+1 STA0035
C SC11(I)=SC11(I)+N*C11(I) STA0036
C SC12(I)=SC12(I)+N*C12(I) STA0037
C SC21(I)=SC21(I)+N*C21(I) STA0038
C SC22(I)=SC22(I)+N*C22(I) STA0039
C NDEG(I)=NDEG(I)+N STA0040

```

10	CONTINUE	STAO041
20	CONTINUE	STAO042
	DO 30 I=1,NX	STAO043
	NDEG(I)=NDEG(I)**2	STAO044
	WRITE(4,250) PER(I),NDEG(I),NORM(I)	STAO045
250	FORMAT(1X,'PERIOD=',F10.3,' DEGREES OF FREEDOM=',15,' STORYS=',15)	STAO046
	WRITE(4,300) SC11(I),SC12(I),SC21(I),SC22(I)	STAO047
300	FORMAT(5X,'C1=',.2E15.4,'C12=',.2E15.4,/,5X,'C21=',.2E15.4,	STAO048
	1'C22=',.2E15.4)	STAO049
	O12=SQRT(REAL(SC12(I))**2+AIMAG(SC12(I))**2)	STAO050
	O12=O12/SQRT(REAL(SC11(I))**2)	STAO051
	O21=SQRT(REAL(SC22(I))**2)	STAO052
	O21=O21/SQRT(REAL(SC21(I))**2+AIMAG(SC21(I))**2)	STAO053
	PHASE=ATAN(AIMAG(SC12(I))/REAL(SC12(I)))*RADDEG	STAO054
	COH=REAL(SC12(I))**2+AIMAG(SC12(I))**2	STAO055
	COH=COH/(REAL(SC11(I))*REAL(SC22(I)))	STAO056
	WRITE(4,400) O12,O21,PHASE,COH	STAO057
400	FORMAT(1X,'** O(C12)=',F12.4,' O(C21)=',F12.4,' PHASE=',F12.4,	STAO058
	3' COH2= ',F12.4)	STAO059
	CALL CONFID(NDEG(I),COH,SC11,SC12,SC21,SC22,O12,PHASE,DELO,DELP)	STAO060
	WRITE(4,600) DELO,DELP	STAO061
600	FORMAT(5X,'DELTA O= ',F12.4,' DELTA PHI= ',F12.4,/) )	STAO062
30	CONTINUE	STAO063
	STOP	STAO064
	END	STAO065

**Appendix D: Programs for calculating  $Q(\omega)$** **Program name: Multi****Subroutines:****Solve****Simul****Runge****Step****Safe****Requires IMSL library and systems library**

```

1 S CHAT (ORDERLIB, SYM^ ) XME XQCAL NO LO N17 S S 72
2 C MULTI
3 C JUNE 30,1980
4 C TO COMPUT RESPONSE FOR MULTI LAYER MODEL
5 C
6 PROGRAM QCAL(HSP)
7 CALL CHANGE("RUN")
8 CALL ASSIGN(3,15,"OUTPUT")
9 REAL I1N,I2N
10 DIMENSION X(4,4),DEPTHM(50)
11 DIMENSION SIGMA(50),C(50),H(50),ANF(50),CNF(50)
12 N=3
13 C
14 C READ IN CONDUCTIVITY MODEL
15 WRITE(59,1)
16 1 FORMAT(1X,"NO. OF SIGMAS?")
17 READ(59,2) NS
18 2 FORMAT(13)
19 DO 10 I=1,NS
20 WRITE(59,3)
21 3 FORMAT(1X,"SIGMA AND DEPTH OF CHANGE IN METERS")
22 READ(59,100) SIGMA(I),DEPTHM(I)
23 100 FORMAT(2F10.3)
24 10 CONTINUE
25 WRITE(3,4)(SIGMA(I),DEPTHM(I),I=1,NS)
26 4 FORMAT(5X,"SIGMA ",E10.3," DEPTHM ",E10.3)
27 C
28 DO 500 JFREQ=1,19
29 X(1,1)=.1
30 X(2,1)=.2
31 X(3,1)=.3
32 X(4,1)=.4
33 X(1,2)=.5
34 X(2,2)=.6
35 X(3,2)=.7
36 X(4,2)=.8
37 X(1,3)=.93
38 X(2,3)=.84
39 X(3,3)=.63
40 X(4,3)=.41
41 X(1,4)=.16
42 X(2,4)=.37
43 X(3,4)=.69
44 X(4,4)=.99
45 P=(FLOAT(JFREQ))*10.**4
46 IF(JFREQ.GE.11) P=(FLOAT(JFREQ-9))*10.**5
47 WRITE(3,501) JFREQ,P
48 501 FORMAT(1X,"* JFREQ ",15," ** INITIAL PERIOD ",E10.3)
49 E1N=1.
50 E2N=1.
51 CALL STEP(P,N,H,NH,C,IMAX,SIGMA,DEPTHM,NS,ZIN)
52 WRITE(3,111) IMAX,NH
53 111 FORMAT(1X,"IMAX= ",13," AND NO. OF STEPS = ",13,/)
54 CALL SAFE(C,NH,H,NH,N,ANF,CNF,IMAX,X,ZIN)
55 6 FORMAT(1X,"USE ANF= ",E10.3," AND CNF= ",E10.3)
56 I1N=E1N/2.-ANF(IMAX)
57 I2N=E2N/2.-CNF(IMAX)
58 7 FORMAT(1X,"I1N ",E10.3," I2N ",E10.3)
59 Q=I1N**2+I2N**2
60 Q=SQRT(Q/(E1N*E1N+E2N*E2N))

```

```
61      PHASE=(I1N*E2N-I2N*E1N)
62      PHASE=ATAN(PHASE/(I1N*E1N+I2N*E2N))
63      WRITE(3,8) Q,PHASE
64      8   FORMAT(1X,"** /Q/ =",E10.3," PHASE= ",E10.3,/)
65      500 CONTINUE
66      CALL EXIT(1)
67      END
```

```

68      SUBROUTINE SAFE(C,IC,H,IH,N,ANF,CNF,IMAX,X,ZIN)
69 C      JULY 7,1980
70 C      UPWARD INTEGRATION, 4 SOLUTIONS, SOLVE
71 C      MATRIX FOR 4 CONSTANTS
72 C
73      DIMENSION C(IC),H(IH),ANF(IMAX),CNF(IMAX),Y(4)
74      DIMENSION X(4,4)
75      DIMENSION AN(50,4),CN(50,4),DAN(50,4),DCN(50,4)
76      DIMENSION DANF(50),DCNF(50),A(4,4),B(4),WKAREA(16)
77 C
78 C      ** INITIALIZE
79      EIN=1.
80      E2N=1.
81      IDCT=3
82      ALPHA=0.001
83      BETA=0.001
84      N=1
85      IA=4
86      IN=4
87      J=1
88      WRITE(3,100)N
89 100  FORMAT(1X,"FOR N= ",15," SKINDEPTHS",/)
90 5    CONTINUE
91 110  FORMAT(1X,"READ IN INITIAL AN,DAN,CN,DCN *** ",/)
92      AN(1,J)=X(1,J)
93      DAN(1,J)=X(2,J)
94      CN(1,J)=X(3,J)
95      DCN(1,J)=X(4,J)
96 120  FORMAT(F10.3)
97      Y(1)=AN(1,J)
98      Y(2)=DAN(1,J)
99      Y(3)=CN(1,J)
100     Y(4)=DCN(1,J)
101     Z=ZIN
102 125  FORMAT(1X,"Y(K) ",4E10.3)
103 C
104 C      SOLVE SIMULTANEOUS EQUATIONS
105 C
106     CALL SIMUL(Z,H,IH,N,C,IC,Y,ANF,CNF,DANF,DCNF,IMAX)
107     DO 10 I=1,IMAX
108     AN(I,J)=ANF(I)
109     DAN(I,J)=DANF(I)
110     CN(I,J)=CNF(I)
111     DCN(I,J)=DCNF(I)
112 10   CONTINUE
113 130  FORMAT(1X,"I ",15," J ",15," AN ",E10.3," DAN ",E10.3,/,5X,
114     1" CN ",E10.3," DCN ",E10.3)
115     J=J+1
116     IF(J.LT.5) GO TO 5
117 C
118 C      DEFINE ELEMENTS OF MATRIX
119 C
120     DO 30 J=1,4
121     A(1,J)=AN(1,J)
122     A(2,J)=CN(1,J)
123     A(3,J)=DAN(IMAX,J)+C(IC)*AN(IMAX,J)
124     A(4,J)=DCN(IMAX,J)+C(IC)*CN(IMAX,J)
125 30   CONTINUE
126 200  FORMAT(1X,/, " ELEMENTS OF MATRIX",/)
127 205  FORMAT(1X,4E10.3)

```

```

128      B(1)=ALPHA
129      B(2)=DETA
130      B(3)=3./2.*C(IC)*E1N
131      B(4)=3./2.*C(IC)*E2N
132  210  FORMAT(1X," B(1)= ",4E10.3,/)
133      CALL LEQTF(A,M,IN,IA,B,IDGT,WKAREA,IER)
134  220  FORMAT(1X,"THE FOUR CONSTANTS ARE" ",4E10.3)
135      WRITE(3,230) IER
136  230  FORMAT(1X,/, " ERROR PARAMETER ",15)
137  C
138  C      USING THEOREM THAT THERE EXISTS ONE SOLUTION .
139  C      Y1=C1*Y11+C2*Y12+C3*Y13+C4*Y14,ETC
140  C
141      DO 40 I=1,IMAX
142      ANF(I)=B(1)*AN(I,1)+B(2)*AN(I,2)+B(3)*AN(I,3)+B(4)*AN(I,4)
143      DANF(I)=B(1)*DAN(I,1)+B(2)*DAN(I,2)+B(3)*DAN(I,3)+B(4)*DAN(I,4)
144      CNF(I)=B(1)*CN(I,1)+B(2)*CN(I,2)+B(3)*CN(I,3)+B(4)*CN(I,4)
145      DCNF(I)=B(1)*DCN(I,1)+B(2)*DCN(I,2)+B(3)*DCN(I,3)+B(4)*DCN(I,4)
146  40  CONTINUE
147  C
148  C      ARE CONTINUITY CONDITIONS MET?
149  C
150      WRITE(3,300) ALPHA,ANF(1)
151  300  FORMAT(/,1X,"ALPHA ",E10.3," ANF(1) ",E10.3)
152      WRITE(3,310) BETA,CNF(1)
153  310  FORMAT(1X,"BETA ",E10.3," CNF(1) ",E10.3)
154      TEST1=(-1)*C(IC)*ANF(IMAX)+(3./2.*C(IC)*E1N)
155      TEST2=(-1)*C(IC)*CNF(IMAX)+(3./2.*C(IC)*E2N)
156      WRITE(3,320) TEST1,DANF(IMAX)
157  320  FORMAT(1X,"TEST1 ",E10.3," COMPARED TO DAN(IMAX) ",E10.3)
158      WRITE(3,330) TEST2,DCNF(IMAX)
159  330  FORMAT(1X,"TEST2 ",E10.3," COMPARED TO DCN(IMAX) ",E10.3)
160      RETURN
161      END

```

```

162      SUBROUTINE SIMUL(Z,H, IH,N,CC, IC,Y,AN,CN,DAN,DCN,IMAX)
163 C      ** AS OF APRIL 28,1980
164 C      CALCULATES SOLUTION TO PAIR OF COUPLED SIMULTANEOUS
165 C      2ND ORDER DIFFERENTIAL EQUATIONS OF FORM  $D^2A/DZ^2=(2*C**2$ 
166 C       $*AN/(C*(Z-1)+1)**2+2*N**2*CN$ , WHERE C IS A GIVEN COEF-
167 C      FICIENT. RETURNS AN AND CN AS FUNCTION OF DEPTH. Z IS
168 C      NONDIMENSIONAL AND VARIES 0 TO 1. REQUIRES FUNCTION RUNGE
169 C
170      DIMENSION AN(IMAX),CN(IMAX),Y(4),H(IH),F(4),CC(IC),DAN(IMAX)
171      DIMENSION DCN(IMAX)
172      INTEGER RUNGE
173 C
174 C      INITIALIZE
175 C
176      50 FORMAT(3X,"** INITIALIZATION **")
177      60 FORMAT(1X,"Y1",E10.3," Y2",E10.3," Y3",E10.3," Y4",E10.3)
178      AN(1)=Y(1)
179      CN(1)=Y(3)
180      DAN(1)=Y(2)
181      DCN(1)=Y(4)
182      65 FORMAT(1X," AN(1)=",E10.3," CN(1)=",E10.3,/,
183      65X,"DAN(1)=",E10.3," DCN(1)=",E10.3,/)
184      I=1
185 C
186 C      START INTEGRATION
187 C
188      4 IF(IH.EQ.1) STEP=H(1)
189      IF(IH.EQ.1) GO TO 5
190      STEP=H(1)
191      68 FORMAT(1X,"I ",.15," STEP ",E10.3)
192      5 K=RUNGE(4,Y,F,Z,STEP)
193      101 FORMAT(9X,"K=",.13," Z=",E10.3)
194      IF(K.EQ.0) GO TO 10
195 C
196 C      DERIVATIVES ARE DEFINED
197 C
198      IF(IC.EQ.1)C=CC(1)
199      IF(IC.NE.1)C=CC(1)
200      104 FORMAT(1X,"C=",E10.3)
201      F(1)=Y(2)
202      F(2)=2*C**2/((C*(Z-1.))+1.))**2)*Y(1)+N**2*2*Y(3)
203      F(3)=Y(4)
204      F(4)=2*C**2/((C*(Z-1.))+1.))**2)*Y(3)-N**2*2*Y(1)
205      102 FORMAT(1X,"F1=",E10.3," F2=",E10.3," F3=",E10.3," F4=",E10.3)
206      GO TO 5
207 C
208 C      WHEN K IS RETURNED AS 0 ,INTEGRATION IS COMPLETED
209 C
210      10 I=I+1
211      200 FORMAT(1X,"I=",.15," Z=",E10.3)
212      AN(I)=Y(1)
213      CN(I)=Y(3)
214      DAN(I)=Y(2)
215      DCN(I)=Y(4)
216      300 FORMAT(5X,"I=",.15," AN(1)",E10.3," CN(1)",E10.3)
217      IF(I.LT.IMAX) GO TO 4
218      IF(I.NE.IMAX) WRITE(3,400)
219      400 FORMAT(9X,"INDEX IMAX IS NOT CONSISTENT")
220      RETURN
221      END

```

```

222      FUNCTION RUNGE(N,Y,F,X,H)
223 C
224 C      THE FUNCTION RUNGE EMPLOYS THE FOURTH-ORDER RUNGE -
225 C      KUTTA METHOD WITH KUTTA'S COEFFICIENTS TO INTEGRATE A
226 C      SYSTEM OF N SIMULTANEOUS FIRST ORDER ORDINARY DIFFERENTIAL
227 C      EQUATIONS  $F(J)=DY(J)/DX$ , ( $J=1,2,\dots,N$ ), ACROSS ONE STEP OF
228 C      LENGTH H IN THE INDEPENDENT VARIABLE X, SUBJECT TO
229 C      INITIAL CONDITIONS  $Y(J)$ , ( $J=1,2,\dots,N$ ). EACH  $F(J)$ , DERI-
230 C      VATIVE OF  $Y(J)$ , MUST BE COMPUTED FOUR TIMES PER INTE-
231 C      GRATION STEP BY THE CALLING PROGRAM. THE FUNCTION MUST BE
232 C      CALLED FIVE TIMES PER STEP (PASS(1)...PASS(5)) SO THAT THE
233 C      INDEPENDENT VARIABLE VALUE X AND THE SOLUTION VALUES
234 C      ( $Y(1)\dots Y(N)$ ) CAN BE UPDATED USING THE RUNGE-KUTTA AL-
235 C      GORITHM. M IS THE PASS COUNTER. RUNGE RETURNS AS ITS VALUE
236 C      1 TO SIGNAL THAT ALL DERIVATIVES (THE  $F(J)$ ) BE EVALUA-
237 C      TED OR 0 TO SIGNAL THAT THE INTERGRATION PROCESS FOR THE
238 C      CURRENT STEP IS FINISHED. SAVEY(J) IS USED TO SAVE THE
239 C      THE INITIAL VALUE OF  $Y(J)$  AND PHI(J) IS THE INCREMENT
240 C      FUNCTION FOR THE J(TH) EQUATION. AS WRITTEN, N MAY BE
241 C      NO LARGER THAN 80. CARRAHAN, LUTHER, + WILKES, APPLIED
242 C      NUMERICAL METHODS, JOHN WILEY + SONS, N.Y., 1969.
243 C
244      INTEGER RUNGE
245      DIMENSION PHI(80),SAVEY(80),Y(N),F(N)
246      DATA N/0/
247 C
248      N=N+1
249 100  FORMAT(7X,"PASS ",I3)
250      GO TO (1,2,3,4,5),M
251 C
252 C      ..... PASS1.....
253 1    RUNGE=1
254      RETURN
255 C
256 C      ..... PASS2.....
257 2    DO 22 J=1,N
258      SAVEY(J)=Y(J)
259      PHI(J)=F(J)
260 22   Y(J)=SAVEY(J)+0.5*H*F(J)
261      X=X+0.5*H
262      RUNGE=1
263      RETURN
264 C
265 C      ..... PASS3.....
266 3    DO 33 J=1,N
267      PHI(J)=PHI(J)+2.0*F(J)
268 33   Y(J)=SAVEY(J)+0.5*H*F(J)
269      RUNGE=1
270      RETURN
271 C
272 C      ..... PASS4.....
273 4    DO 44 J=1,N
274      PHI(J)=PHI(J)+2.0*F(J)
275 44   Y(J)=SAVEY(J)+H*F(J)
276      X=X+0.5*H
277      RUNGE=1
278      RETURN
279 C
280 C      ..... PASS5.....
281 5    DO 55 J=1,N

```

```
232 55 Y(J)=SAVEY(J)+(PHI(J)+F(J))*H/6.0  
233     H=0  
234     RUNGE=0  
235     RETURN  
236 C  
237     END
```

```

288      SUBROUTINE STEP(P,N,H,NH,C,NZ,SIGMA,DEPTHM,NSS,ZIN)
289 C
290 C      SEPT.4,1980 (NOV25,1980)
291 C      TO DEFINE STEP SIZES GIVEN CONDUCTIVITY PROFILE
292 C      P=PERIOD(SEC),N=SKIN DEPTHS NORMALIZATION,H(1)=
293 C      STEP SIZE,NH=NO. OF STEPS, CC(1)=N*DELTA/(6371*
294 C      10**3),NZ=NO.OF DEPTHS Z=0 TO 1,I.E. IMAX IN SUB.
295 C      SAFE.
296 C
297      DIMENSION H(50),HH(50),DEPTH(50),DELTA(50),CC(50),Z(50)
298      DIMENSION SIGMA(50),C(50),DEPTHM(50)
299      NSS=NSS
300      PI=3.1415
301      FREQ=1./P
302      DO 20 I=1,NS
303      DELTA(I)=SQRT(2.*10.**7/(8.*PI**2*FREQ*SIGMA(I)))
304      C(I)=N*DELTA(I)/(6371.*10.**3)
305      DEPTH(I)=DEPTHM(I)
306      IF(I.EQ.1) DEPTH(I)=1.-DEPTH(I)/(N*DELTA(I))
307      IF(I.NE.1) DEPTH(I)=DEPTH(I-1)-((DEPTHM(I)-DEPTHM(I-1))/
308      1(N*DELTA(I)))
309      IF(C(I).GE.1.) DEPTH(I)=1.
310      IF (DEPTH(I) .GT. 1.) WRITE(59,10),I,DEPTH(I)
311 10      FORMAT("ERROR I =",I5,"DEPTH(I) = ",E10.2)
312      IF(DEPTH(I).LT.0.)NS=I
313      IF(DEPTH(I).LT.0.) GO TO 21
314 20      CONTINUE
315      GO TO 22
316 21      DEPTH(NS)=0.
317 22      NH=0
318      WRITE(3,200)(J,DEPTH(J);DELTA(J),C(J),J=1,NS)
319 200      FORMAT(1X,"J ",I3," DEPTH ",E10.3," DELTA ",E10.3," C ",E10.3)
320      DO 30 I=1,NS
321      DO 25 J=1,5
322      IF(I.EQ.1) HH(NH+J)=(1.-DEPTH(I))/5.
323      IF(I.NE.1) HH(NH+J)=(DEPTH(I-1)-DEPTH(I))/5.
324      CC(NH+J)=C(I)
325      IF(HH(NH+J).EQ.0) CC(NH+J)=C(I+1)
326      IF(HH(NH+J).EQ.0)WRITE(3,5)(NH+J),I,DEPTH(I)
327 5      FORMAT(1X,"SPECIAL CONDITIONS NH+J=",I3," I ",I3,"DEPTH ",E10.3)
328 C      **NOTE CONDITIONS ON STEP HH **
329 25      CONTINUE
330      NH=NH+5
331 30      CONTINUE
332      Z(1)=DEPTH(NS)
333 300      FORIAT(/,1X,"THERE ARE ",I3," STEPS",/)
334      DO 40 I=1,NH
335      K=NH+1-I
336      H(I)=HH(K)
337      C(I)=CC(K)
338      Z(I+1)=Z(I)+H(I)
339 400      FORMAT(1X,"I ",I3,"Z= ",E10.3,"TO Z= ",E10.3," H= ",E10.3)
340 40      CONTINUE
341      NZ=NH+1
342      IF(Z(NZ).NE.1.) Z(NH)=1.-Z(NH)
343      WRITE(3,450)(I,Z(I),Z(I+1),H(I),C(I),I=1,NH)
344 4      FORMAT(/,1X,"FINAL Z S ,H S, AND C S ",/)
345 450      FORMAT(1X,"I ",I3,"Z= ",E10.3,"TO Z= ",E10.3," H= ",E10.3,
346      1" C= ",E10.3)
347      ZIN=Z(1)
348      RETURN
349      END

```

```

350      SUBROUTINE LEQTIF (A,M,N,IA,B,IDGT,WKAREA,IER)
351 C
352 C-----S-----LIBRARY 3-----
353 C
354 C      FUNCTION          - LINEAR EQUATION SOLUTION - FULL STORAGE
355 C                      - MODE - SPACE ECONOMIZER SOLUTION.
356 C      USAGE            - CALL LEQTIF (A,M,N,IA,B,IDGT,WKAREA,IER)
357 C      PARAMETERS      A  - INPUT MATRIX OF DIMENSION N BY N CONTAINING
358 C                      - THE COEFFICIENT MATRIX OF THE EQUATION
359 C                      - AX = B.
360 C                      - ON OUTPUT, A IS REPLACED BY THE LU
361 C                      - DECOMPOSITION OF A ROWWISE PERMUTATION OF
362 C                      - A.
363 C      M                - NUMBER OF RIGHT-HAND SIDES.(INPUT)
364 C      N                - ORDER OF A AND NUMBER OF ROWS IN B.(INPUT)
365 C      IA               - NUMBER OF ROWS IN THE DIMENSION STATEMENT
366 C                      - FOR A AND B IN THE CALLING PROGRAM. (INPUT)
367 C      B                - INPUT MATRIX OF DIMENSION N BY M CONTAINING
368 C                      - RIGHT-HAND SIDES OF THE EQUATION AX = B.
369 C                      - ON OUTPUT, THE N BY M SOLUTION X REPLACES B.
370 C      IDGT             - INPUT OPTION.
371 C                      - IF IDGT IS GREATER THAN 0, THE ELEMENTS OF
372 C                      - A AND B ARE ASSUMED TO BE CORRECT TO IDGT
373 C                      - DECIMAL DIGITS AND THE ROUTINE PERFORMS
374 C                      - AN ACCURACY TEST.
375 C                      - IF IDGT EQUALS ZERO, THE ACCURACY TEST IS
376 C                      - BYPASSED.
377 C      WKAREA           - WORK AREA OF DIMENSION GREATER THAN OR EQUAL
378 C                      - TO N.
379 C      IER              - ERROR PARAMETER
380 C                      - TERMINAL ERROR = 12B+N.
381 C                      - N = 1 INDICATES THAT A IS ALGORITHMICALLY
382 C                      - SINGULAR. (SEE THE CHAPTER L PRELUDE).
383 C                      - WARNING ERROR = 32+N.
384 C                      - N = 2 INDICATES THAT THE ACCURACY TEST
385 C                      - FAILED.
386 C                      - THE COMPUTED SOLUTION MAY BE IN ERROR
387 C                      - BY MORE THAN CAN BE ACCOUNTED FOR BY
388 C                      - THE UNCERTAINTY OF THE DATA.
389 C                      - THIS WARNING CAN BE PRODUCED ONLY IF
390 C                      - IDGT IS GREATER THAN 0 ON INPUT.
391 C                      - SEE CHAPTER L PRELUDE FOR FURTHER
392 C                      - DISCUSSION.
393 C      PRECISION        - SINGLE
394 C      REQD. IMSL ROUTINES - LUDATF,LUELMF,UERTST
395 C      LANGUAGE          - FORTRAN
396 C-----
397 C
398 CC+-----
399 CC+
400 CC+      LAWRENCE LIVERMORE LABORATORY
401 CC+      NUMERICAL MATHEMATICS GROUP -- MATHEMATICAL SOFTWARE LIBRARY
402 CC+-----
403 CC+
404 CC+
405 CC+      CLASS TWO ROUTINE:      LEQTIF
406 CC+      EDITION:      5
407 CC+      DATE LAST CHANGED: 76-04-01
408 CC+
409 CC+      CLASS TWO ROUTINES ARE MADE AVAILABLE BY NMC AS A SERVICE TO THE

```

**Appendix E: Glossary of Symbols**

## Glossary of Symbols

$a$	radius of the earth
$A_n$	series coefficient for $p$
$\bar{B}$	magnetic induction
$C_n$	series coefficient for $p$
$C_{ij}$	cross power spectra for series $i$ and $j$
$\hat{C}_{ij}$	cross power estimate
$c$	normalized skin depth = $N \delta/a$
$c_1$	constant coefficients
$\bar{D}$	electric displacement field; magnetic disturbance field
DS	disturbance local-time inequality
Dst	storm time variation
$E$	activation energy
$\bar{E}$	electric field
$E_{1n}, E_{2n}$	series coefficients for $e_1 = e_1^0(t)$
$e_\ell^m(t)$	external magnetic field variation of order $m$ , degree $\ell$
$f$	frequency, cycles/sec
$F_i$	differential equations
$F( )$	fourier transform of
$\bar{H}$	magnetic field intensity
$I_{1n}, I_{2n}$	series coefficients for $i_1 = i_1^0(t)$
$i_\ell^m(t)$	internal field variation of order $m$ degree $\ell$
$\bar{J}_f$	free current density

M.	counting index
N	counting index; number of skin depths
$n, n_i$	number of degrees of freedom
p	scalar part of poloidal field $\vec{S}$
$P_{ij}$	coefficients
$P_n^m, P_l^o$	legendre polynomials
Q	response function
$\hat{Q}$	estimate of response function
q	electric charge
$\vec{r}$	radius vector
r	radius
S	selectivity
$\vec{S}$	poloidal vector field
Sq	quiet time daily variations
T	total time; total thickness
t, $t_n$	time
$t_{1i}, t_{2j}$	thickness of ith slab (jth slab) with conductivity $\sigma_1$ ( $\sigma_2$ )
U	potential
$W(w_i - w_n)$	Gaussian window
x, $\bar{x}$	variable
$Y_i$	derivatives for finite difference algorithm
z	normalized radial distance

Greek

$\alpha$	constant
$\beta$	constant
$\delta$	skin depth
$\Delta V$	change in volume
$\gamma_{12}$	coherency between series 1 and 2
$\tilde{\epsilon}_n$	arbitrary coefficient
$\epsilon$	permittivity (electric)
$\lambda$	longitude
$\mu$	permeability (magnetic); ion mobility
$\emptyset$	phase
$\tilde{\emptyset}$	function
$\rho$	= $1/\sigma\mu$
$\sigma$	conductivity
$\Sigma$	summation
$\theta$	latitude
$\omega$	frequency, rad/sec

## BIBLIOGRAPHY

- Andersen, R. S., J. F. Devane, S.-A. Gustafson and D. E. Winch,  
"The qualitative character of the global electrical conductivity of the earth," *Phys. Earth Planet. Inter.*, 20, pp. 15-21, 1979.
- Banks, R. J. "Geomagnetic variations and the electrical conductivity of the upper mantle," *Geophys. J. R. Astron. Soc.*, 17, pp. 457-487, 1969.
- Banks, R. J., "The overall conductivity distribution of the earth," *J. Geomagn. Geoelec.*, 24, pp. 337-351, 1972.
- Backus, G., "A class of self-sustaining dissipative spherical dynamos," *Annals of Physics*, 4, pp. 372-447, 1958.
- Bailey, R. C., "Inversion of the geomagnetic induction problem," *Proc. R. Soc.*, 315, pp. 185-194, 1970.
- Bendat, J. S. and A. G. Piersol, Random Data: Analysis and Measurement Procedures, Wiley-Interscience, New York, 1971.
- Birch, F., "Density and composition of the upper mantle: first approximation as an olivine layer," in The Earth's Crust and Upper Mantle, ed. P. J. Hart, Am. Geophysical Union, Washington, D. C., pp. 18-36, 1969.
- Blackman, R. B. and J. W. Tukey, The Measurement of Power Spectra, Dover Publications, New York, 1958.
- Boyd, F. R. and P. H. Nixon, "Experimental and field studies in igneous petrology," Annual Report of the Director Geophysical Laboratory, Carnegie Institute, Washington, D. C., pp. 431-445, 1973.
- Boyce, W. E. and R. C. DiPrima, Elementary Differential Equations, John Wiley & Sons, Inc., New York, 1969.
- Bullard, E. C. and R. L. Parker, "Electromagnetic induction in the ocean," The Sea, ed. A. E. Maxwell, v. 4, Wiley-Interscience (John Wiley & Sons), pp. 695-730, 1970.
- Cain, J. C. and R. A. Langel, "Geomagnetic survey by the polar orbiting geophysical observatories," in World Magnetic Survey 1957-1964, ed. A. J. Zmuda, et al., IAGA Bulletin, 28, 1971.

- Carmichael, I. S. E., F. J. Turner, and J. Verhoogen, Igneous Petrology, McGraw-Hill, New York, 1974.
- Chapman, S., "The solar and lunar diurnal variations of the earth's magnetism," *Phil. Trans. R. Soc.*, A218, pp. 1-118, 1919.
- Chapman, S. and Price, A. T., "The electrical and magnetic state of the interior of the earth as inferred from terrestrial magnetic variations," *Philos. Trans. R. Soc. London, ser. A*, 229, pp. 427-460, 1930.
- Cox, C. S., J. H. Filloux, and J. C. Larsen, "Electromagnetic studies of ocean currents and electrical conductivity below the ocean floor," The Sea, v. 4, John Wiley, New York, pp. 637-693, 1970.
- Didwall, E. M. and R. A. Langel, "Storm-time magnetic field variations: implications for earth conductivity models," *Trans. AGU*, v. 57 (Fall), p. 908, 1976.
- Didwall, E. M. and R. A. Langel, "Internal and external magnetic field variations as determined from satellite magnetic storm data," *Trans. IAGA*, NO. 41, (Seattle), 1977.
- Didwall, E. M., "Continuous upper mantle conductivity models and their application to satellite data," *Trans. AGU*, v. 61, (Spring), no. 17, p. 226, 1980.
- Duba, A., "Electrical conductivity of olivine," *J. Geophys. Res.*, 77, pp. 2483-2495, 1972.
- Duba, A. and I. A. Nicholls, "The influence of oxidation state on the electrical conductivity of olivine," *Earth Planet. Sci. Lett.*, 18, pp. 59-64, 1973.
- Duba, A., J. Ito and J. C. Jamieson, "The effect of ferric iron on the electrical conductivity of olivine," *Earth Planet. Sci. Lett.*, 18, pp. 279-284, 1973.
- Duba, A., H. C. Heard and R. N. Schock, "Electrical conductivity of olivine at high pressure and under controlled oxygen fugacity," *J. Geophys. Res.*, 79, pp. 1667-1673, 1974.
- Duba, A., H. C. Heard, A. Pininskai and R. N. Schock, "Electrical conductivity and the geotherm. Proc. Int. Conf. on Geothermometry and Geobarometry. Penn. State Univ., Oct., 1975.

- Duba, A., "Are laboratory electrical conductivity data relevant to the earth," *Acta Geodaet., Geophys. et Montanist. Acad. Sci. Hung. Tomus 11 (3-4)*, pp. 485-495, 1976.
- Eckhardt, D., K. Larner and T. Madden, "Long period magnetic fluctuations and mantle electrical conductivity estimates," *J. Geophys. Res.*, 68, pp. 6279-6286, 1963.
- Eggler, D. H. and I. Kushiro, "Free energies of decarbonation reactions at mantle pressures: I. Stabilities of the assemblage forsterite-enstatite-magnesite in the system  $MgO-SiO_2-CO_2-H_2O$  to 60 kbar," *Am. Mineral.* 64, pp. 288-293, 1979.
- Garland, G. D., "Correlation between electrical conductivity and other geophysical parameters," *Phys. Earth Planet. Inter.*, 10, pp. 220-230, 1975.
- Grant, F. S. and G. F. West, Interpretation Theory in Applied Geophysics, McGraw-Hill, New York, 1965.
- Gough, D. I., "The geophysical significance of geomagnetic variation anomalies," *Phys. Earth Planet. Inter.*, 7, pp. 379-388, 1973.
- Gough, D. I., "Electrical conductivity under western North America in relation to heat flow, seismology, and structure," *J. Geomagn. Geoelec.*, 26, pp. 105-123, 1974.
- Haggerty, S. E. "Opaque mineral oxides in terrestrial igneous rocks," Oxide Minerals, ed. D. Rumble III, Mineralogical Soc. of Am., Washington, D. C., 1976.
- Hermance, J. F. and Grillot, C. R., "Correlation of magnetotelluric, seismic and temperature data from southwest Iceland," *J. Geophys. Res.*, 75, pp. 6582-6591, 1970.
- Hermance, J. F., A. Nur and S. Bjornsson, "Electrical properties of basalt: relation of laboratory to in situ measurements," *J. Geophys. Res.*, 77, pp. 1424-1429, 1972.
- Jady, R. J., "The conductivity of spherically symmetric layered earth models determined by Sq and longer period magnetic variations," *Geophys. J. R. astr. Soc.*, 36, pp. 399-410, 1974(a).
- Jady, R. J., "Conductivity models and Bank's data," *Geophysics J. R. Astron. Soc.*, 37, pp. 447-452, 1974(b).

- Jenkins, G. M. and D. G. Watts, Spectral Analysis and its Applications, Holdenday, San Francisco, 1969.
- Kittel, C., Introduction to Solid State Physics, John Wiley & Sons, Inc., New York, 1971.
- Lahiri, B. N. and A. T. Price, "Electromagnetic induction in non-uniform conductors, and the determination of the conductivity of the earth from terrestrial magnetic variations," Phil. Trans. Roy. Soc., A237, pp. 509-540, 1939.
- Lamb, H., "On electrical motions in a spherical conductor," Philos. Trans. R. Soc. London, A174, pp. 519-539, 1883.
- Langel, R. A., "Near-earth magnetic disturbance in total field at high latitudes, 1, Summary of data from Ogo 2, 4 and 6," J. Geophys. Res., 79, pp. 2363-2371, 1974.
- Langel, R. A., "Near-earth satellite magnetic field measurements: a prelude to MAGSAT," EOS, 60, no. 38, pp. 667-670, 1979.
- Larsen, J. C., "An introduction to electromagnetic induction in the ocean," Phys. Earth Planet. Int., 7, pp. 389-398, 1973.
- Larsen, J. C., "Low frequency (0.1-6.0 cpd) electromagnetic study of deep mantle electrical conductivity beneath the Hawaiian islands," Geophys. J. R. astr. Soc., 43, pp. 17-46, 1975.
- Lorrain, P. and D. R. Corson, Electromagnetic Fields and Waves, W. H. Freeman and Co., San Francisco, 1970.
- Marsh, B. D. and E. M. Didwall, "Thermal regime of the upper mantle based on electrical conductivity derived from satellite magnetic field measurements," NASA Grant no. NSG-5269 technical report, 1979.
- Mayhew, M. A. "A computer program for reduction of Pogo satellite magnetic anomaly data to common elevation and to the pole," contract no. S-41625-B, Business & Technological Systems, 1980.
- Misener, D. J., "Cationic diffusion in olivine to 1400°C and 35 kbar," Conference on Geochemical Transport and Kinetics, Arlie House, Carnegie Institute of Washington Publication 634, pp. 117-129, 1973.
- Nitsan, U., "Stability field of olivine with respect to oxidation and reduction," J. Geophys. Res., 79, pp. 706-711, 1974.

- Parker, R. L., "The inverse problem of electrical conductivity in the mantle," *Geophys. J. R. astr. Soc.*, 22, pp. 121-138, 1970.
- Price, A. T., "The induction of electric currents in nonuniform thin sheets and shells," *Quart. J. Mech. Appl. Math.*, 2, pp. 283-310, 1949.
- Rikitake, T., "Electromagnetic induction within the earth and its relation to the electrical state of the earth's interior," *Bull. Earthquake Res. Inst.*, 28, pp. 45-98.
- Rikitake, T., Electromagnetism and the Earth's Interior, Elsevier, Amsterdam, 1966.
- Ringwood, A. E., "Composition of the crust and upper mantle," in The Earth's Crust and Upper Mantle, ed. P. J. Hart, Am. Geophysical Union, Washington, D. C., 1969.
- Ringwood, A. E., Composition and Petrology of the Earth's Mantle, McGraw-Hill, New York, 1975.
- Roden, R. B., "The effect of an ocean on magnetic diurnal variations," *Geophys. J. Roy. Astr. Soc.*, 8, pp. 375-387, 1964.
- Schmucker, U., "Anomalies of geomagnetic variations in the southwestern United States," *Bull. Scripps Inst. Oceanogr.*, 13, 1970.
- Shankland, T. J. and H. S. Waff, "Partial melting and electrical conductivity anomalies in the upper mantle," *J. Geophys. Res.*, 82, pp. 5409-5417, 1977.
- Stacey, F. D., Physics of the Earth, John Wiley & Sons, New York, 1977.
- Swift, C. M., Jr., "A magnetotelluric investigation of an electrical conductivity anomaly in the southwestern United States," Ph.D. thesis, Dept. of Geol. and Geophys., Mass. Inst. of Technol., Cambridge, 1967.
- Thayer, R. E., "Telluric-magnetotelluric investigations of regional geothermal processes in Iceland," Ph.D. thesis, Dept. of Geol. Sci., Brown Univ., Providence, R. I., 1975.

VITA

Edna Mary Didwall

Born: [REDACTED]

Education:

High School: Perry Hall Senior High, Perry Hall, MD, 1970

B.S. in Physics: University of Maryland, College Park, 1974  
with honors in Physics

M.S. in Metallurgy: Carnegie-Mellon University, Pittsburgh, PA,  
1974

Ph.D. in Geophysics: Johns Hopkins University, Baltimore, MD,  
1980 (to be awarded 1981)

Honors: Phi Beta Kappa, Phi Kappa Phi, Sigma Pi Sigma, Sigma Xi